

**DEVELOPMENT OF HYDROLOGIC AND VADOSE MODELS TO
IMPROVE GROUNDWATER MANAGEMENT IN THE OWENS VALLEY**

**A Final Report Prepared by The County of Inyo Water Department
For the State of California, Department of Water Resources, Grant Agreement
No. 460001827 under the Local Groundwater Management Assistance Act**

Robert Harrington and Aaron Steinwand

**with contributions by Dani Or, Univ. of Connecticut; Wesley Danskin, U.S.
Geological Survey; Jan Hendrickx, New Mexico Technical Institute; and Jim
Stroh, The Evergreen State College.**

November 10, 2003

Executive Summary

The County of Inyo and the City of Los Angeles and its Department of Water and Power have adopted a Long Term Groundwater Management Plan to manage groundwater and surface water in the Owens Valley to avoid adverse changes to phreatophytic vegetation while continuing to supply water to Los Angeles. Experience gained through monitoring and research during the last decade revealed the ineffectiveness of existing monitoring and management procedures. The purpose of this research project was to improve prediction tools used to evaluate the potential effects of proposed groundwater pumping. Specifically, this project focused on revision and testing of existing groundwater and vadose zone models and collection of field measurements to study the conceptualization of the models.

A post-audit for the period 1989-2002 was completed for a regional groundwater model of the Owens Valley originally prepared by Danskin (1998). In addition, the model was revised to separate the water balance components into custom MODFLOW packages to facilitate evaluation of each component. The model now simulates the period 1963-2002. It successfully simulated the drawdown due to the high pumping of 1987 through 1990 and the subsequent period of low pumping to allow water table recovery. The post-audit confirmed the earlier conclusions that the primary influence in most areas of the valley is pumping. Transient simulations supported conclusions based on steady state simulations that the time frame for response of the groundwater system was five to ten years. This suggests that there may be a lag of as much as a decade for the groundwater system to fully respond to changes in natural

hydrologic inputs such as runoff or evapotranspiration or management of pumping and recharge. Future work to enhance the use of the model should focus on refinement of historical data inputs, testing of additional future scenarios, and further revision of the model itself

In work associated with the model revision, we experimented with two methods to construct estimates of spatial evapotranspiration (ET), a major component of the groundwater budget of the basin. A series of ET maps for the post audit period was developed based on field and remote sensing vegetation measurements and empirically derived transpiration coefficients (Kc). Future work will incorporate the ET maps into the groundwater model to examine the effect of different ET estimates on model performance. SEBAL (Surface Energy Balance Algorithm for Land) is an alternative method developed recently that estimates ET directly from satellite measurements. Results of initial tests of the method conducted as part of this project were promising and generated interest in the scientists developing the technique to use the Owens Valley as a test site for their research.

A field investigation was conducted to measure ET using micrometeorological methods to compare with vegetation based Kc methods like those used to prepare the ET maps for the groundwater model. Along with the ET and vegetation measurements, soil water and water table measurements were collected to account for sources and locations of plant uptake. These results were used to evaluate and examine the parameterization of a vadose zone water balance model for phreatophytes that can account for direct groundwater uptake. Turbulent fluxes of heat and water measured by the eddy covariance ET system did not account for approximately one-third of the available energy similar as has been observed in other studies. Based on a side-by-side comparison with Bowen ratio instruments that rely on different theory to measure ET, we

developed recommendations to correct the ET measurements to account for all the available energy. After correction for energy imbalance, the measured seasonal ET generally agreed with estimates derived from Kc models and LAI measurements when the site conditions met assumptions of the Kc models. The sensitivity of the Kc estimates to correctly sampling the peak leaf area, however, suggests the practice of obtaining a single vegetation measurement is potentially error prone.

The portion of ET derived from the water table was estimated from the water balance as the difference between measured ET, soil water depletion, precipitation, and evaporation. Direct uptake accounted for 70 to 80% of ET for high cover sites with water table depths of 1 to 3 m. The field results suggest that a general relationship may exist that relates the partitioning of plant uptake (ET) to depth to water table. Additional field results are necessary as well as simulations using the existing partitioning function to determine which approach more accurately models changes in soil water. The vadose zone model was revised during this project to take advantage of experimental data collected since it was developed. The stochastic model of reference ET was updated by incorporating an additional 10 years of data obtained from the California Irrigation Management Information System station in the Owens Valley, and the model code was revised to allow input of site specific estimates of Kc as well as empirical Kc and vegetation measurements. This added flexibility allows use of the best available ET estimates. Future model revisions will be to incorporate and test model performance with the functions developed from the results of the field investigation of the soil water balance partitioning.

TABLE OF CONTENTS

I. Introduction	1
II. Task 1: Groundwater model	3
Model Development	3
Introduction.....	3
Materials and Methods	5
Post-audit	5
Zonebudget	8
Evapotranspiration (ET) maps	9
ET depth function.....	21
Results and Discussion	22
Post-audit	22
ET maps	26
ET depth function.....	33
Conclusions	35
Field ET investigation.....	39
Introduction.....	39
Materials and Methods	40
Site selection.....	40
Eddy covariance instrumentation and theory	49
Quality control	53
Bowen ratio instruments and theory.....	54

Soil water and groundwater measurements	57
Vegetation measurements.....	58
Comparison of EC and of Kc estimates	58
Results and Discussion	63
Site characteristics.....	63
EC energy balance components and closure	78
Eddy covariance results.....	90
Comparison of EC and T_{Kc} results	96
Conclusions	107
III. Task 2: Vadose Zone model.....	108
Field investigation	108
Introduction.....	108
Materials and Methods	108
Site selection and instrumentation	108
Soil characterization.....	109
Soil Water Balance (SWB) and Partitioning	110
Results and Discussion.....	114
Soil Water Balance (SWB) and Partitioning	114
Conclusions	123
Vadose Zone KF model development/improvements	123
Introduction.....	123
Materials and Methods	125

Results and Discussion	125
CIMIS ETr model	125
Site-Scale Transpiration Coefficients.....	128
KW evaluation and model simulation.....	128
Conclusions	132
IV. Public Outreach and Technical Presentations	132
Presentations	133
V. References	134
VI. Summary of Costs and Disbursements	140
Appendix A: Daily eddy covariance, energy balance component, and transpiration model results.	141
Appendix B: Soil characterization data for EC sites.	214

LIST OF FIGURES

Figure 1. Area of Los Angeles owned lands mapped during vegetation inventory in 1984-87 and general vegetation classification into phreatophytic and nonphreatophytic types.....	10
Figure 2. Example of vegetation cover in the Owens Valley in 1984 measured with SMA analysis of Landsat data. The boundaries of the vegetation map correspond with the groundwater model domain.	16
Figure 3. (A) Histogram of T for all parcels with T_{poly} estimates. (B) Histogram of the fraction of T_{poly} contributed by species without assigned T_s values.....	27
Figure 4. Example of estimated ET for the Owens Valley in 1984 using SMA, transpiration coefficients, and LADWP vegetation inventory.....	28
Figure 5. Example of the time series of ET, depth to groundwater, and precipitation for one site instrumented with an eddy covariance tower.....	29
Figure 6. Map of daily ET for September 12, 2002 derived using SEBAL.....	31
Figure 7. Approximate contributing area upwind of an eddy-covariance stations in unstable conditions according to Gash (1986). Reasonable values were assumed for roughness height, stability, wind speed, and zero-plane displacement; z is instrument height and h is canopy height.....	40
Figure 8. Aerial photograph and measurement locations for ET, soil water, and LAI BLK100.	42
Figure 9. Aerial photograph and EC, soil water and LAI measurement locations at ET site BLK9.	43
Figure 10. Aerial photograph and EC, soil water and LAI measurement locations at ET site PLC045.....	44
Figure 11. Aerial photograph and EC, soil water and LAI measurement locations at ET site FSL138.....	45
Figure 12. Aerial photograph and EC, soil water and LAI measurement locations at ET site PLC018.....	46
Figure 13. Aerial photograph and EC, soil water and LAI measurement locations at ET site PLC074.....	47
Figure 14. Aerial photograph and EC, soil water and LAI measurement locations at ET site PLC185.....	48
Figure 15. Energy balance components measured at BLK100.	50
Figure 16. Latent heat flux from three collocated systems at BLK100.	55
Figure 17. Transpiration coefficients (Kc_{ij}) and fitted models for saltgrass (<i>Distichlis spicata</i>) and alkali sacaton (<i>Sporobolus airoides</i>).	60
Figure 18. Transpiration coefficients (Kc_{ij}) and fitted models for Nevada saltbush (<i>Atriplex lentiformis</i> ssp. <i>torreyi</i>), rabbitbrush (<i>Chrysothamnus nauseosus</i>) and greasewood (<i>Sarcobatus vermiculatus</i>).	61
Figure 19. Depth to water in two test well located near BLK100. Test well 850T is adjacent to the EC station; 454T is located south east of the site, adjacent to the LA Aqueduct.....	64
Figure 20. Depth to water in test well 586T located near BLK009.....	64

Figure 21. Depth to water in test well 485T located south of PLC045 and estimated DTW at PLC 045.	65
Figure 22. Depth to water in test well 746T located at FSL138.....	65
Figure 23. Depth to water in test well test well 12UT located at PLC074.	66
Figure 24. Soil water content 2 profiles for spring, summer, and fall conditions in four access tubes at BLK100 in 2000.....	68
Figure 25. Soil water content 2 profiles for spring, summer, and fall conditions in four access tubes at BLK100 in 2001.....	69
Figure 26. Soil water content 2 profiles for spring, summer, and fall conditions in four access tubes at BLK009 in 2001.....	70
Figure 27. Soil water content 2 profiles for spring, summer, and fall conditions in two access tubes at PLC045 in 2001.....	71
Figure 28. Soil water content 2 profiles for spring, summer, and fall conditions in four access tubes at BLK100 in 2002.....	72
Figure 29. Soil water content 2 profiles for spring, summer, and fall conditions in four access tubes at FSL138 in 2002.....	73
Figure 30. Soil water content 2 profiles for spring, summer, and fall conditions in two access tubes at PLC018 in 2002.....	74
Figure 31. Soil water content 2 profiles for spring, summer, and fall conditions in four access tubes at BLK074 in 2002.....	75
Figure 32. Soil water content 2 profiles for spring, summer, and fall conditions in three access tubes at PLC182 in 2002.....	76
Figure 33. LAI for all sites. Values are the average of four transects.	77
Figure 34. Plant cover of all species (fraction) for all sites. Values are the average of four transects.	77
Figure 35. Example of the energy balance closure error for EC system on half hourly basis at BLK 100 during the period of BR system operation.....	79
Figure 36. Wind speed at BLK 100 measured with eddy covariance and Bowen Ratio instruments in 2002.....	80
Figure 37. <i>EB</i> for BLK100 in 2000 and 2001.....	81
Figure 38. <i>EB</i> for BLK009 and BLK045 in 2001.....	81
Figure 39. <i>EB</i> for PLC018, PLC074 and BLK100 in 2002.....	82
Figure 40. <i>EB</i> for PLC185 and FSL138 in 2002.....	82
Figure 41. Daytime Bowen ratio (<i>H/IE</i>) at BLK100 measured with eddy covariance and Bowen Ratio instruments in 2002. Only daytime b are shown because for either system, nighttime b tended to be highly erratic due to the small magnitude and variable sign of <i>IE</i>	85
Figure 42. Latent heat flux at BLK 100 measured with eddy covariance and Bowen Ratio instruments in 2002. EC latent heat flux has been corrected using Equation 18.....	86
Figure 43. All uncorrected ET measured by EC systems.	88
Figure 44. All corrected ET measured by EC systems.	88
Figure 45. Half-hourly energy balance components measured at PLC185 (top graph) and BLK100 (bottom graph). Latent heat flux has been corrected for EB.....	89

Figure 46. ET at BLK100 in 2000 measured with the EC system and estimated using field measurements and transpiration coefficients (Equation 17). EC measurements corrected and uncorrected for energy balance closure error are presented.	92
Figure 47. ET at BLK100 in 2001 measured with the EC system and estimated using field measurements and transpiration coefficients (Equation 17). EC measurements corrected and uncorrected for energy balance closure error are presented.	92
Figure 48. ET at BLK009 in 2001 measured with the EC system and estimated using field measurements and transpiration coefficients (Equation 17). EC measurements corrected and uncorrected for energy balance closure error are presented.	93
Figure 49. ET at PLC045 in 2001 measured with the EC system and estimated using field measurements and transpiration coefficients (Equation 17). EC measurements corrected and uncorrected for energy balance closure error are presented.	93
Figure 50. ET at BLK100 in 2002 measured with the EC system and estimated using field measurements and transpiration coefficients (Equation 17). EC measurements corrected and uncorrected for energy balance closure error are presented.	94
Figure 51. ET at FSL138 in 2003 measured with the EC system and estimated using field measurements and transpiration coefficients (Equation 17). EC measurements corrected and uncorrected for energy balance closure error are presented.	94
Figure 52. ET at PLC018 in 2002 measured with the EC system and estimated using field measurements and transpiration coefficients (Equation 17). EC measurements corrected and uncorrected for energy balance closure error are presented.	95
Figure 53. ET at PLC074 in 2002 measured with the EC system and estimated using field measurements and transpiration coefficients (Equation 17). EC measurements corrected and uncorrected for energy balance closure error are presented.	95
Figure 54. ET at PLC185 in 2002 measured with the EC system and estimated using field measurements and transpiration coefficients (Equation 17). EC measurements corrected and uncorrected for energy balance closure error are presented.	96
Figure 55. Measured LAI for dominant species at BLK100 in 2000 and LAI model in the Kc model scaled to the LAI used to calculate T_{Kc} . LAI is the mean of the four transects.	99
Figure 56. Measured LAI for dominant species at BLK100 in 2001 and LAI model in the Kc model scaled to the LAI used to calculate T_{Kc} . LAI is the mean of the four transects.	100
Figure 57. Measured LAI for dominant species at BLK009 in 2001 and LAI model in the Kc model scaled to the LAI used to calculate T_{Kc} . LAI is the mean of the four transects.	101
Figure 58. Measured LAI for dominant species at PLC045 in 2001 and LAI model in the Kc model scaled to the LAI used to calculate T_{Kc} . LAI is the mean of the four transects.	102
Figure 59. Measured LAI for dominant species at BLK100 in 2002 and LAI model in the Kc model scaled to the LAI used to calculate T_{Kc} . LAI is the mean of the four transects.	103
Figure 60. Measured LAI for dominant species at PLC074 in 2002 and LAI model in the Kc model scaled to the LAI used to calculate T_{Kc} . LAI is the mean of the four	

transects.	104
Figure 61. Measured LAI for dominant species at PLC074 in 2002 and LAI model in the Kc model scaled to the LAI used to calculate T_{Kc} . LAI is the mean of the four transects.	105
Figure 62. Measured LAI for dominant species at PLC185 in 2002 and LAI model in the Kc model scaled to the LAI used to calculate T_{Kc} . LAI is the mean of the four transects.	105
Figure 63. Measured LAI for dominant species at FSL138 in 2002 and LAI model in the Kc model scaled to the LAI used to calculate T_{Kc} . LAI is the mean of the four transects.	106
Figure 64. Measured LAI for dominant species at PLC018 in 2002 and LAI model in the Kc model scaled to the LAI used to calculate T_{Kc} . LAI is the mean of the four transects.	106
Figure 65. Nighttime soil evaporation measured by EC method at BLK100. Note the strong seasonal trend. Lines represent model predictions based on water table depth (Equation 20).	112
Figure 66. Hydrograph for monitoring well 419T. The magnitude of the intra-annual fluctuations do not correspond with pumping 1991 to 2003 and increase when the water is near the root zone (2m).water table to well below the root zone (approximately 2 m).	115
Figure 67. Diurnal fluctuations in water table depth (WTD) near EC station in BLK100 (well 850T). Notice a reduction in drawdown rate (smaller slope) during nighttime. $ET(EC)=ET_{corr}$	117
Figure 68. Diurnal fluctuations in water table depth (WTD) near EC station in PLC074 (well 012UT). Notice a reduction in drawdown rate (smaller slope) during nighttime. $ET(EC)=ET_{corr}$	117
Figure 69. Soil water characteristic for BLK100 soil measured in the lab (and fitted model) and inferred from measured water content vs. height above the water table during April of 2000, 2001, and 2002.	119
Figure 70. Fraction of ET supplied by direct uptake from the water table as a function of DTW at the beginning of the growing season. DTW values for PLC018 is an estimate and could be deeper (i.e. >4.8m). DTW for PLC185 was determined at the time of access tube installation.	121
Figure 71. T_{gw} scaled by maximum LAI as a function of DTW. DTW values for PLC018 is an estimate and could be deeper (i.e. >4.8m). DTW for PLC185 was determined at the time of access tube installation.	122
Figure 72: Mean daily ETr and its standard deviation (STD) estimated by the modified Penman equation from climatic data collected at Bishop, California (CIMIS, 2002, station #35).	126
Figure 73. Site-scale Kc data, average, and fitted Fourier model for BLK100. Fourier model coefficients: A(1) -0.20, B(1)-0.064, A(2) and B(2) 0.0; $r^2 = 0.91$	129
Figure 74. Changes in relative water table depth (DTW/RTD, where $RTD_{max}=2500$ mm) in BLK100 during 2001. KW was based on the power function with $b=3$, and the site Kc adjusted by the water table contribution as reflected by KW [calculated as:	

adjusted $KC = (1-KW)*Kc(EC)$. The area between the Kc curves reflects the contribution of direct uptake from water table to site ET_{corr}	130
Figure 75. Measured and modeled changes in S at BLK100 for 2000-2002 using the revised water table uptake expression.	131

LIST OF TABLES

Table 1. Vegetation plant communities and miscellaneous land classes mapped in the Owens Valley during 1984-87.....	11
Table 2. Values and source of annual T_a assigned to species. The values have been normalized to 100% cover to facilitate calculations.....	13
Table 3. Post-audit scenarios.....	23
Table 4. ET calculated by SEBAL remote sensing algorithm and measured. EC ET is eddy covariance ET corrected for energy imbalance for September 12, 2002.....	32
Table 5. Correlation (r) matrix for winter precipitation (October 1 to April 1) measured at seven stations maintained by LADWP in the Owens Valley for 1986-2001.....	34
Table 6. Eddy covariance site characteristics. Range of depth to water during the growing season is given. Precipitation values are annual totals beginning October 1 the previous year. Except for PLC45, April to October rain was less than 15mm.....	41
Table 7. Dates of EC station operation.....	49
Table 8. Statistics of ET tower comparison at BLK100, alkali meadow site in 2000.....	54
Table 9. Day of year for maximum LAI in the Kc models, the LAI sampling DOY used to determine T_{Kc} , and DOY of actual measured maximum LAI for the dominant species at each site.....	62
Table 10. ET_{corr} Fourier model coefficients and r^2 for each site-year.....	91
Table 11: Eddy covariance ET corrected for energy balance closure and T estimated from Kc models and measured LAI and ETr_i . Vegetation measurements taken nearest the date of maximum LAI for the dominant species in Kc models were used (Table 9). Measured and predicted fluxes are the sum of daily totals for the period with available corrected eddy covariance measurements and integrated for the entire growing season using the fitted Fourier model (March 25-October 15).....	97
Table 12: Soil water balance components and calculation of T_{gw} for EC sites. The values represent growing season totals (March 25 to October 15.....	114
Table 13. Measured diurnal changes in water table depths, daily ET (eddy covariance method), and estimated specific yield for BLK 100 during summer of 2003 (Specific yield is estimated assuming ET was a result of uptake from water table only).....	118
Table 14. Estimated model parameters for standardized mean daily ETr series for 1983-2001 in Bishop, California. Data are from CIMIS Station #35).....	127

I. Introduction

The Owens Valley is a long, narrow valley on the eastern slope of the Sierra Nevada in Inyo County, California. It is a closed basin drained by the Owens River which terminates at saline Owens Lake. Although the climate of the valley floor is arid (mean precipitation of 10 to 15 cm), snowmelt runoff from the Sierra Nevada creates a shallow water table that supports approximately 70,000 acres of native phreatophytic shrubs and grasses and riparian areas. Since the early 1900's, the water resources of the Owens Valley have been managed by the Los Angeles Department of Water and Power (LADWP) as the primary water supply for the city. Nearly the entire floor of the valley is owned by Los Angeles and most is leased for grazing and irrigated agriculture. The Owens River and small creeks emanating from the Sierra Nevada are diverted into the Los Angeles Aqueduct below Tinemaha Reservoir and delivered to Los Angeles. In addition to surface water sources, Los Angeles has constructed approximately 95 groundwater wells to supply local water uses and for export.

In 1991, the County of Inyo and the City of Los Angeles and its Department of Water and Power adopted a Long Term Groundwater Management Plan (Plan) to settle two decades of litigation over the effects of Los Angeles' export of groundwater from the Owens Valley. The Plan requires management of groundwater and surface water in the Owens Valley to avoid adverse changes to phreatophytic vegetation while continuing to supply water to Los Angeles. The technical information required for implementation of the Plan is based upon vadose zone water and vegetation monitored at permanent monitoring sites located in wellfield areas throughout the Owens Valley. Each monitoring site is linked to nearby pumping wells.

Predicted transpiration values derived from vegetation measurements are compared to the plant-available water stored in the vadose zone. If available water at a site is insufficient to meet the projected vegetation water demand, pumping from the wells linked to the site is halted to allow water table recovery to replenish the water stored in the vadose zone. Pumping can only resume when the vadose zone water is restored to levels sufficient to meet plant requirements when the wells were turned off. This monitoring and management program was implemented to minimize excessive lowering of the water table below plant root zones that would result in extended periods of water stress and decline in vegetation cover.

In addition to permanent monitoring sites, vegetation response to pumping is monitored at other locations throughout the Valley. Selected areas encompassing approximately 8000 acres inside and outside wellfields are annually resampled to compare with the Plan's baseline vegetation conditions based on conditions mapped in 1984-1987. Further, depth to groundwater is regularly monitored by the County and LADWP at approximately 800 piezometers. These data are used to prepare depth to groundwater maps in areas of groundwater-dependant vegetation. The vegetation and groundwater results are integrated into a geographic information system to track whether the vegetation protection goals of the Agreement are being met and are used to develop and review the annual pumping programs proposed by LADWP.

Monitoring and management provisions of the Plan were initiated during 1989. In 1987 and 1988, high amounts of groundwater pumping (more than 200,000 acre feet/year) lowered the water table below the plant root zone under many areas of the valley. Under the Plan, groundwater pumping was greatly reduced in the fall of 1989, but vegetation had already declined below the Plan's baseline conditions in many areas. From 1989 to the present, the

LADWP and the County have agreed to promote water table recovery by reducing annual groundwater pumping below the amount allowed under the original provisions of the Plan. Since 1990, in some areas of the valley groundwater levels and cover of perennial vegetation have recovered to pre-drought levels, but some areas of wellfields have not fully recovered.

Water table and vegetation decline observed during the 1980s and research conducted during the last decade have demonstrated the need to evaluate the effectiveness of existing monitoring and management procedures and to improve prediction tools to evaluate the potential effects of proposed groundwater pumping (Steinwand, 2000a and b; Steinwand and Harrington, 2003). Since its inception, the Plan explicitly recognized the need for ongoing scientific investigations to better achieve its goals.

The purpose of this project was to improve existing groundwater and vadose zone groundwater models that can be used to evaluate the impact of groundwater pumping on groundwater levels and water availability for native vegetation. Field data collected as part of this project and available information collected since the original development of the models will be applied in conjunction with model revisions to accomplish this task.

II. Task 1: Groundwater model

This task consisted of two subtasks, groundwater model development and field investigation of evapotranspiration using micrometeorological methods.

Model Development

Introduction

Research examining the relationship between groundwater pumping and environmental

change was conducted in the 1980's by Inyo County and LADWP with assistance from the U.S. Geological Survey and others. From that effort, the USGS produced a basin-wide MODFLOW application which spanned the period 1963-1988 (Danskin, 1998). This model will be the starting point for further development of numerical groundwater modeling tools in this project.

Numerical models are well suited to exploring hypothetical scenarios because they are based on approximate representations of the physical principles of groundwater flow, and they can generate a spatially complete hydrologic prediction to provide a regional picture of hydrologic response to imposed conditions. Numerical models are time consuming and expensive to calibrate requiring much information to characterize the system, and the uncertainty in model predictions is hard to quantify. The extensive data on the hydrologic, geologic, and vegetation in the Owens Valley, however, make numerical models a particularly attractive method to apply to improve groundwater management (Danskin, 1998; Hollett et al., 1991).

The purpose of this task was to develop numerical groundwater models for critical areas of the Owens Valley that can be used to evaluate the impact of groundwater pumping, climatic variations, surface water management, and other hydrologic changes on groundwater levels. Components of this task contained in the original proposal included a post-audit of the Danskin (1998) model, application of the MODFLOW zonebudget package to develop finer grid models, and development of alternative methods to determine ET, which is the upper boundary condition of the model domain. Under this grant, the model was updated through 2002 and has the capability of simulating future scenarios through 2020, an arrangement which serves to both test the performance of the model in simulating the period 1989-2002, and provide Inyo County and LADWP a tool with which to evaluate future scenarios.

Materials and Methods

Post-audit

Danskin (1998) calibrated his model for steady state conditions using data from 1963 and for transient conditions using data from 1963-1984. Subsequently, Inyo and Los Angeles have collected an extensive database of groundwater levels, pumping, and environmental conditions to test the original calibrated model. A post-audit was completed to evaluate the performance of the model and to develop model input and output for the period subsequent to the calibration/validation period. The post audit included a simulation of observed conditions and an evaluation of the management alternatives presented in Danskin (1998).

The methodology used for the post-audit was to mimic as much as possible the data sets and approach used during the original development of the model. Inyo County and LADWP developed the data sets for the post-audit period (1989-2002) based on descriptions in WSP2370-H and discussions with Wes Danskin, the developer of the original model and consultant retained for the present work. For the purpose of post-auditing, no changes were made to the hydrostratigraphic framework or numerical discretization of the model. The model continued to use annual stress periods, and it models water-years 1963 through 2002. Future scenarios with differing management alternatives were simulated for transient conditions through water year 2020. Transient-mode simulations appeared to be more illustrative of the groundwater system than the steady-state model scenarios used in WSP2370-H. Additionally, the groundwater model code was modified with additional packages so that each specified flux (e.g. discharge from pumped wells, underflow, recharge from tributary streams, etc.) was simulated as a discrete item. The preprocessor modifications allowed for a more direct accounting of the MODFLOW water

budget, but did not affect simulated results. The modeling was done on a UNIX computer system using MODFLOW-88. Much of the actual preparation of the data sets was done using Excel and Emacs, with some manual entry.

The same pre-processing and post-processing programs were used for the original calibration and the post-audit with minor changes for size of arrays and length of simulation. The philosophy from the calibration period of using percent annual runoff as an index of recharge from tributary streams, ungaged runoff, and canals was retained. There remains a lingering question whether the percentages reflect the same historical base period, but this discrepancy would only alter the percent annual runoff by a percent or two. All categories of fluxes were maintained as before except for pumped and flowing wells. The data requirements and preprocessor modifications required for each water budget component are discussed below.

Stream recharge. Additional data required for the stream recharge component were the percent of normal runoff for the post-audit period, which were obtained from LADWP's Totals and Means records.

Agriculture recharge. Additional data required for the agricultural recharge component were the percent of normal runoff for the post-audit period, which were obtained from LADWP's Totals and Means records.

Evapotranspiration. The evapotranspiration component was treated as constant in the original model, therefore no changes were necessary to apply this concept to the post-audit period.

Canal recharge. Additional data required for the canal recharge component were the percent of normal recharge for the post-audit period and the years for which the Geiger and

Collins canals were operated, which were determined from LADWP's Totals and Means records.

Groundwater recharge. Additional data required for the groundwater recharge component were uses and losses for the Laws, Bishop, Big Pine, and Lone Pine areas, and overhead and spillgate releases for the Blackrock-Thibaut, and Lone Pine areas, which were obtained from LADWP's Totals and Means records. Some data for 1989-1992 were estimated because the records in Totals and Means only extended back to 1993. Typically this was done by taking the average of the 1993-2000 record.

Groundwater pumping. The post-audit included a philosophy of separating pumped and flowing well discharge, which was done for water years 1971 through 2002. The pre-processing program for pumpage was modified in minor ways to separate pumped and flowing well discharge. A few pumped wells put into service after the original calibration period (water year 1988) were added to the post-audit. Additional data required for the groundwater pumping component was obtained from LADWP pumping records. Locations and screened intervals for wells constructed since the completion of the original model were obtained from site visits and well construction diagrams. The groundwater pumping preprocessor was modified to accommodate the additional time spanned by the post-audit period.

Underflow. The underflow component was constant in the original model, so no changes were necessary.

Ungaged recharge. Additional data required for the ungaged recharge component were the percent of normal runoff for the post-audit period, which were obtained from LADWP's Totals and Means records. The ungaged recharge preprocessor was modified to accommodate the additional time spanned by the post-audit period.

To ensure that the post-audit was the same model that was used during calibration, fluxes from the post-audit simulation were compared with those published in Table 11 in WSP2370-H. Differences were always less than 0.5% (often less than 0.1%) and were attributable to round-off error.

The post-audit evaluation of model performance was based on visual comparison of simulated and measured hydrographs and a review of the model water budget, which were the same criteria used during the original development of the model. The post-processing program that generated hydrographs, published as Plate 3 in WSP2370-H, was used with more recently measured groundwater levels. No new wells were evaluated as part of the post-audit, mostly to achieve the dual goal of expediency and symmetry with the original calibration. Groundwater fluxes were evaluated on a valley-wide basis to insure that the fluxes were reasonable. No other critique of fluxes was done, including any comparison with measured spring flow or estimated evapotranspiration.

No direct comparison between the post-audit results and the specific scenarios described in WSP2370-H was done, choosing instead to focus first on incorporating historical data through water-year 2002 and general projections through 2020. A post-audit comparison of prior scenarios would be possible and might be illustrative considering the differences that occurred after 1988. The main difference between the earlier scenarios and the actual data was a decrease in pumpage, which resulted in less decline in groundwater levels than was suggested might occur.

Zonebudget

The purpose of this effort was to subdivide the regional flow model into wellfield-sized

individual models. The water balance for each smaller model would be derived from the regional model using the Zonebudget MODFLOW package. This work was slated to be performed after completion of the post-audit. Unfortunately, time to complete the post-audit spanned the time-frame of the project, and this task was not completed or funded by this grant.

Evapotranspiration (ET) maps

The MODFLOW groundwater model of Danskin (1998) applied a constant maximum ET rate at each cell to determine the upper boundary condition of the model domain. Spatial models of ET based on vegetation conditions and remote sensing techniques were developed for the Owens Valley to be linked to the MODFLOW application using a GIS. A time series of ET for the post-audit period was developed from existing remotely sensed thematic maps of vegetation cover (Elmore et al., 2000) and transpiration coefficients (Steinwand, 1999b; Steinwand et al., 2001). Additionally, satellite data were analyzed using an analytic model (SEBAL) to prepare an instantaneous estimate of spatial ET for the valley to test the applicability of this remote sensing method for use in the groundwater model.

Vegetation-based ET map. This method to estimate ET combined measures of vegetation cover with estimates of the transpiration (T) rate per unit of vegetation. It assumes that the primary contributor to ET is transpiration. This assumption was tested during the development of the vadose zone model (see Section III below)

The spatially distributed data consisted of a vegetation community map which included measurements of the species composition and cover for most polygons (Figure 1). The dominant vegetation of Los Angeles-owned land in the Owens Valley was inventoried and mapped by

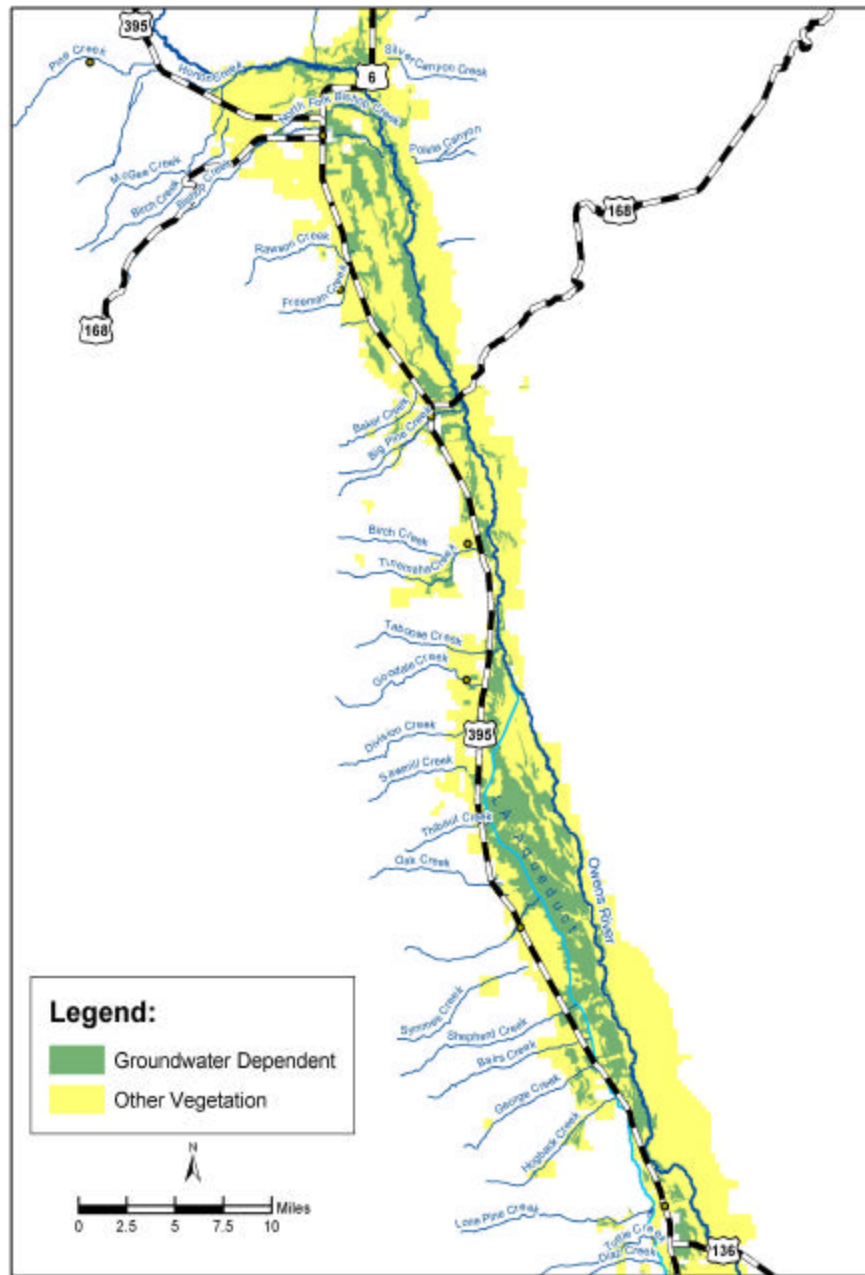


Figure 1. Area of Los Angeles owned lands mapped during vegetation inventory in 1984-87 and general vegetation classification into phreatophytic and nonphreatophytic types.

Table 1. Vegetation plant communities and miscellaneous land classes mapped in the Owens Valley during 1984-87.

Code Number	Community
14000	Barren Lands
34100	Mojave Creosote Bush Scrub
34210	Mojave Mixed Woody Scrub
34300	Blackbrush Scrub
35100	Great Basin Mixed Scrub
35210	Big Sagebrush Scrub
36110	Desert Saltbush Scrub
36120	Desert Sink Scrub
36130	Desert Greasewood Scrub
36140	Shadscale Scrub
46000	Alkali Playa
35400	Rabbitbrush Scrub
36150	Nevada Saltbush Scrub
45310	Alkali Meadow
45320	Alkali Seep
45340	Rabbitbrush Meadow
45350	Nevada Saltbush Meadow
52320	Transmontane Alkali Marsh
61610	Great Basin Riparian Forest
61700	Mojave Riparian Forest
63600	Great Basin Riparian Scrub
63810	Tamarisk Scrub
11000	Irrigate Agriculture
13100	Permanent Lakes/Reservoirs
13200	Intermittent Ponds
45330	Rush/Sedge Meadow
45500	Non-native Meadow
76100	Black Locust Woodland

LADWP between 1984 and 1987. Vegetation map polygons were delineated into visually contiguous assemblages of plants with relatively similar cover and composition. Historic and current land-use maps also were consulted to delineate non-native or miscellaneous land cover classes (e.g. agriculture and urban lands). Color aerial photographs (scale 1:12,000) taken in

July 1981 were used as the basemap. Ultimately, the polygons were transferred to USGS 7.5' quadrangle maps. Black-and-white air photo prints from 1944 (1:24,000) and 1968 (1:12,000) were also used to verify abandoned agriculture. Field sampling was conducted on most parcels to adjust the parcel boundaries if necessary and to quantify vegetation cover and composition using the line-point method (Kuchler, 1967). Vegetation cover was defined as the crown cover of all live plants in relation to the ground surface. Species composition is synonymous with relative cover and was expressed as a percent of the total live cover. A minimum of five transects were run on each sampled parcel, but if the vegetation cover was particularly heterogeneous, up to twelve transects were run. Vegetation cover and percent composition of up to twelve dominant species were entered into a computer database. Polygons were classified according to (Cheatham and Haller, 1975), as revised to plant community descriptions (Holland, 1986). This system was further refined for the Owens Valley by adding six additional plant communities, non-native vegetation, and miscellaneous lands categories (Table 1). The classification system used is primarily floristic; hence, parcels with similar species composition were grouped together.

The annual T rate (T_{poly}) for each vegetation polygon was computed by

$$T_{poly} = C_p \sum_{s=1}^q T_s f_s \quad (1)$$

where f_s is the fraction (by cover) of species s and C_p is the average vegetation cover for the polygon. T_s is the annual transpiration for a species normalized to 100% cover assuming sufficient soil water/water table conditions. T_s was either determined from the literature or from transpiration coefficients developed previously for the five most prevalent species using,

Table 2. Values and source of annual T_a assigned to species. The values have been normalized to 100% cover to facilitate calculations.

Species	Abbreviation	T_s (cm/yr)	Source
<i>Artemisia tridentata</i>	ARTRT	35.5	Steinwand (1998); Branson et al. (1976)
<i>Atriplex confertifolia</i>	ATCO	59.1	Steinwand (1998); Branson et al. (1976)
<i>Atriplex lentiformis</i> ssp. <i>torreyi</i>	ATTO	102.9	Steinwand et al. (2001) and this report
<i>Krascheninnikovia lanata</i>	CELA	31.7	Steinwand (1998); Branson et al. (1976)
<i>Chrysothamnus nauseosus</i>	CHNA2	224.9	Steinwand et al. (2001) and this report
<i>Chrysothamnus viscidiflorus</i>	CHVI8	177.5	Miller (1988)
<i>Distichlis spicata</i>	DISP2	90.3	Steinwand (1999b) and this report
<i>Grayia spinosa</i>	GRSP	33.3	Steinwand (1998); Branson et al. (1976)
<i>Juncus balticus</i>	JUBA	75.5	Miller et al. (1982)
	LAKES	170.2	Lee (1912)
<i>Populus fremontii</i>	POFR3	191.0	Blaney (1954) and references therein
	PONDS	170.2	Lee (1912)
<i>Rosa woodsii</i>	ROWO	48.9	Robinson (1970)
<i>Salix gooddingii</i>	SAGOV	115.6	Robinson (1970)
<i>Salsola tragus</i>	SAKAT	52.0	Schillinger and Young (2000)
<i>Salix</i> sp.	SALIX	115.6	Robinson (1970)
<i>Sarcobatus vermiculatus</i>	SAVE4	192.5	Steinwand et al. (2001) and this report
<i>Sporobolus airoides</i>	SPAI	92.0	Steinwand (1999b) and this report
<i>Tamarix ramosissima</i>	TARA	92.0	Gay and Fritschen (1979); Ball et al. (1994)
<i>Tetradymia axillaris</i>	TEAX	56.0	Steinwand (1998); Branson et al. (1976)
<i>Typha latifolia</i>	TYLA	112.0	Blaney (1954) and references therein
<i>Typha</i> sp.	TYPHA	112.0	Blaney (1954) and references therein

$$T_s = \sum_{j=1}^n \sum_{i=1}^m Kc_{ij} ETr_j \quad (2)$$

where ETr_j is the reference evapotranspiration for day j , and Kc_{ij} is the transpiration coefficient for species i on day j normalized to 100% cover (Table 2). Normalization to 100% cover in Equations 1 and 2 was simply for convenience in performing calculations utilizing the fraction of live cover. Transpiration coefficients are a dimensionless ratio of actual ET (in this case T) to a

reference or potential ET typically determined over an irrigated grass or alfalfa reference crop (Allen et al., 1998). Coefficients for the five most common phreatophytic species were developed from an extensive database of stomatal conductance, ET_r , and LAI measurements collected by LADWP, USGS, and Inyo County in the Owens Valley (Steinwand, 1999a and b; Steinwand et al., 2001). ET_{r_j} was derived from the California Irrigation Management Information System at Bishop, California by averaging the reference ET for several years. Cover of species without T_s values were assigned the weighted average T_s of the known species. The contribution of this subjective procedure affects the level of confidence in the T_{poly} estimate, and therefore, it was quantified separately for each polygon. For polygons where greater than 20% of the T_{poly} was due to species for which T_s was not available, the mean T_{poly} of polygons belonging to the same Holland class with less than 20% of T_{poly} attributable to unquantified species was assigned.

Several sources were used to assemble T_s values for common Owens Valley species. Ideally, T_s of all species would be known from measurements taken locally, but few species have been evaluated by local studies. Values of T_s from published studies on several species were used to increase the number of species with assigned T_s . The primary limitations to extracting values from other studies were the variable methods to measure plant cover and T. Sometimes only ET was measured, in which case only measurements where E could be reasonably assumed to be minimal were used. The alternative of relying solely on Kc models derived in the Owens Valley would reduce the number of parcel datasets amenable to derive T_{poly} . Also, T_s for some species reasonably can be assumed to be smaller than the dominant phreatophytic species, and without assigned T_s derived from the literature, these would be ignored or as in this project

assigned the weighted average T_s of phreatophytes.

To develop the ET time series for the years following the initial vegetation mapping, plant cover was estimated from satellite imagery using spectral mixture modeling, where the spectra for each pixel is modeled as a linear combination of bare soil, shadow, and vegetation end members (Elmore et al., 2000). LandSat Thematic Mapper images in late summer or early fall (preferably September) were obtained from 1984 to 2001. Late summer scenes were chosen to minimize the influence of varying phenology and leaf cover of spring annuals on estimates of vegetation abundance. The data sets were coregistered, spectrally calibrated to temporally invariant features, and georeferenced. The LandSat data were processed using the SMA model to estimate percent live plant cover for each pixel (28.5m X 28.5m). The estimates are considered accurate to $\pm 4.0\%$ live cover. All mixture modeling was performed by Brown University as part of a previous study, and the results in GIS format were provided to Inyo County. Full details of the SMA model are given in Elmore et al. (2000).

Assuming temporal variation in T is largely due to changes in cover that reflect changes in water availability (Nichols, 2000), T_{poly} for polygons calculated from the initial vegetation map were adjusted each year based on average remotely-sensed cover (Figure 2). Manning et al. (1999) compared the SMA time series estimates of vegetation cover for the period 1991-1997 with cover measurements determined using field methods similar to those in the original vegetation mapping. SMA cover agreed with field sampling approximately for one third of the 98 polygons examined, but the two methods gave the same measures of cover or were systematically offset (i.e. parallel time series) for 69 of the polygons. Because temporal trends of remotely-sensed cover were more reliable than the magnitude, disagreement between field-

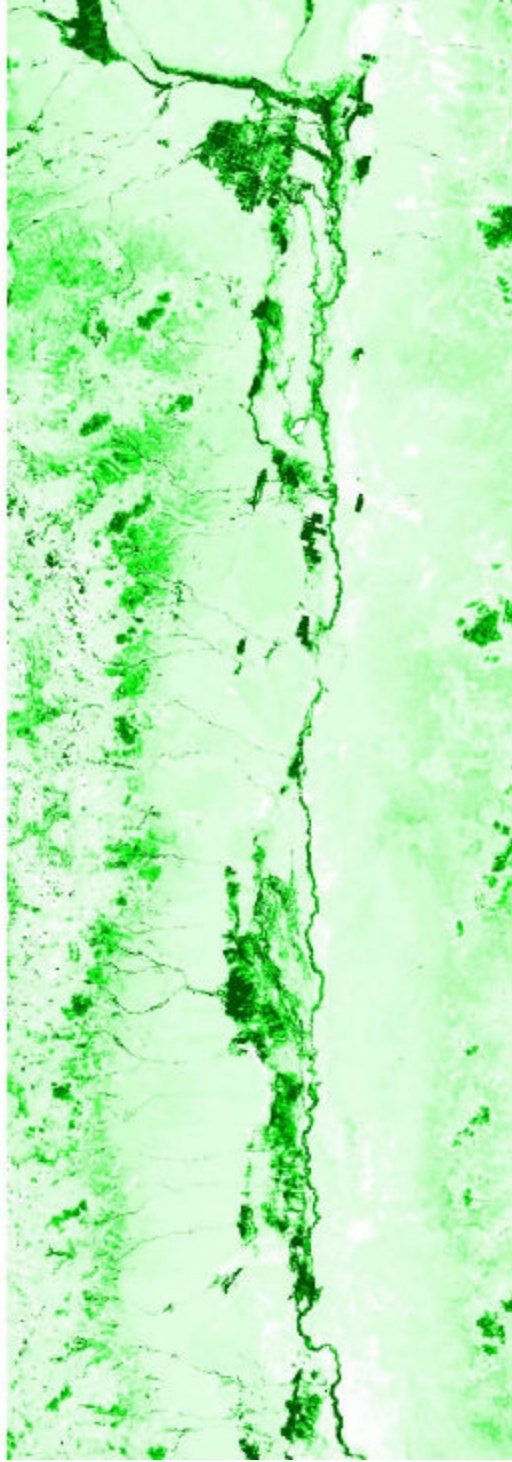


Figure 2. Example of vegetation cover in the Owens Valley in 1984 measured with SMA analysis of Landsat data. The boundaries of the vegetation map correspond with the groundwater model domain.

mapped and remotely-sensed vegetation cover was resolved by normalizing the results by the ratio of mapped cover with remotely-sensed cover of the years when the polygons were mapped. T_{poly} for each polygon for each year was then averaged over each MODFLOW cell to obtain the maximum transpiration rate for each cell.

Remote sensing ET map. The Surface Energy Balance Algorithm for Land (SEBAL) is a physically-based algorithm to estimate ET by solving the surface energy balance on an instantaneous time scale for every pixel of a satellite image (Bastiaanssen et al. 1998a,b, 2002; Bastiaanssen 2000). The method is based on the computation of surface albedo, surface temperature, and vegetation index from multispectral satellite data. For this project, one Landsat Thematic Mapper image for September 12, 2002 was provided by Brown University for analysis conducted by Jan Hendrickx of New Mexico Technical Institute. The SEBAL results were compared with the results of the field measurements of ET using the eddy covariance stations. Although developed recently, the SEBAL algorithm has been applied for water balance estimations (e.g. Pelgrum and Bastiaanssen 1996), irrigation performance assessment studies (e.g. Roerink et al. 1997), and in weather prediction studies (e.g. Van de Hurk et al. 1997). The technique is not commonplace, and this analysis was not contemplated in the original proposal. Therefore, the theoretical development of method is described below. SEBAL evaluates the components of the energy balance and determines the ET rate as the residual,

$$R_n - G - H = IE \quad (3)$$

where R_n is the net incoming radiation flux density (W m^{-2}), G is the ground heat flux density (W m^{-2}), H is the sensible heat flux density (W m^{-2}), and IE is the latent heat flux density (W m^{-2})

or ET rate. The parameter λ is the latent heat of vaporization of water (J kg^{-1}) and E is the vapor flux density ($\text{kg m}^{-2} \text{s}^{-1}$).

The primary challenge to implement this approach was to partition the available energy ($R_n - G$) into λE and H . R_n was estimated from the surface albedo spatial variability (calculated from Thematic Mapper bands 1-5 and 7), surface temperature (from Thematic Mapper band 6), and solar radiation calculated from standard astronomical formulae (Iqbal, 1983). The ground heat flux G is determined through semi-empirical relationships with R_n , surface albedo, surface temperature, and Normalized Difference Vegetation Index (NDVI) calculated from Thematic Mapper bands 3 and 4 (Bastiaanssen 2000; Bastiaanssen et al. 1998a, b, 2002). The most complicated factor to solve for is H ,

$$H = \rho_a c_p \frac{T_{aero} - T_a}{r_{ah}} \quad (4)$$

where ρ_a is the density of air (kg m^{-3}), c_p is the specific heat of air ($\text{J kg}^{-1} \text{K}^{-1}$), r_{ah} is the aerodynamic resistance to heat transfer (s m^{-1}), T_{aero} is the surface aerodynamic temperature, and T_a is the air temperature either measured at a standard screen height or the potential temperature in the mixed layer (Brutsaert et al., 1993). The aerodynamic resistance to heat transfer is affected by wind speed, atmospheric stability, and surface roughness (Brutsaert, 1982). The simplicity of Equation 4 is quite deceptive since T_{aero} cannot be measured by remote sensing. Remote sensing techniques measure the radiometric surface temperature T_{rad} which is not the same as the aerodynamic temperature. The two temperatures usually differ by 1 to 5 °C. Unfortunately, an uncertainty of 1 °C in $T_{aero} - T_a$ can result in a 50 W m^{-2} uncertainty in H

(Campbell and Norman, 1998) which could be approximately equivalent to 1 mm per day of ET. Although many investigators have tried to solve this problem by adjusting r_{ah} or using an additional resistance term, no generally applicable method has been developed yet (Kustas and Norman, 1996).

SEBAL overcomes the problem of inferring the aerodynamic temperature from the radiometric temperature and the need for near-surface air temperature measurements by directly estimating the temperature difference between T_1 and T_2 taken at two arbitrary levels z_1 and z_2 without explicitly deriving the absolute temperature. The temperature difference for a dry surface without evaporation is obtained from the inversion of the sensible heat transfer equation with latent heat flux $\lambda E=0$ so that $H=R_n-G$ (Bastiaanssen et al., 1998a, 2002),

$$T_1 - T_2 = \Delta T_a = \frac{H r_{ah}}{r_a c_p} \quad (5)$$

For a wet surface all available energy R_n-G is used for evaporation (λE) so that $H=0$ and $\Delta T_a=0$. Field observations have indicated that land surfaces with a high ΔT_a are associated with high radiometric temperatures and those with a low ΔT_a with low radiometric temperatures (e.g. moist irrigated fields have a much lower ΔT_a than dry rangelands). The two unknowns in Equation 5, ΔT_a and the aerodynamic resistance to heat transfer r_{ah} , are affected by wind speed, atmospheric stability, and surface roughness (Brutsaert, 1982). For heterogeneous landscapes a wind speed near the ground surface is required for each pixel. Wind speed is not affected by local surface heterogeneities at a height of 200 m above ground level and is obtained by an upward extrapolation of a wind speed measurement at 2 or 10 m to 200 m using a logarithmic wind

profile. The wind speed at each pixel is obtained by a downward extrapolation using the surface roughness, which is determined for each pixel using an empirical relationship between surface momentum roughness z_{om} , Normalized Difference Vegetation Index (NDVI), and the surface albedo α ,

$$z_{om} = \exp[(a \times NDVI / \alpha) + b] \quad (6)$$

where a and b are correlation regression coefficients derived from a plot of $\ln(z_{om})$ versus $NDVI/\alpha$ for two or more sample pixels representing specific vegetation types. The end result of all these calculations is the determination of a r_{ah} and ΔT_a for each pixel. Field measurements by several authors (Bastiaanssen et al., 1998b; Wang et al., 1998; Frank and Beven, 1997; and Farah, 2001) have shown that the relationship between T_{rad} and ΔT_a is linear,

$$\Delta T_a = c_1 T_{rad} - c_2 \quad (7)$$

where c_1 and c_2 are the linear regression coefficients valid for one particular moment (the time and date the image is taken) and landscape. By using the minimum and maximum values of ΔT_a as calculated for the coldest and warmest pixel(s), the extremes of H are used to find the regression coefficient c_1 and c_2 to prevent outliers of H -fluxes. The internal auto-calibration process of SEBAL (Equation 7) eliminates the need for actual measurements of T_{rad} and/or ΔT_a as well as for atmospheric corrections. Thus, the surface temperature T_{rad} is used as a distribution parameter to partition of the sensible and latent heat fluxes. ΔT_a varies above the land surface as it is indexed to T_{rad} , but it does not require actual measurements on the ground or atmospheric corrections. This new approach has only recently been validated (Bastiaanssen et al., 1998a,b; Bastiaanssen, 2000). SEBAL results are most sensitive for the selection of the cold and warm

pixel which determine the outcome of the auto-calibration process. SEBAL is rather insensitive for errors in parameters as NDVI and atmospheric disturbances (Hendrickx et al., 2002).

ET depth function

In the original groundwater model, ET was varied temporally according to a linear function relating maximum ET to depth to groundwater. In the model, maximum ET (the valley-wide average ET) occurred when DTW was at the surface, and it decreased linearly to zero at a depth of 4.5 m. A potentially more robust relationship was developed by deriving an empirical relationship using multiple linear regression and an extensive dataset of depth to water, precipitation, and vegetation cover (to estimate ET) collected during routine monitoring by Inyo County and LADWP. As part of the Plan, Inyo County and Los Angeles established 33 permanent vegetation monitoring transects between 1987 and 1989; 22 are located in wellfield areas, 8 are control sites. Most sites are adjacent to an LADWP monitoring well. Depth to water was measured each month, and vegetation cover and composition were measured using point frame methods (Goodall, 1952; Groeneveld, 1997) each year in late June or early July. Precipitation on the valley floor was measured at seven locations by LADWP.

The multiple linear regression models were based on an annual time step to predict midsummer vegetation cover as a function of vegetation cover the preceding year, DTW at the beginning of the growing season (generally the shallowest water table), and valley-wide average precipitation the preceding winter. In the Owens Valley, winter precipitation predominates; usually summer rain is sparse. The annual time step of the regression models was selected to conform with the groundwater model time step.

Results and Discussion

Post-audit

Five scenarios were tested with the updated model. The scenarios were designed to test the new data-sets and to demonstrate the sensitivity of the model to runoff, groundwater pumpage, and recharge. They were not designed to illustrate a specific management plan. The simulation period was a combination of the historical period (1963-1988), the post-audit period (1989-2002), and future conditions (2003-2020). For each scenario and time period, descriptions of three flux components, percent runoff, pumpage, and groundwater recharge are summarized in Table 3.

Scenario 1. Average runoff, zero pumping. The primary goal of this scenario was to view the effect of average runoff without pumping. Can the model reasonably simulate this condition or will it become numerically unstable? This scenario in some respects represents the unmanaged system, though it includes some groundwater recharge resulting from water management activities. One of the purposes of Scenario 1 is to demonstrate that the model can simulate a high, stable water table, unaffected by pumping after 1988. Another purpose was to critique the separation of pumpage into discharge from pumped well and discharge from flowing wells.

The results of this simulation met these goals reasonably well, and also demonstrate the significant effect pumping has on the system. The results also confirm that the response time of the basin is on the order of 5 to 10 years – the time necessary for a significant change in recharge or discharge to equilibrate throughout the system. A comparison of the pumpage data from the original data sets and the newly acquired data set for 1972-88 shows that there are differences. It

Table 3. Post-audit scenarios.

Scenario 1. Average runoff, zero pumping.			
Period	% Runoff	Pumpage	Groundwater recharge
1963-1988	original model	original model	original model
1989-2002	100% of long-term average	0%	same as WSP 2370-H projection (mean of 1985, 1986, 1988)
2003-2020	100% of long-term average	0%	same as WSP 2370-H projection (mean of 1985, 1986, 1988)
Scenario 2. Historical runoff, zero pumping.			
Period	% Runoff	Pumpage	Groundwater recharge
1963-1988	original model	same as scenario 1	original model
1989-2002	additional data	"	additional data
2003-2020	100% of long-term average	"	same as WSP 2370-H projection (mean of 1985, 1986, 1988)
Scenario 3. Historical runoff and pumping.			
Period	% Runoff	Pumpage	Groundwater recharge
1963-1988	same as scenario 2	original model	same as scenario 2
1989-2002	"	additional data	"
2003-2020	"	100% of long-term average	"
Scenario 4. Average future runoff and pumping.			
Period	% Runoff	Pumpage	Groundwater recharge
1963-1988	same as scenario 2	original model	same as scenario 2
1989-2002	"	additional data	"
2003-2020	"	2001 water-year (76,318 AF)	"
Scenario 5. Transient future runoff and pumping.			
Period	% Runoff	Pumpage	Groundwater recharge
1963-1988	same as scenario 2	original model	original model
1989-2002	"	additional data	additional data
2003-2020	"	water-years 1992-2002 followed by 1992-1997	water-years 1992-2002 followed by 1992-1997

was not obvious why some values for selected wells were different by as much as 100%. The

total annual pumpage was very similar in most cases, but the two data sets were not as comparable as expected.

Scenario 2. Historical runoff, zero pumpage. The goal of this scenario is simply to extend Scenario 1 with runoff data for the new period. Any bias in developing the runoff and recharge data would likely become evident, as would any long-term trend in the data. Results indicate that there does not seem to be any bias in the new recharge data. The trend of the simulated groundwater levels is reasonable and does not appear to be affected by any difference in philosophy between the initial period (1963-88) and the later period (1989-2002).

Scenario 3. Historical runoff and pumping. The purpose of this scenario is to add new pumpage and flowing well data to Scenario 2. Similar to Scenario 2, the goal was to identify any unintended bias in developing, processing, or incorporating the data into the model.

Results indicate that no bias is visually discernible. The new data for pumping wells seems to work well. For water-years 1989-02, the model performed remarkably like the original calibration period 1963-88. Measured groundwater levels and simulated heads in areas that matched well during the initial period continued to match well during the later period; areas where heads were offset in some fashion continued to be offset. Essentially no hydrographs converged or diverged. If they had, it likely would indicate a problem with the model.

Scenario 4. Average future runoff and pumping. The goal of this scenario is to extend the post-audit simulation into the future using reasonably average conditions. The runoff is fixed at 100% of the long-term mean, and pumpage is fixed at a typical value for the years just prior to 2003. This scenario is in essence a future steady-state, but the transient simulation demonstrates the time needed to reach this steady-state. This approach is better and more illustrative than

simply running a steady-state solution as was done for the four alternatives in the earlier modeling effort.

In general, there is a slight upward trend in groundwater levels. This result suggests that the pumpage of about 75,000 acre-feet per year is in balance with the amount of recharge. This is the same result that was found during the testing of water management alternatives described in the earlier modeling effort.

Scenario 5. Transient future runoff and pumping. The purpose of this scenario is to demonstrate a dynamic version of Scenario 4 by incorporating climatic variability. This scenario addresses the question, What response is likely to occur from a typical pattern of varying runoff and pumpage? A recent historical period (1993-2002) was identified that had similar statistics to much longer periods, for example 1935-2002. The cumulative percent runoff was used to select the precise period so that there would not be mass balance discrepancies in moving the simulation from historical conditions in 2002 to hypothetical conditions in 2003 and beyond. This means that there should not be an artificial gain or loss of water from the basin as a result of moving into the future period. To achieve this goal, the cumulative percent runoff curve was manipulated by hand, offsetting it in time, and then rematching one curve on top of the other. This process resulted in 1992 matching 2002.

The 10-year period of runoff also needs to have a range of wet and dry years that are comparable to historical conditions. In essence, the period is a sine curve with a short decline, a long rise, and short decline in runoff, ending about where it started in terms of cumulative runoff for the period. Statistical comparison shows that 1993-2002 substantiates that 1993-2002 is a reasonable period to use as it represents a period of zero net change in storage, and contains

reasonably representative wet and dry periods.

Results of Scenario 5 indicate that there is a range of response of the groundwater system over this period. Compared to the historical period, the response is less because the wet and dry periods do not last as long as during the 1960's (drought) or 1980's (wet period). Therefore, Scenario 5 should be viewed as modest fluctuations, less than would result from simulating the historical period 1963-2002. Simulating this period as a scenario is a worthy effort, but beyond the scope of this first task of the post audit.

ET maps

Vegetation based ET maps. Transpiration was calculated for 1677 of the 2126 polygons delineated on the vegetation map; 449 polygons had no vegetation or had no plant species with assigned T_s . Most of the 449 polygons were irrigated lands, urban lands, barren lands, or playa. The distribution of T for the 1677 parcels is shown in Figure 3. Average T was 24.4 cm/year, but the distribution was highly skewed, and the median was probably a better measure of central tendency (19.2 cm/year). Most parcels dominated by phreatophytes had transpiration estimates greater than average precipitation. Some parcels with degraded vegetation were predicted to transpire less than average precipitation. LandSat data, SMA model results, and the vegetation base map produced a map like Figure 4 for each year during 1984-2001. Figure 5 shows an example how the ET rate changes through time for a single MODFLOW cell. Also shown in Figure 5 are depth to water and precipitation, both of which exhibit the expected correlation with ET. Our method contrasts with other recent efforts to develop regional ET rates for Great Basin vegetation. The satellite imagery was used here only to assess the fractional cover of vegetation, whereas other workers (Laczniaak, et al., 1999; Nichols, 2000) have used imagery to classify

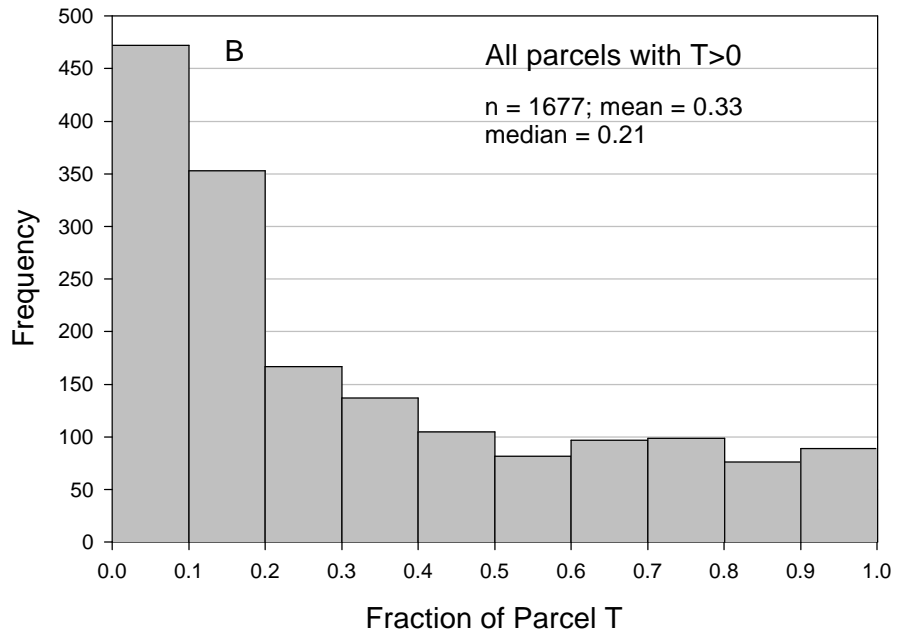
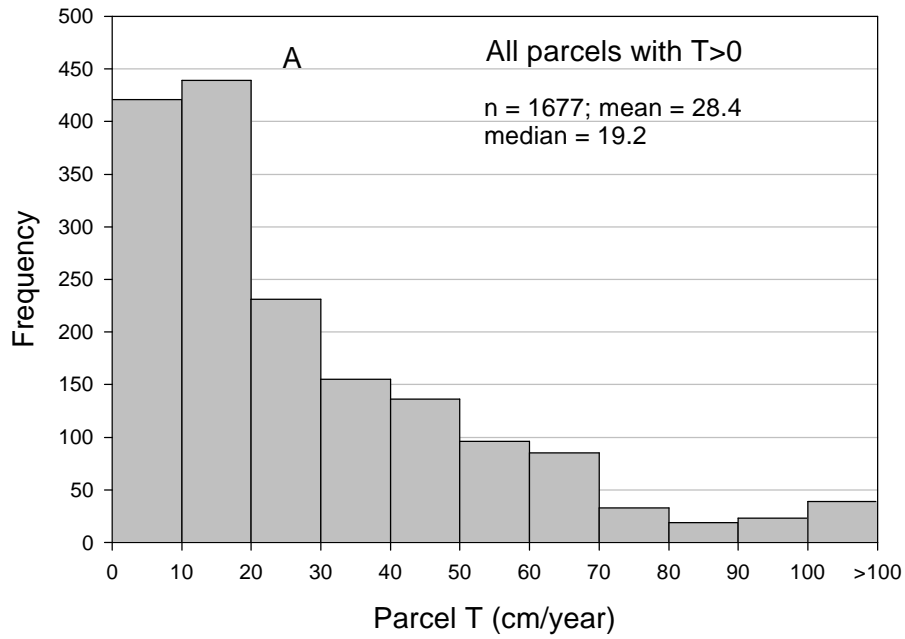


Figure 3. (A) Histogram of T for all parcels with T_{poly} estimates. (B) Histogram of the fraction of T_{poly} contributed by species without assigned T_s values.

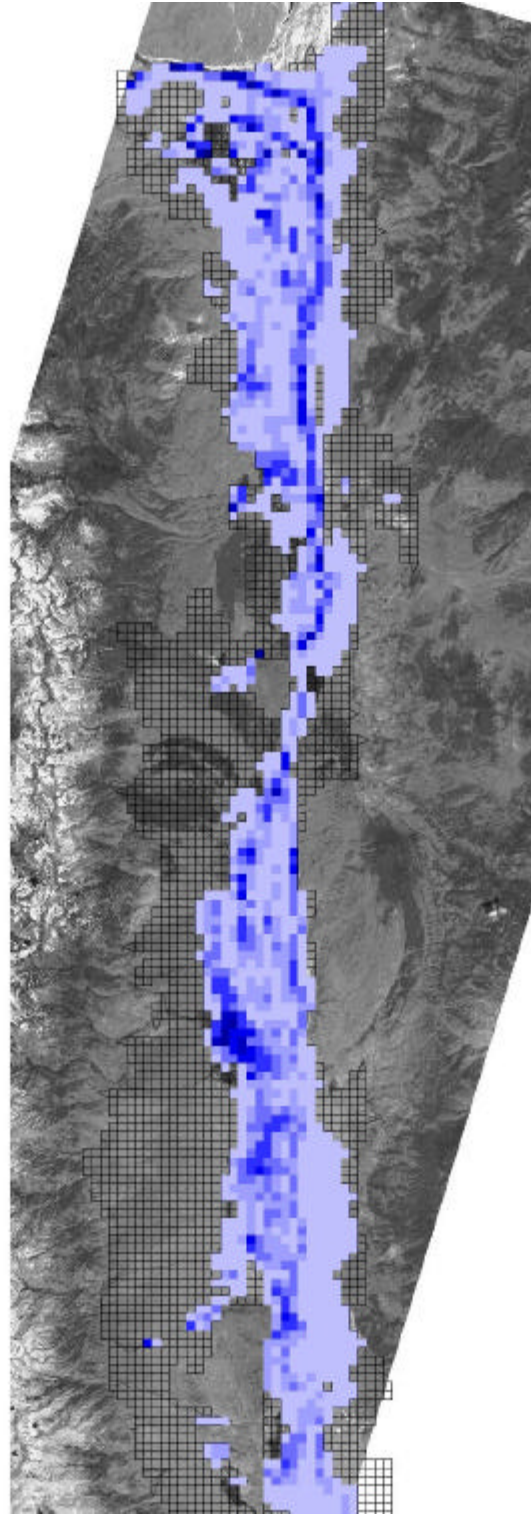


Figure 4. Example of estimated ET for the Owens Valley in 1984 using SMA, transpiration coefficients, and LADWP vegetation inventory.

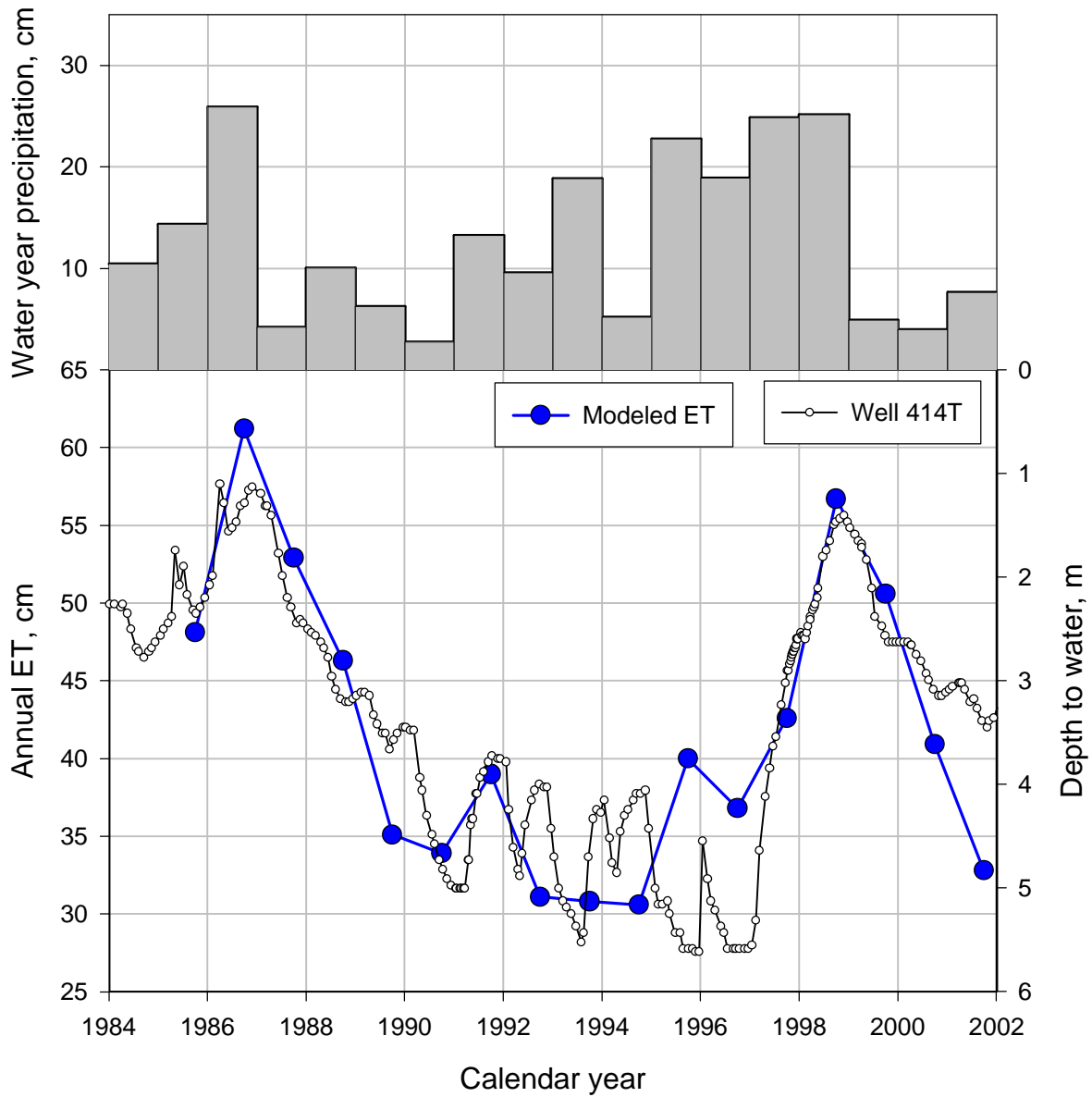


Figure 5. Example of the time series of ET, depth to groundwater, and precipitation for one site instrumented with an eddy covariance tower.

vegetation cover type. Such methods are efficient where there are no preexisting vegetation maps, but if such maps can be constructed or are available from preexisting work, this method allows such information to be used. The parameters required by the MODFLOW ET package are maximum ET rate, ET surface elevation, and ET extinction depth. T_{poly} represents well-watered vegetation at the cover estimated from the imagery, which is analogous the maximum rate required by MODFLOW. However, drought stress or pumping reduces vegetation cover, and the remotely-sensed cover for the early 1990's represents drought stressed vegetation, not well watered vegetation. Alternatively, the computed ET could be considered the actual ET rate. While this could be implemented in MODFLOW, it removes the feedback between ET rates and water table fluctuations. It is presently unclear whether ET as computed above best serves as the maximum ET rate or the actual ET rate. Figure 5 suggests that it may be more correct to treat the computed ET as the maximum rate consistent with the assumptions in the transpiration coefficients of well watered conditions. This would allow for reduced actual ET when the water table is deeper than the plant rooting zone, but resolution of this question will require experimentation with the groundwater model that was beyond the scope of this component of the project.

This method presumes that relatively detailed information about vegetation community composition is efficacious for computing regional ET. It may be the case that a coarser scheme of vegetation classification (e.g., groundwater dependent meadow or groundwater dependent scrub) would provide a simpler or more robust method of computing ET.

Remote sensing ET map. The ET map for the SEBAL analysis is presented in Figure 6. Most of the phreatophytic vegetation on the valley floor transpired less than 3mm day^{-1} . Areas

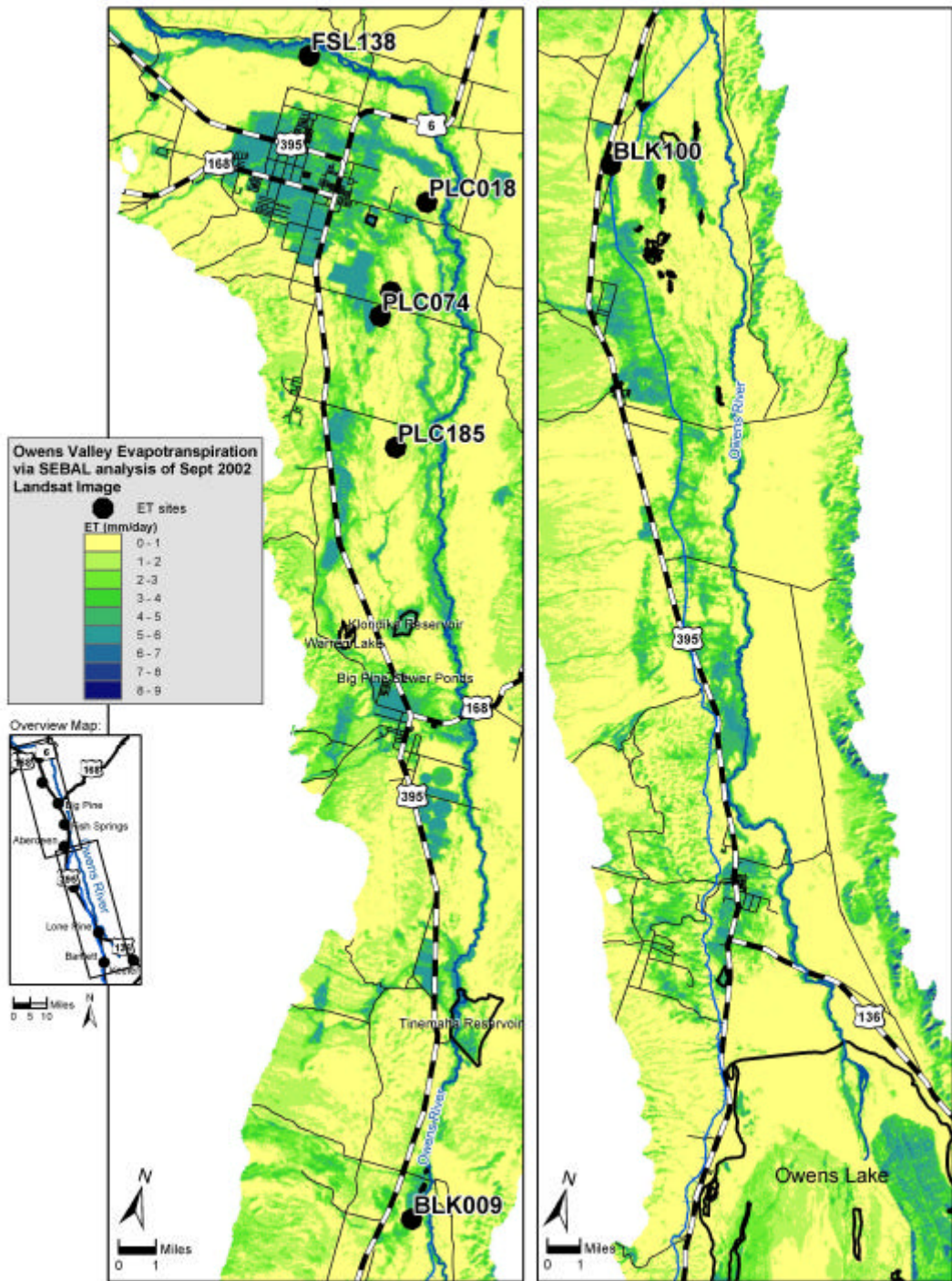


Figure 6. Map of daily ET for September 12, 2002 derived using SEBAL.

Table 4. ET calculated by SEBAL remote sensing algorithm and measured. EC ET is eddy covariance ET corrected for energy imbalance for September 12, 2002.

Site	SEBAL ET (mm/day)			EC ET (mm/day)
	EC site pixel	mean of 9 pixels	mean of 25 pixels	
FSL138	3.0	3.0	3.1	3.0 [^]
PLC018	0.5	0.6	0.6	0.2
PLC074	2.3	2.6	2.7	0.6
PLC185	0.4	0.3	0.3	0.5
BLK100	2.0	2.0	2.0	1.8

[^]: estimated value as described in the text.

of expected higher ET such as the riparian areas adjacent to the Owens River and creeks emanating from the Sierra Nevada and irrigated lands were clearly distinguished by the SEBAL algorithm. SEBAL produced relatively high ET estimates along the White/Inyo Mountain front (east side) and on rock outcrops on alluvial fans on the west side of the valley. Vegetation in these locations probably was senescent this late in the summer suggesting that additional research is need to examine the application of SEBAL for areas of high relief and/or shade. Four of the five EC stations were operating on the date the LandSat data were collected, September 12, 2002. The EC station at FSL138 ceased functioning on September 5, 2002 preventing a direct comparison of the methods. ET at the EC station was estimated for September 12 based on CIMIS ETr and the average site-scale Kc for the 5 days preceding station malfunction (0.61 ± 0.04).

Table 4 compares ET measurements on the ground with eddy covariance towers with ET estimates from SEBAL. The agreement between ET ground measurements and ET SEBAL estimates was very good for both high and low transpiration sites except for PLC074. The large

difference between the ET ground measurement and ET SEBAL was probably due to the spatial resolution of the thermal band of LandSat 7. The thermal band has a pixel size of 60×60 m, and even after careful georeferencing of a LandSat image, the true location of any given pixel may be within two or three pixels of the location on the image. For site PLC074 a shift of two pixels (120 m) to the west would include an irrigated area not sensed by the tower measurements, while a similar shift to the east would encounter depression with slightly higher cover of grasses. Both these areas probably had a higher ET than the footprint sensed by tower and, thus, the SEBAL ET overestimated the true ET. The data in Table 4 support this argument since the ET values are increasing when averaged over a larger area around the tower (from 1 to 9 to 25 pixels); the larger the area of averaging, the more irrigated or riparian land was included increasing the SEBAL derived ET estimate.

Especially encouraging were the SEBAL ET estimates of sites FSL138, BLK100, and PLC185 that were very close to the ET ground measurements. This result together with results in the riparian areas of the Middle Rio Grande Valley by Dr. Hendrickx's group indicate that SEBAL may be a reliable method for determination of ET in areas with phreatophytic and riparian vegetation. For future testing of SEBAL in the Owens Valley, it is recommended to locate the eddy covariance towers in locations that cover a sufficiently large homogeneous area to eliminate the problems with georeferencing of the thermal band.

ET depth function

Several multiple linear regression models were developed to explore the relationship between vegetation cover, depth to water table and precipitation. Total plant cover was used as the independent variable as a surrogate quantity related to ET (Nichols, 2000). Transpiration

Table 5. Correlation (r) matrix for winter precipitation (October 1 to April 1) measured at seven stations maintained by LADWP in the Owens Valley for 1986-2001.

	Bishop	Tinemaha	Intake	Independence	Alabama gates	Lone Pine	Big Pine
Bishop	1						
Tinemaha	0.93	1					
Intake	0.92	0.92	1				
Independence	0.90	0.95	0.86	1			
Alabama gates	0.93	0.86	0.92	0.84	1		
Lone Pine	0.90	0.84	0.89	0.81	0.98	1	
Big Pine	0.94	0.95	0.90	0.96	0.85	0.82	1

estimates determined using methods described above were not used as the independent variable for this initial analysis because those values are linearly related to plant cover (Steinwand et al., 2001) and because the accuracy of those estimates is under investigation as part of this study.

Development of appropriate dependent variables required exploration of various transformations of the raw data. Plant cover at each site would be expected to respond uniquely to changes in the driving variables because of differing vegetation, soil, and antecedent groundwater conditions. Simply relating depth to water and precipitation with plant cover for sites with a widely varying range of characteristics was not successful. Site specific response could be addressed by preparing models for each location, but the relatively small data sets and lack of replicated measurements makes this a questionable practice. Also, it would be much simpler to incorporate a generalized relationship into the groundwater model. Several strategies were implemented to address the problem of site specificity. Plant cover the previous year was added as a dependent variable and the DTW was standardized to produce a variable with zero

mean and standard deviation equal to 1 (Snedecor and Cochran, 1988). Cover and depth to water data were site specific, but precipitation stations were not located at all sites. The appropriate scale to average the precipitation variable was examined by preparing a correlation matrix of precipitation at the seven locations. Winter precipitation was correlated for all pairs of gauges (Table 5) suggesting little advantage to using data from an individual gauge in favor of a spatially aggregated average for the valley.

Several multiple linear regression models were attempted using various combinations of transformed dependent variables. This work is considered preliminary, but the results were promising. For sites located in wellfields, the tentative relationship developed is given below,

$$Cov = 0.66 * Cov_{prev} + 0.83 * Ppt - 1.38 * DTW_{stand} - 2.48 \quad (8)$$

where Cov is total vegetation cover (%), Cov_{prev} is total vegetation cover the previous year, Ppt is average valley winter precipitation, and DTW_{stand} is standardized DTW. Model coefficients were rational, e.g. increasing DTW corresponds with lower predicted cover. The model accounted for 62% of the variance ($r^2 = 0.62$), and all regression coefficients were significant ($p < 0.05$). A similar model was developed for control areas, but as expected, the pumping variable was not significant. Work on this modeling effort continues, including using estimated T as the independent variable and revision of the DTW variable to include threshold values.

Conclusions

In general, the post-audit confirmed the conclusions stated in WSP2370-H that the primary influence in most areas of the valley is pumping. The effect of recharge is most evident on the alluvial fans and in regions such as Laws with less confined aquifers. The scenarios

demonstrated that pumpage tends to have a localized short-term effect, whereas recharge has a more diffuse, long-term effect. The post-audit results successfully simulated the drawdown due to the high pumping of 1987 through 1990 and the subsequent period of recovery. The time frame for response of the groundwater system which was identified in WSP2370-H to be on the order of five to ten years is supported by the transient simulations. This means that there may be a lag of as much as a decade for the system to fully respond to changes in either the natural hydrologic inputs such as runoff or evapotranspiration or human management of pumping and recharge.

Alternative 1 in WSP2370-H examined continued operations at 1988 pumping levels, or about 141,000 acre-feet of pumping, which was substantially more pumping than the 60,000 to 90,000 acre-feet that occurred during the post-audit period. It was noted in WSP2370-H that one of the greatest uncertainties in the results stated in WSP2370-H was how groundwater management would evolve in the future. Alternative 3, which examined increases or decreases in pumping, predicted that groundwater extraction (including 8,000 to 10,000 acre-feet of artesian flow) would have to be approximately 75,000 acre-feet to maintain 1984 groundwater levels. Actual water levels during the post-audit period bear out this conclusion of WSP2370-H.

These observations suggest that the model can continue to be useful in critiquing proposed changes in water management and bracketing the likely long-term effects that will result. Identifying these hydrologic effects by actual monitoring may be difficult or impossible because of the commingling effect of other stresses and the widespread presence of hydrologic buffers as described in WSP2370-H.

This effort has resulted in several significant achievements. The model now simulates

conditions in the basin from 1963 to 2002 in the same manner as it had for the original calibration period (1963-1988). Performance of the model over this extended period was shown to be similar to the original calibration period. The five scenarios examined in this effort generally corroborated the results of Danskin (1998). Water balance components were separated into separate custom MODFLOW packages, including separation of pumped and flowing wells. Future work to enhance the use of the model falls into three categories: refinement of historical data, testing of additional future scenarios, and revision of the model itself.

Refinement of historical data. During development of the simulation period 1989-2002, data for some years had to be estimated from adjacent years, in particular for groundwater recharge. The cumulative effect of these estimates is not believed to significantly alter model performance, at least at the valley-wide scale. It seems likely, however, that credibility of the model would be enhanced by taking additional effort to find specific annual values and to resolve differences between data used in WSP2370-H and that used in the post audit. Other historical input data that may be refined are the flow/recharge regression relationships that determine stream channel recharge, and spatially varying evapotranspiration parameters.

Testing of additional future scenarios. Prior to making any changes in the model code, it may be efficient to test additional future scenarios of interest to Inyo County, LADWP, or others. The scenarios evaluated as part of the post-audit were developed with the goal of testing model sensitivity and the conceptualization of the general hydrologic system, rather than with the goal of evaluating any specific management plan.

Revision of the model. Significant enhancements to the MODFLOW computer code have been made since the original valley-wide model was developed. These improvements include a

more accurate way to simulate faults, streams, and reservoirs, and efficient methods for extracting local sub-models from regional models. Application of these capabilities will likely allow for an improved ability to critique management alternatives and inspect the effect of management changes.

Two methods to construct estimates of spatial ET were developed by this project. A series of ET maps for the post audit period was developed by combining field vegetation measurements, remote sensing measurements of plant cover, empirically derived transpiration coefficients, and transpiration estimates from the scientific literature. These maps can be readily converted into the MODFLOW application to test the sensitivity of the groundwater model to different ET estimates. Future work will be to repeat the transient model simulations for the post-audit period using the new spatial ET estimates and compare those results with the simulations prepared during this study. While not contemplated in the original proposal, the interest generated by the field ET measurements collected by this study and the ongoing cooperative study with LADWP prompted testing of the remote sensing algorithm SEBAL to estimate ET in the Owens Valley. Based on the promising initial results presented in this report, Dr. Hendrickx, New Mexico Technical Institute is seeking additional funding to further test this method in Owens Valley. His group also is processing additional LandSat scenes from 2002 to prepare additional comparisons with the EC groundtruth measurements from this study. Further research will refine the SEBAL method and test whether SEBAL results can be combined with reference ET measurements to develop Kc models to estimate seasonal or annual ET rates.

Field ET investigation

Introduction

There are several methods of measuring ET using micrometeorological measurements (Brutsaert, 1982; Shuttleworth, 1993). All micrometeorological methods measure variables near the land surface (i.e., a few meters above the plant canopy) to determine fluxes of energy, momentum, or trace gases. Micrometeorological methods have been used in previous cooperative studies to measure water vapor fluxes from phreatophytic vegetation (Duell, 1990; Gay, 1992; Duell, 1992; Stannard, 1992), but these measurements were not made concurrently with the necessary vegetation cover measurements to undertake the comparison between micrometeorological results and estimates based on vegetation cover measurements and transpiration coefficients.

The micrometeorological method used in this project was the eddy covariance (EC) method. The eddy covariance method has gained predominance among micrometeorological methods recently because of its minimal theoretical assumptions and improved instrumentation (Shuttleworth, 1993). An advantage of the eddy covariance method is that it is the most direct measurement of sensible and latent heat fluxes that is possible with micrometeorological methods. Inyo County and LADWP have jointly conducted a study to collect eddy covariance ET measurements to compare with transpiration coefficient models in Steinwand et al. (2001) and in the Plan. Because of the similar study design, data from the LADWP funded equipment are included in this report.

The purpose of this task was to measure ET using micrometeorological methods to provide an independent measurement for comparison with estimates from existing transpiration

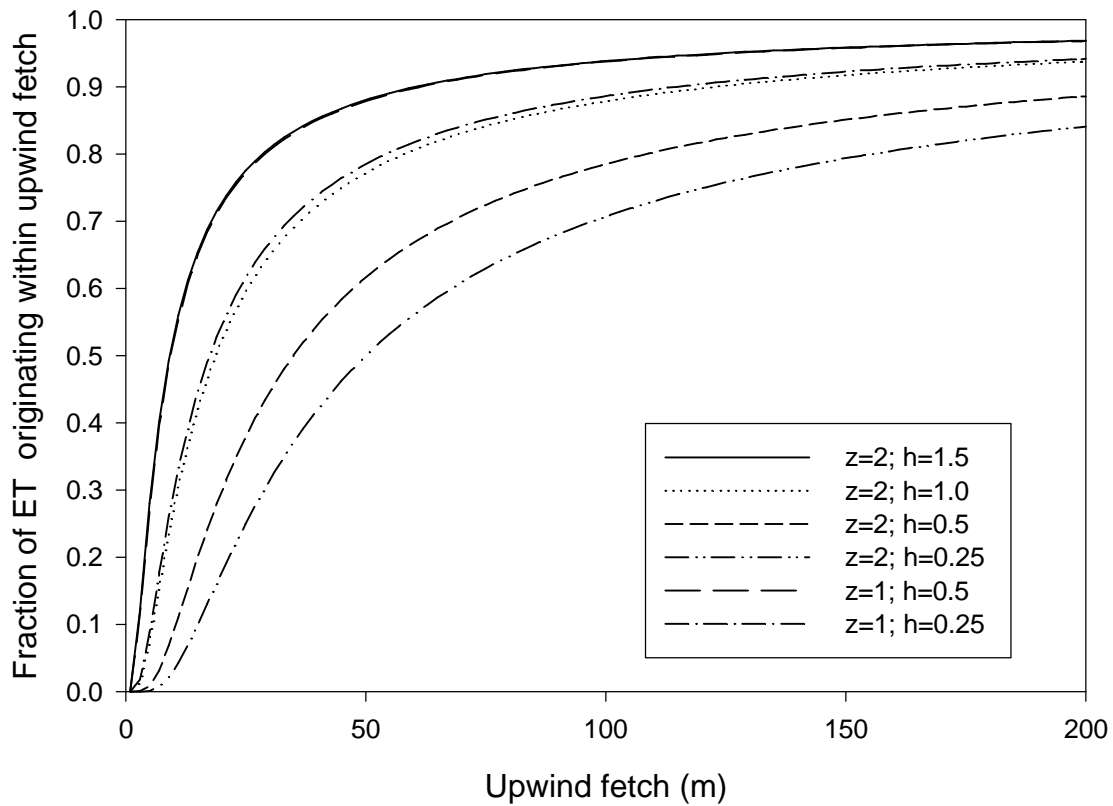


Figure 7. Approximate contributing area upwind of an eddy-covariance stations in unstable conditions according to Gash (1986). Reasonable values were assumed for roughness height, stability, wind speed, and zero-plane displacement; z is instrument height and h is canopy height.

coefficients.

Materials and Methods

Site selection

Sites were selected based on species composition, depth to the water table, and fetch. EC stations were placed in both mixed and monocultural sites ranging from alkali meadow to scrub sites. Except for PLC018 and PLC045, the intent was to select sites with DTW sufficient to

Table 6. Eddy covariance site characteristics. Range of depth to water during the growing season is given. Precipitation values are annual totals beginning October 1 the previous year. Except for PLC45, April to October rain was less than 15mm.

Year	Site	Vegetation type	Dominant Species [^]	Depth to water (m)	Precipitation (mm)
2000	BLK 100	alkali meadow	SPAI, DISP	2.0-2.5	35.6
2001	BLK 100	alkali meadow	SPAI, DISP	2.2-3.0	71.1
	BLK 9	rabbitbrush meadow	CHNA, SPAI	2.6-3.2	71.1
	PLC 45	Nev.saltbush scrub	ATTO	3.8-4.1(est.)	105.9
2002	BLK 100	alkali meadow	SPAI, DISP	2.3-3.2	32.5
	FSL 138	alkali meadow	DISP, LETR, SPAI	1.2-2.1	21.8
	PLC 18	rabbitbrush scrub	CHNA	>5.0	34.5
	PLC 74	Nev. saltbush meadow	SAVE, ATTO, DISP	2.1-2.4	31.5
	PLC 185	desert sink scrub	SAVE	>4.0	31.5

[^]grasses: SPAI, *Sporobolus airoides*; DISP, *Distichlis spicata*; LETR, *Leymus triticoides*. shrubs: CHNA, *Chrysothamnus nauseosus*; ATTO *Atriplex lentiformis ssp. torreyi*; SAVE, *Sarcobatus vermiculatus*.

subirrigate the vegetation, but deep enough to minimize surface evaporation. This provision was to allow valid comparisons of measured ET (i.e. minimize E) with the vegetation-based transpiration estimates. Methods in Gash (1986) were used to estimate the size of the potential area contributing to the EC measurements to guide selection of sites (Figure 7). Sites with obvious boundaries between dissimilar vegetation and hydrologic conditions within approximately 150 m of the site were avoided. All the sites were undisturbed by water spreading or irrigation.

Locations of the EC sites is shown on Figures 8 to 14, and environmental characteristics of the sites are summarized in Table 6. Each EC tower was fenced to prevent range cattle from



Figure 8. Aerial photograph and measurement locations for ET, soil water, and LAI BLK100.



Figure 9. Aerial photograph and EC, soil water and LAI measurement locations at ET site BLK9.



Figure 10. Aerial photograph and EC, soil water and LAI measurement locations at ET site PLC045.



Figure 11. Aerial photograph and EC, soil water and LAI measurement locations at ET site FSL138.

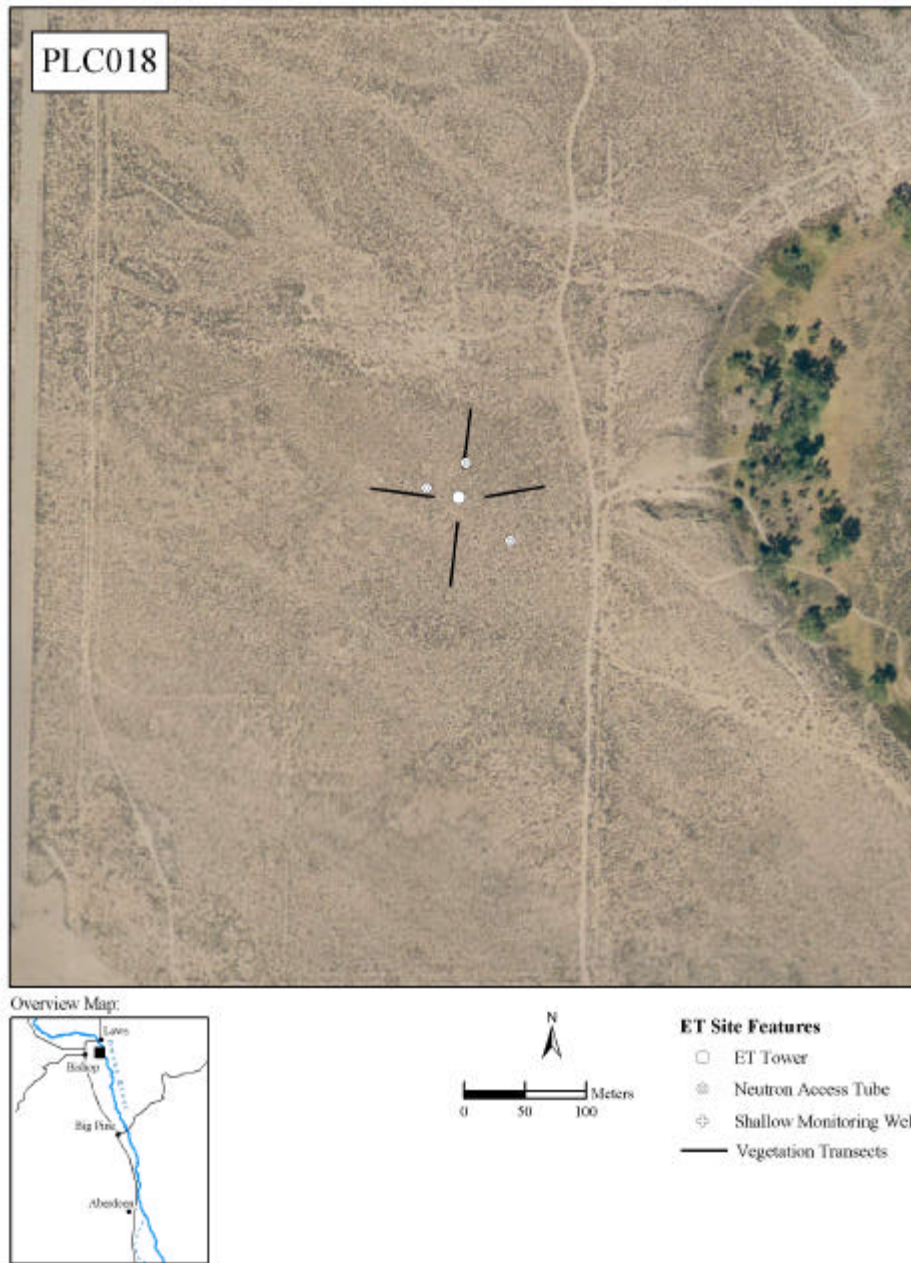


Figure 12. Aerial photograph and EC, soil water and LAI measurement locations at ET site PLC018.

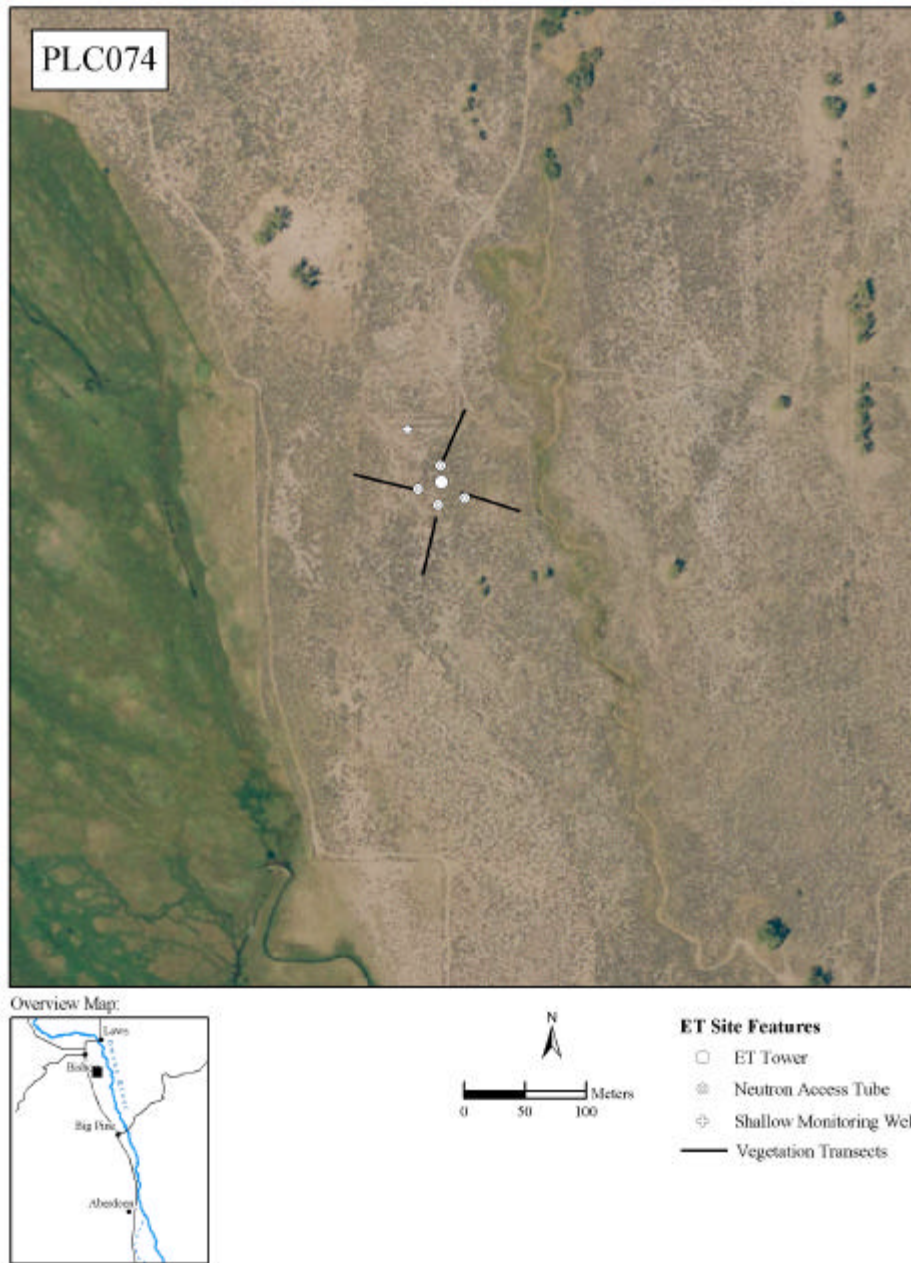


Figure 13. Aerial photograph and EC, soil water and LAI measurement locations at ET site PLC074.

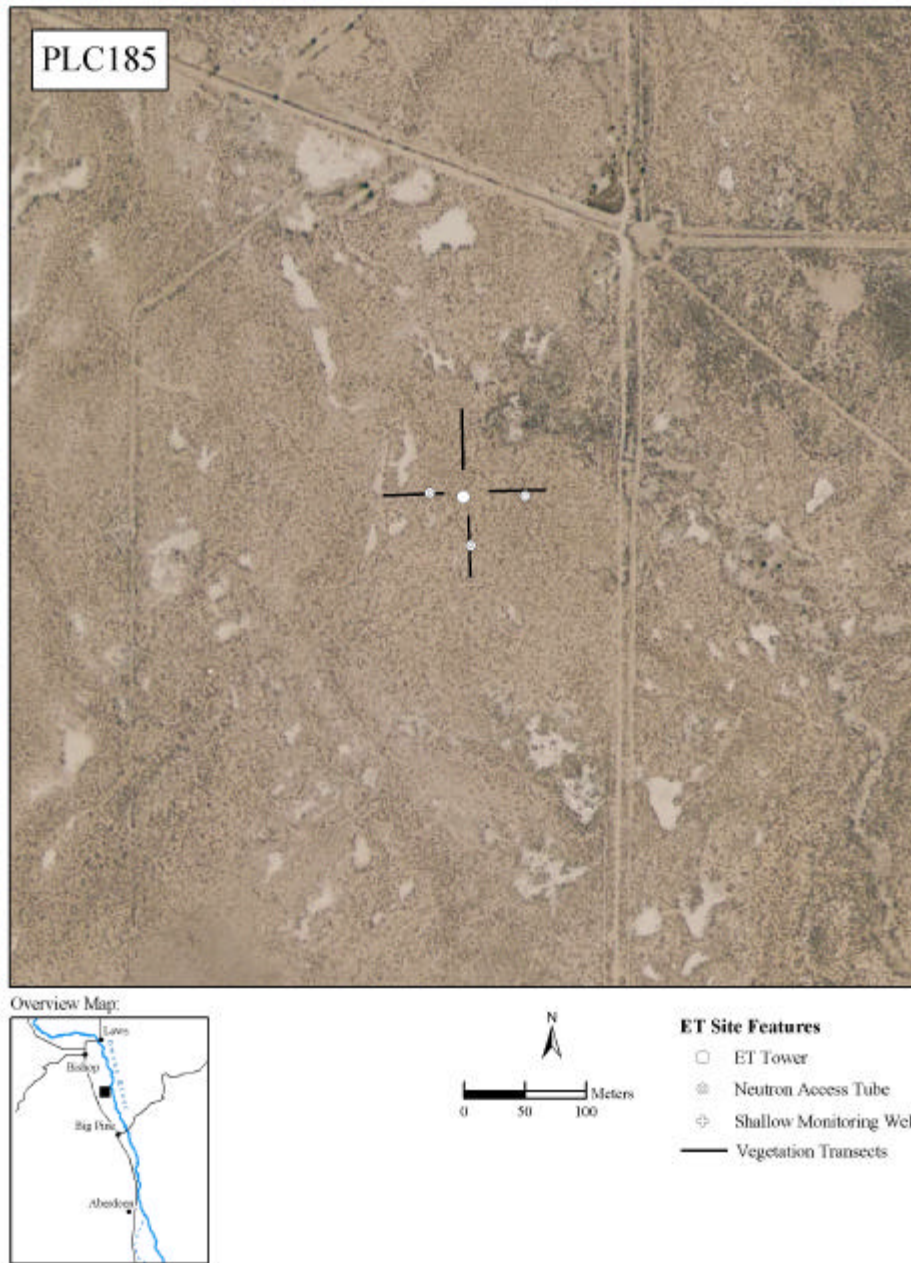


Figure 14. Aerial photograph and EC, soil water and LAI measurement locations at ET site PLC185.

Table 7. Dates of EC station operation.

Year	Site	Date established	Date removed
2000	BLK 100	April 21	January 8, 2001
2001	BLK 100	March 7	November 27
	BLK 9	April 11	November 27
	PLC 45	April 10	November 27
2002	BLK 100	March 12	October 2
	FSL 138	May 3	September 11
	PLC 18	May 2	October 8
	PLC 74	May 25	October 7
	PLC 185	May 24	October 7

damaging the instruments. The fenced enclosure at BLK00 was expanded in 2001 to include the vegetation because of observed grazing impacts adjacent to the tower enclosure late in the growing season and over winter. Table 7 shows the dates ET measurements began and ended each year. In all years, EC measurements encompass the majority of the growing season, approximately March 25 to October 15.

Eddy covariance instrumentation and theory

The EC method of measuring turbulent fluxes uses fast response sensors to measure rapid changes in vertical wind speed and scalar quantities (e.g. water vapor density or air temperature) to compute the flux of the scalar by means of the covariance between the vertical wind and the scalar (Arya, 2001). The latent heat flux is,

$$LE = ET = \overline{lw'r_v'} \quad (9)$$

and the sensible heat flux is,

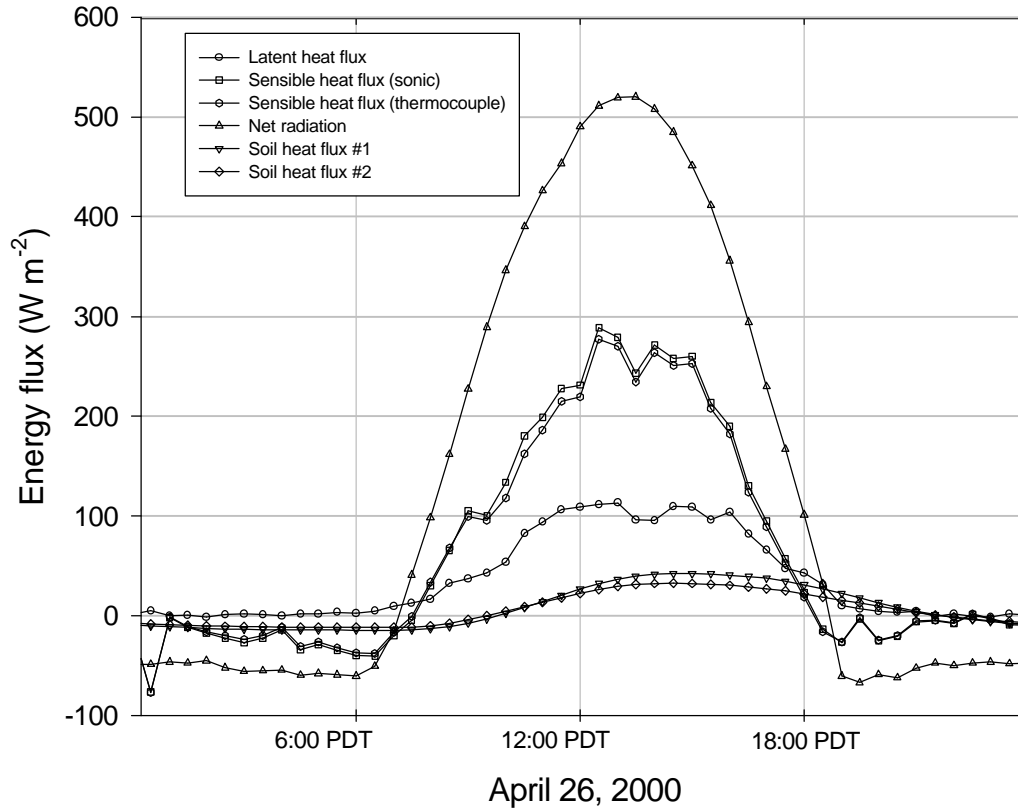


Figure 15. Energy balance components measured at BLK100.

$$H = \rho C_p \overline{w'T'} \quad (10)$$

where w is the vertical wind speed (m s^{-1}), ρ_v is the water vapor density (kg m^{-3}), ρ is the mean air density (kg m^{-3}), C_p is the specific heat of air ($\text{J kg}^{-1} \text{K}^{-1}$), T is the air temperature (primes indicating deviations from the time-averaged mean). The vertical wind speed was measured with a Campbell CSAT sonic anemometer (Campbell Scientific Inc., 1998a), the water vapor density

was measured with a Campbell KH20 krypton hygrometer (Campbell Scientific Inc., 1989), and air temperature was measured using a fine-wire thermocouple, all of which were mounted 2.5 m above the land surface. Sensible heat flux was calculated using both the temperature as calculated from the sonic anemometer and as measured by the fine wire thermocouple, and the two methods had close agreement at BLK100 (Figure 15). The fine wire thermocouples were replaced repeatedly due to breakage which resulted in an intermittent record; therefore, the sonic temperature was used in calculating the seasonal sensible heat flux. The data were acquired and the covariance computed at 10 Hz, and fluxes were averaged over 30 minute intervals. The EC system has the advantage that the computed covariance theoretically provides a direct measure of the scalar flux at the point of measurement. Difficulties in the EC method arise in the demands made on the instrumentation to acquire data at the necessarily rapid sampling rate, and the fact that the measurements in practice are non-collocated volume averages rather than collocated at a point as assumed by Equations 9 and 10.

The EC measurements were corrected for absorption of the krypton hygrometer ultraviolet beam by oxygen (Campbell Scientific Inc., 1998b), and for the effect of fluctuating air density (Webb et al., 1980). These corrections were implemented as,

$$IE = I \left(\overline{w' r_v'} + \frac{r_v H}{r C_p T} + \frac{F k_o H}{k_w T} \right) \quad (11)$$

where F is a factor to account for the fraction of oxygen in air (gm K J^{-1}), k_o is the oxygen absorption coefficient ($0.0045 \text{ m}^3 \text{ gm}^{-1} \text{ cm}^{-1}$), and k_w is the water vapor absorption coefficient ($0.154 \text{ m}^3 \text{ gm}^{-1} \text{ cm}^{-1}$). The first term in the parentheses is the uncorrected EC vapor flux, the second term corrects for fluctuations in air density, and the third term corrects for the effect of

oxygen on the krypton hygrometer.

Though not necessary to make the EC estimate of turbulent fluxes, the EC system was also equipped with a REBS Q-7.1 net radiometer (Campbell Scientific Inc., 1996a), soil heat flux plates (Campbell Scientific Inc., 1999), soil temperature sensors, and a frequency domain reflectometer (Campbell Scientific Inc., 1996b) for measuring soil wetness. These additional instruments allow the energy balance to be computed. Two soil heat flux plates were installed at a depth of 8 cm a few feet apart, and soil temperature thermocouples were installed at depths of 2 and 6 cm between the flux plates. The soil heat flux at the soil surface was computed by correcting the heat flux at the flux plate for thermal storage in the soil above the flux plates,

$$G = G_z + \Delta z \frac{\Delta T}{\Delta t} (C_w \mathbf{q}_v \mathbf{r}_w + \mathbf{r}_b C_s) \quad (12)$$

where G_z is the average of the two flux plates (W m^{-2}), Δz is the depth of the flux plates, ΔT is the average change in temperature of the two soil temperature thermocouples ($^{\circ}\text{C}$), Δt is the time interval over which the flux is averaged (s), C_w is the specific heat capacity of water ($4.18 \text{ J g}^{-1} \text{ K}^{-1}$), \mathbf{q}_v is the volumetric soil water content (0.066 cm^3 water per cm^3 of soil), \mathbf{r}_w is the density of water (1.00 gm cm^{-3}), \mathbf{r}_b is the measured soil bulk density (1.11 gm cm^{-3}), and C_s is the specific heat capacity of dry soil material ($0.87 \text{ J gm}^{-1} \text{ K}^{-1}$). Soil bulk density and water content were determined by oven drying of soil samples, and the specific heat capacity of dry soil material was taken from Campbell and Norman, Table 8.2 (1998).

The sign convention adopted throughout this report is as follows: net radiation is positive when directed toward the land surface, sensible and latent heat fluxes are positive when directed away from the land surface, and soil heat flux is positive when directed into the soil.

Quality control

Several quality control measures were implemented to ensure accurate data were collected. The towers were instrumented to measure all components of the energy balance (EB) to allow an independent check of the ET measured by the EC methods using,

$$EB = R_n - G - H - IE \quad (13)$$

EB should equal zero if canopy heat storage, photosynthetic absorption of solar radiation, and advective energy transport processes are negligible. EC measurements collected during this study and others (Bidlake, 2001; Bidlake 2002; Berger et al., 2001; Sumner, 1996; Duell, 1990) have found that EB does not achieve closure, with the sum of the turbulent fluxes ($H + IE$) measured by the EC instruments generally being less than the available energy ($R_n - G$). Results of the analysis of Equation 13 are described more fully in a separate section below.

Post processing of the EC data included inspection of the record for anomalies in all data streams, inspection of the turbulent flux data for sonic anemometer spikes or signal losses. If more than 5% of the 10 Hz signal from the eddy covariance sensors was lost over a thirty-minute sampling interval, that interval was discarded. Routine maintenance and data downloads were done at roughly weekly intervals when the instruments were deployed. Typically, during each of these site visits, the data were downloaded, the windows on the hygrometer were cleaned, the net radiometer domes were cleaned, the sonic anemometer and net radiometer were checked for level, the solar panel was cleaned, and sensor output was examined to make sure all sensors were recording correctly. Upon the completion of measurements each season, the EC instruments

Table 8. Statistics of ET tower comparison at BLK100, alkali meadow site in 2000.

	Tower 1	Tower 2	Tower 3
mean LE flux (W m^{-2})	32.87	34.26	33.89
standard deviation	47.03	48.61	48.36
% of mean of all towers (33.67 W m^{-2})	97.6%	101.7%	100.6%

were removed from the field for return to the factory for recalibration.

During the period July to October, 2000, 62 days of data were collected where three EC systems collected concurrent ET, air temperature, and humidity measurements at BLK100. For this comparison, the instrument towers were placed about 4 meters apart, arrayed roughly perpendicular to the mean wind direction. The most significant data gaps are in the net radiation record, which lost data during the interval from day of year (DOY) 119 to 130 due to a problem with the datalogger program, from DOY 177 to 180 due to a break in the instrument cable, and from DOY 284 through 294 due to a broken radiometer dome. All three systems were powered down and instruments removed from the field during the period DOY 242-245 due to inclement weather. Short intervals of data were lost when the transducer heads of the sonic anemometer were wet due to rain. Simultaneous operation of the collocated systems showed that latent heat fluxes measured by the three systems agreed closely with one another. Table 8 compares the statistics of the latent heat fluxes measured by each system, and Figure 16, shows the 30-minute latent heat fluxes over the period September 1 through 4.

Bowen ratio instruments and theory

Energy fluxes measured by the EC system were compared to fluxes measured with a collocated Bowen ratio (BR) system to examine the EB closure problem and to develop

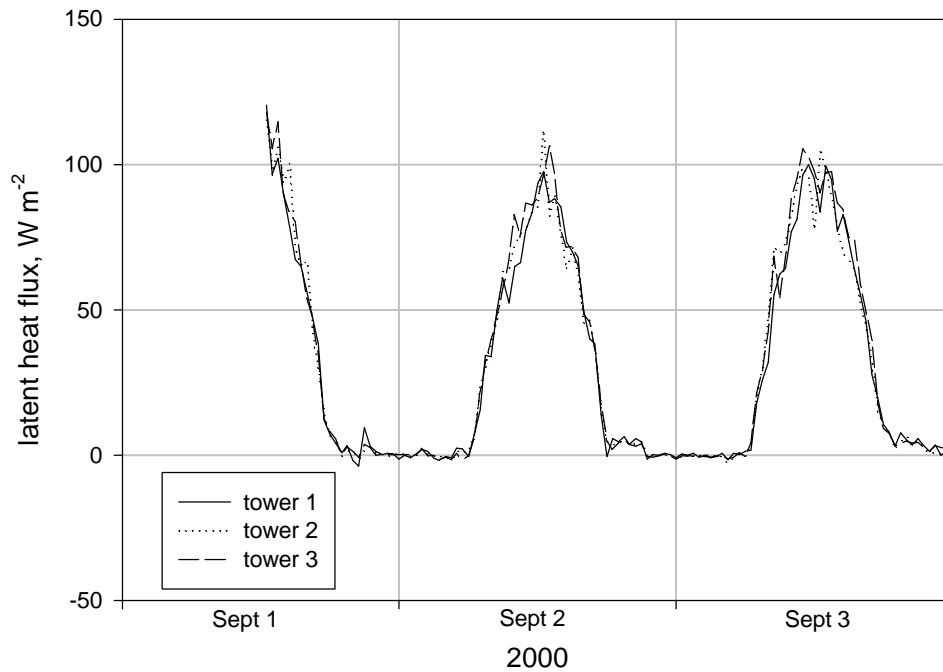


Figure 16. Latent heat flux from three collocated systems at BLK100.

recommendations for processing the EC data to estimate ET. A BR system was installed and operated by Dr. Jim Stroh, Evergreen State College, from August 23 to September 3, 2002 at BLK100. The instrument towers were located 5 m apart in an east-west alignment so wakes on the lee side of each tower would not interfere with the other tower during the prevailing afternoon southeasterly winds. The net radiometers were mounted 5 m apart and 3 m south of their respective instrument towers.

The BR methods relies on different assumptions and instrumentation than the EC to

estimate fluxes. Agreement between the two methods would strongly corroborate the results, and disagreement between the methods can help determine likely sources of error. The BR method uses measurements of water vapor density and temperature at two heights to compute the average gradients near the surface, and then by equating the eddy diffusivity for sensible and latent heat, uses Equation 3 and the measured Bowen ratio ($b = H/LE$) to compute the turbulent fluxes. Beyond its use in the BR method, b is significant as a measure of the relative partitioning of available energy between sensible and latent heat. The BR system consists of fine wire thermocouples mounted at 1.0 and 2.0 m above the surface, a chilled mirror hygrometer, an air pump and routing system that alternately directs an air stream from the upper and lower sensor arms to the hygrometer, a net radiometer, soil heat flux plates, and soil temperature sensors. Fluxes were averaged over 20 minute intervals. The BR method has the advantage that the instrumentation is relatively simple compared to the EC method, but has the disadvantage that energy balance is used to compute the fluxes. The energy balance cannot be used as a check on the internal consistency of the computed fluxes, and any errors in measuring available energy affect the computation of the turbulent fluxes. The chilled mirror hygrometer has a limited range of environmental conditions under which it will function properly. In very dry conditions, very warm conditions, or very cool conditions, formation of frost on the mirror surface confounds the dew point measurement. The early fall season was chosen for operation of the BR system at this site because it was expected that conditions would be within the applicable range of the chilled mirror hygrometer. Soil heat flux was computed as described for the EC systems.

Two sources of error that are common to both BR and EC measurements are the

mismatch between the sampling areas ("footprints") of the various sensors used to compute fluxes and energy balances, and the variability of the landscape within the footprint. For example, the sonic anemometer and krypton hygrometer combine to sense water vapor flux integrated over a footprint with a radius on the order of 100 m, whereas the calculation of soil heat flux has a footprint of about a square meter. Similar mismatches of measurement areas or volumes are present in the BR instrumentation. Because the land surface properties that affect the energy balance are spatially heterogeneous, these footprint mismatches limit the precision with which the energy balance at a point can be estimated.

Soil water and groundwater measurements

Three or four access tubes were installed adjacent to the vegetation transects, usually to just above the water table. Only one access tube extended to depths below 1m at PLC045 because augered holes collapsed repeatedly in the dry, sandy soil. Access tubes were constructed of PVC except at PLC018 where aluminum tubes were used. The neutron gauge was calibrated by regressing volumetric water content (q) of samples collected during access tube installation against neutron gauge count ratio (count/field standard count) recorded at the sampling depths. Determination of q followed Blake and Hartage (1986) and Allen et al. (1993). Soil cores of a known volume were collected, weighed, and dried at 105 °C for 24 hrs to determine the gravimetric water content (g water/g soil) and bulk density (g soil/cm³ soil). Volumetric water content is the product of gravimetric water content and bulk density (assuming the density of water is 1 g/cm³). Soil water was measured biweekly during the growing season and approximately monthly in winter. Soil depths below 20 cm were monitored in 15 cm

increments. Shallow depths (0-8 cm) were monitored using gravimetric sampling. Existing on-site test wells were monitored at FSL138, PLC074, BLK009, and BLK100 (beginning in February, 2001). Nearby test wells were monitored at PLC045, and BLK100 (before February, 2001). Sites PLC018 and PLC185 were not located near test wells.

Vegetation measurements

Four 50 m transects aligned north, south, east, and west of the ET station enclosures were established at each site. Point frame measurements with 50 cm pin spacing were conducted approximately monthly, and first contacts and all contacts with green live, green leaves or stems were recorded by species to determine leaf area index (LAI) (Goodall, 1952). Plant cover was calculated as the fraction of pins that contacted at least one green leaf or stem. Contact frequency (total contacts / total pins) was used to calculate LAI according to,

$$LAI = \frac{N}{K} \quad (14)$$

where N is contact frequency for a species and K is an extinction coefficient determined empirically for common Owens Valley species (Groeneveld, 1997). Extinction coefficients for species not examined by Groeneveld (1997) were assigned a value of 0.5, which was a typical value for the common species.

Comparison of EC and of Kc estimates

Transpiration coefficients are a dimensionless ratio of actual ET (in this case T) to a reference or potential ET typically determined over an irrigated grass or alfalfa reference crop. The general form of transpiration coefficients is,

$$Kc = \frac{actualET}{referenceET} \quad (15)$$

Once the Kc for a plant species (usually a crop) is known, actual ET for another site or time can be derived from measurements of reference ET by rearranging Equation 15. Transpiration coefficients take several forms based on modifications for precipitation, growing season weather, time-varying leaf area/canopy closure, or irrigation (Allen et al., 1998).

Transpiration coefficients from Steinwand (1999b) and Steinwand et al. (2001), measured LAI, and measured reference ET were used to calculate transpiration (T_{Kc}) using:

$$T_{Kc} = \sum_{j=1}^n \sum_{i=1}^m (Kc_{ij} ETr_i LAI_j) \quad (16)$$

where: ETr_i is reference ET for day i , n is number of species, Kc_{ij} is the transpiration coefficient for species j on day i , LAI_j is the midsummer LAI for species j . The Kc models were developed from a large database of stomatal conductance, reference ET, and leaf area index for the five most common Owens Valley plant species and assume soil water conditions are not limiting (Figures 17 and 18). ETr_i was derived at a weather station in Bishop using a modified Penman equation by the California Irrigation Management Information System. Changes in LAI during the growing season were incorporated during the construction of the Kc models by relying on models of daily LAI normalized to peak LAI=1.0. Hence, Equation 16 only requires a single LAI measurement near the peak of the growing season to adjust the Kc to provide site-specific estimates of ET. LAI of the dominant species at each site determined on the date nearest the maximum LAI in the Kc models was used in Equation 16. Dates of LAI measurements used to compute T_{Kc} are given in Table 9. LAI of minor species for which no Kc models were available

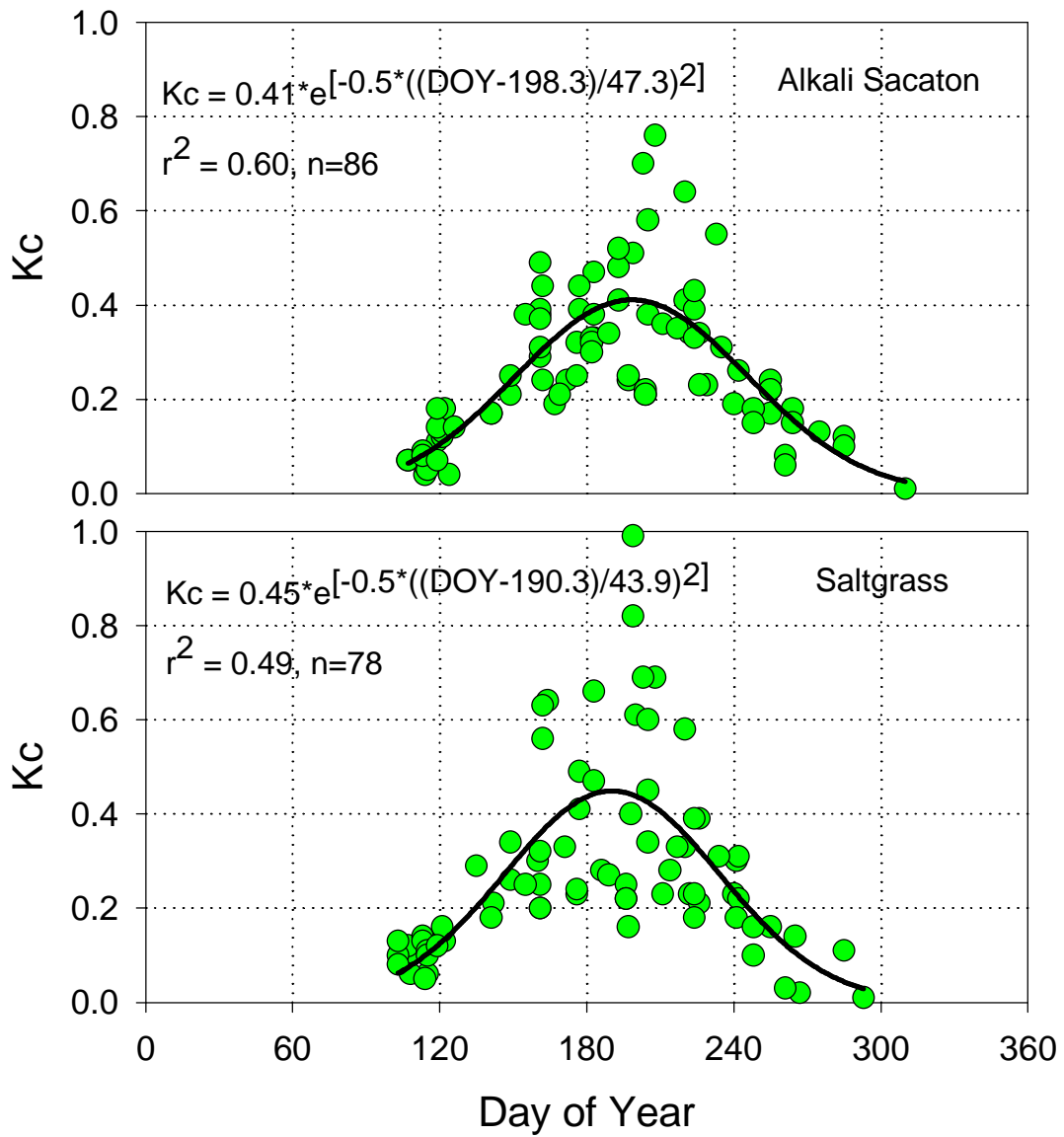


Figure 17. Transpiration coefficients ($K_{c_{ij}}$) and fitted models for saltgrass (*Distichlis spicata*) and alkali sacaton (*Sporobolus airoides*).

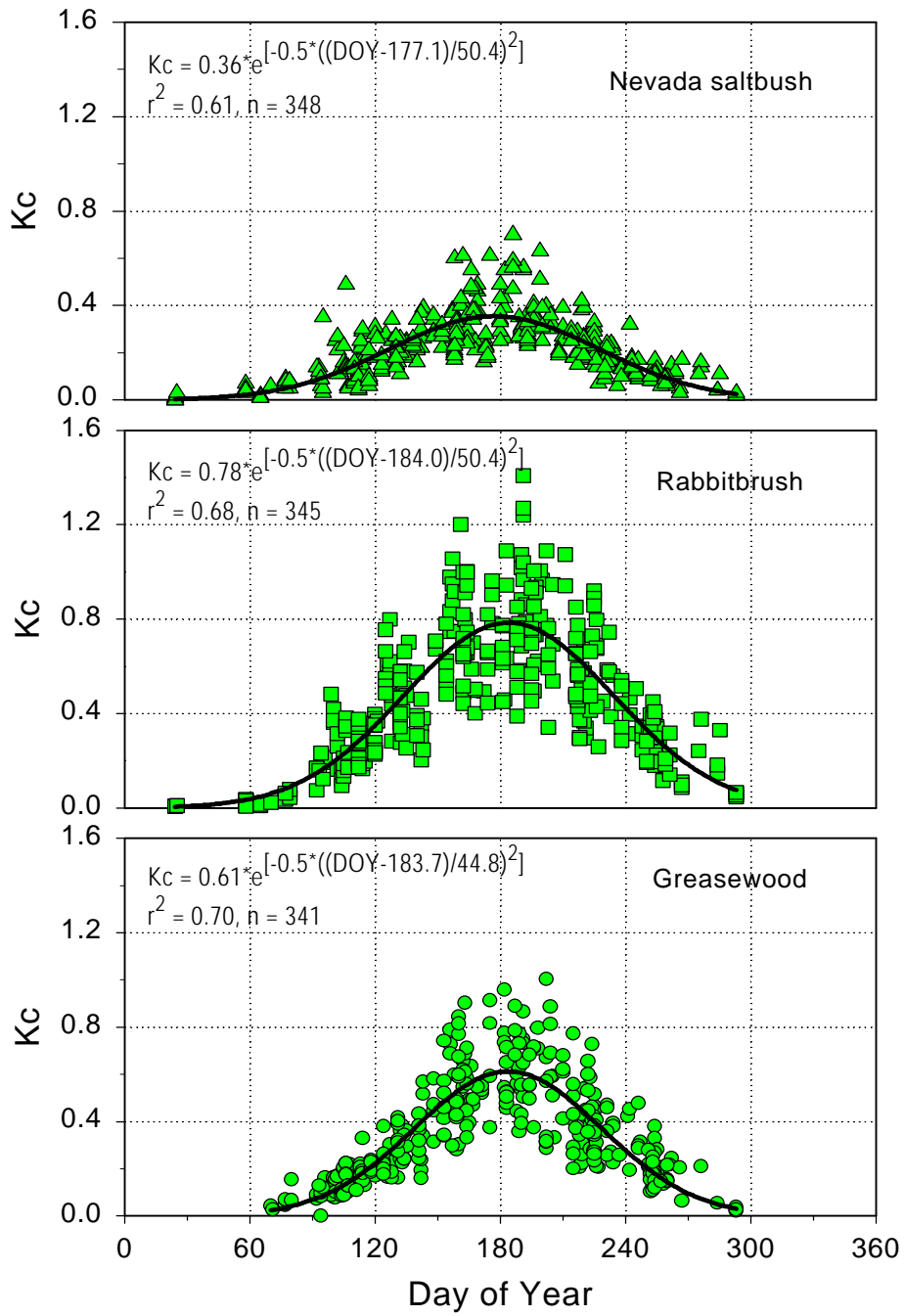


Figure 18. Transpiration coefficients ($K_{c_{ij}}$) and fitted models for Nevada saltbush (*Atriplex lentiformis* ssp. *torreyi*), rabbitbrush (*Chrysothamnus nauseosus*) and greasewood (*Sarcobatus vermiculatus*).

Table 9. Day of year for maximum LAI in the Kc models, the LAI sampling DOY used to determine T_{Kc} , and DOY of actual measured maximum LAI for the dominant species at each site.

Year	Site	Dominant species [^]	Kc LAI model maximum DOY	LAI sampling DOY	Measured LAI maximum DOY
2000	BLK 100	SPAI, DISP2	201, 189	189	188, 250
2001	BLK 100	SPAI, DISP2	201, 189	190	253, 220
	BLK 9	CHNA2, SPAI	184, 201	192	135, 165
	PLC 45	ATTO	163	162	162
2002	BLK 100	SPAI, DISP2	201, 189	191	217,154
	FSL 138	DISP, LETR5,JUBA	189, 201	190	190 (DISP2)
	PLC 18	CHNA2	184	190	154
	PLC 74	SAVE4, ATTO, DISP2	174, 163, 189	156	156,156,186
	PLC 185	SAVE4	174	156	128

[^]: grasses; SPAI, *Sporobolus airoides*; DISP2, *Distichlis spicata*; LETR5, *Leymus triticoides*. shrubs; JUBA, *Juncus Balticus*; CHNA2, *Chysothamnus nauseosus*; ATTO *Atriplex lentiformis* ssp. *torreyi*; SAVE4, *Sarcobatus vermiculatus*.

was apportioned among the species with Kc values based on their relative proportion of total LAI.

The ET record at all sites contained gaps due to instrument failure or was truncated before the end or after the beginning of the growing season. To prevent the comparison of measured and predicted fluxes from being confounded by the partial record, the EC data were fit to a Fourier model like that used to predict reference ET (ETr, described below). This model was chosen because of its demonstrated ability to model the seasonal changes in evaporative demand in the Owens Valley represented by ETr (Or and Groeneveld, 1994). Fitting the Fourier model also permitted site to site comparisons and year to year comparisons of transpiration between uniform limits for integration. Daily ET_{corr} was modeled using a Fourier series with two

harmonics using procedures described by Salas et al., (1980). ET_{corr} is the daily ET measured by the EC system corrected for the energy imbalance (described below). The first two harmonics series is given by,

$$\overline{ET_{corr}} = \langle ET_{corr} \rangle + \sum_{j=1}^2 \left[A(j) \cos\left(\frac{2\pi ij}{365}\right) + B(j) \sin\left(\frac{2\pi ij}{365}\right) \right] \quad (17)$$

where i is the day of year, $\langle ET_{corr} \rangle$ is mean daily ET for the entire year, $A(1)$, $A(2)$, $B(1)$, and $B(2)$ are model coefficients. Occasionally the fitted model was poorly constrained and gave negative values during winter when EC data were lacking. When this occurred, daily ET was assumed to be 0.01 mm day^{-1} and the model was revised. This procedure was largely for graphical purposes. The effect on the comparison with Kc models was negligible because only the daily ET or T values during the period with ET_{corr} data or during the growing season were summed.

Results and Discussion

Site characteristics

Depth to water measured at the EC sites is presented in Figures 19 to 23. Typically, the shallowest depth to water occurred in the spring (March or April) and declined to maximum depth at end of the growing season (October). FSL138 was an exception where maximum depth to water occurred in July and August. Water tables at all sites increased during the winter the vegetation was senescent. Test well 850T was installed at BLK100 in 2001, but based on the comparison with nearby test well 454T, DTW fluctuations were similar in all three years EC measurements were collected. No piezometer was located near PLC018 and PLC185. Soil water content at PLC018 at depth was nearly at limiting water content for sandy soil suggesting

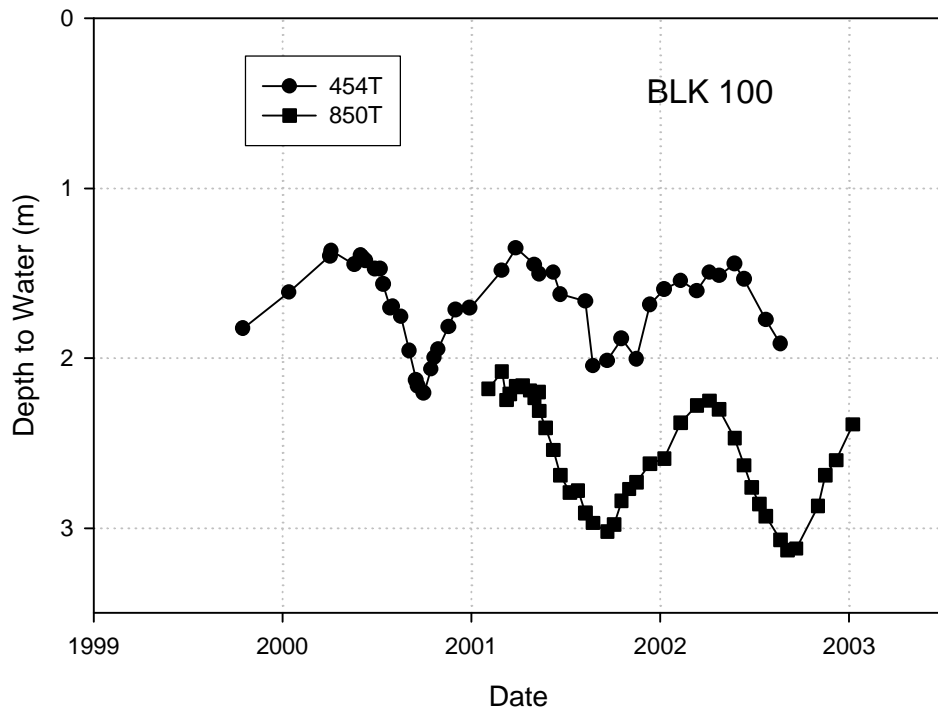


Figure 19. Depth to water in two test well located near BLK100. Test well 850T is adjacent to the EC station; 454T is located south east of the site, adjacent to the LA Aqueduct.

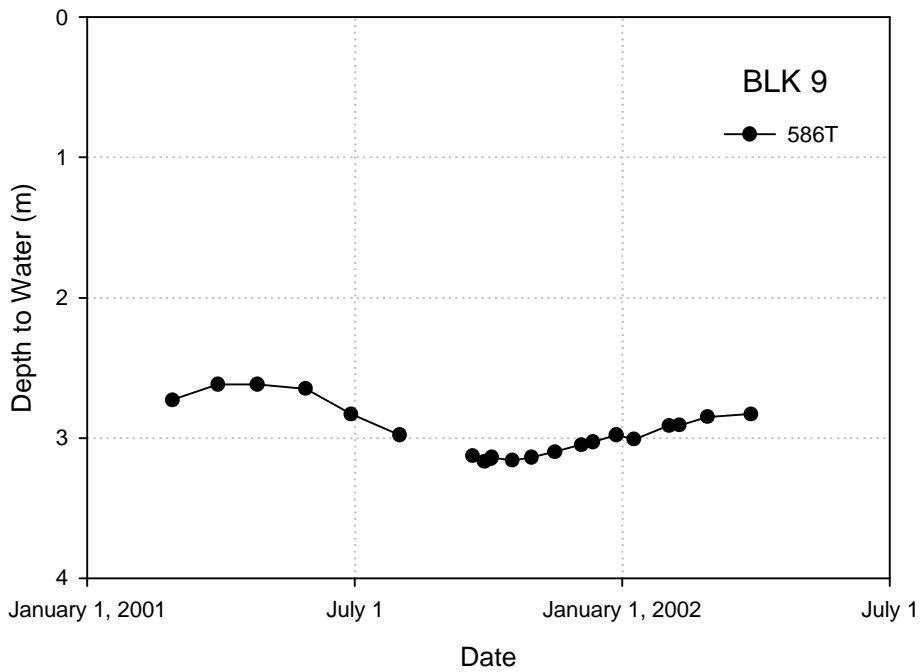


Figure 20. Depth to water in test well 586T located near BLK009.

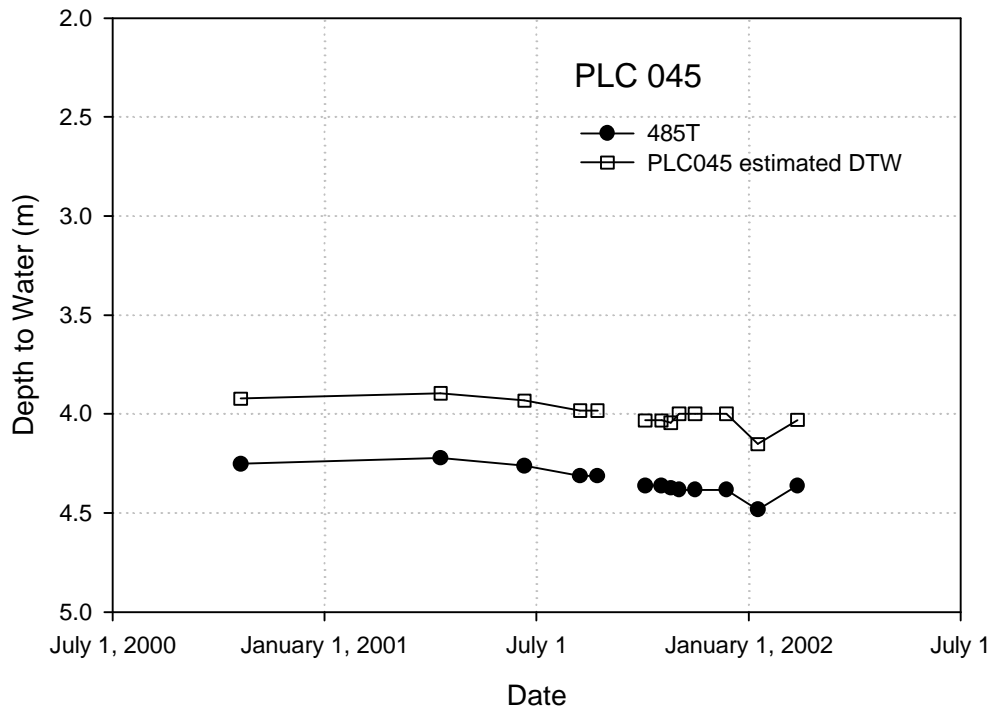


Figure 21. Depth to water in test well 485T located south of PLC045 and estimated DTW at PLC 045.

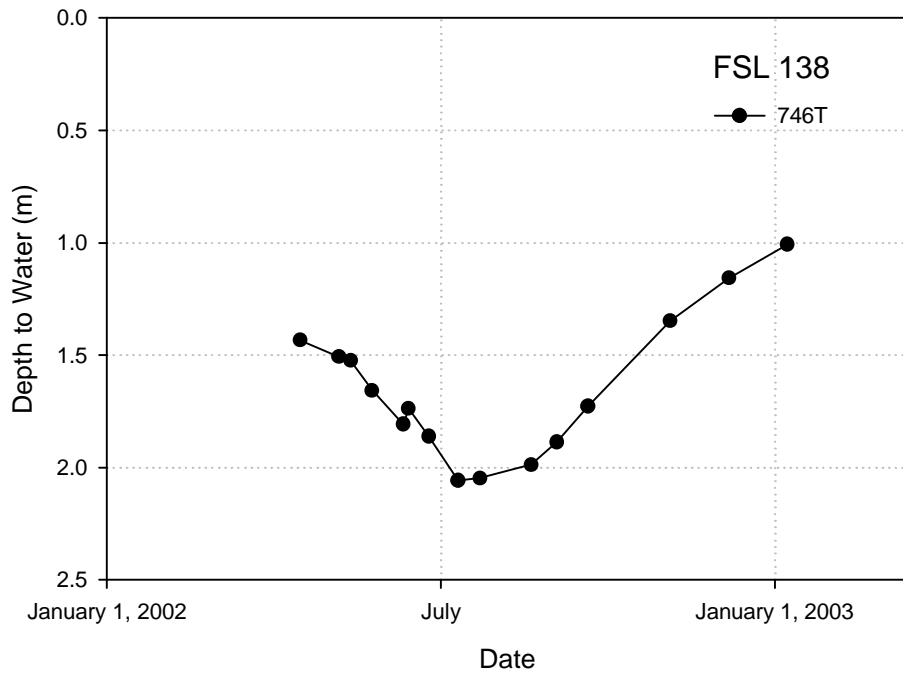


Figure 22. Depth to water in test well 746T located at FSL138.

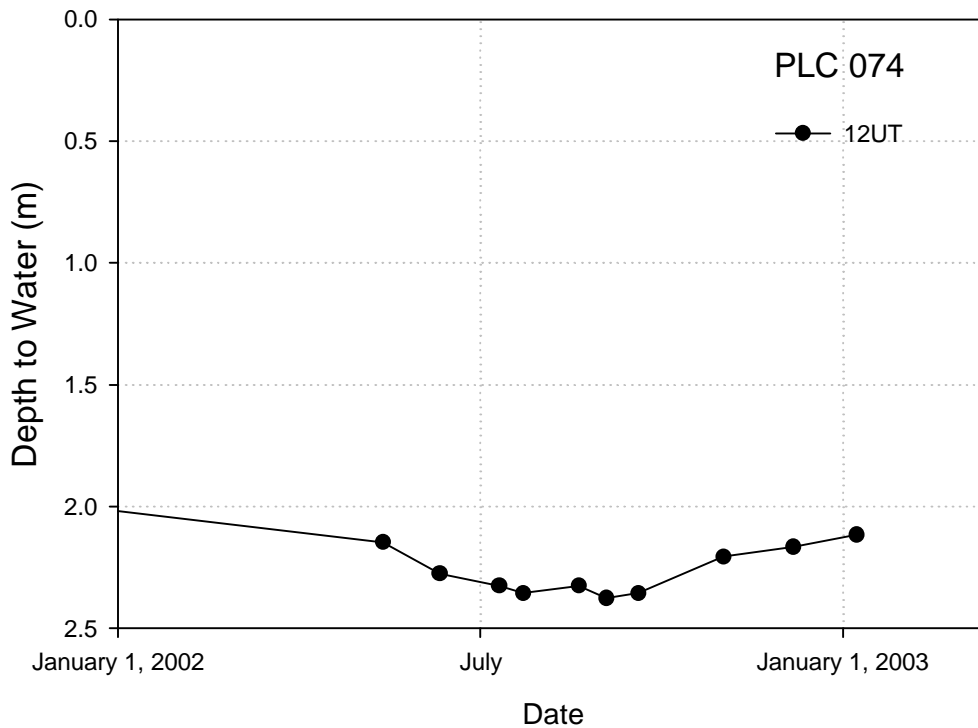


Figure 23. Depth to water in test well test well 12UT located at PLC074.

depth to water was always deeper than 5 m. The water table was encountered at PLC185 during access tube installation in the spring 2002. The water table was approximately 4 m which probably represents the high stand during the growing season. Depth to water at PLC045 was estimated from the initial water table depth (3.9m) observed during access tube installation and fluctuations observed at a test well 485T in similar vegetation 0.5 km from the site.

Precipitation preceding the growing seasons each year 2000-2002 consisted of small events, and total precipitation was below normal (about 130 mm) in all years (Table 6). Only two summer storms in July 2001 were of significant size during the project to affect either ET or LAI

measurements, and only at PLC045.

Soil water profiles collected at each access tube, including the shallow gravimetric measurements are presented in Figures 24 through 32. An example of spring, midsummer, and fall conditions are presented for each access tube. Even though estimates of limiting water content are not available, it is evident from the high values that ample soil water was available for plant uptake at sites BLK100 (all years), BLK009, and FSL138. Soil water content at BLK100 fluctuated throughout the profile reflecting the coupling with the water table fluctuations (i.e. capillarity and drainage) and plant uptake. The attempt to discriminate between these two processes is described in the vadose zone model section below. Tube 2 at BLK100 (1002) was located in a small 2m² slickspot nearly devoid of vegetation. At that location, θ in the upper 1.1 m was relatively constant except for precipitation/evaporation suggesting the importance of plant uptake in controlling soil water in the upper part of the soil at vegetated locations. The soil at BLK009 can be divided into three zones. Above 0.9 m, the soil was affected by infiltrating rain. Soil water content was relatively static at intermediate depths (0.90 to 1.50-2.00 m depending on location). Below the intermediate zone, soil water was coupled to water table fluctuations. At PLC045, soil water increased to 0.50-0.90 m due to winter and summer rains, but below 0.9 m, θ was less than 5% which is approximately the limiting value expected for sandy soils (McCuen et al., 1981). The extreme limit of capillarity above the water table extended to 3.2 m during access tube installation in early spring. Soil water at PLC018 was dry similar to PLC045 except the limit of capillarity was below the deepest monitoring depth of 4.7 m. PLC074 also had very sandy soils (Appendix B), but the water table was relatively

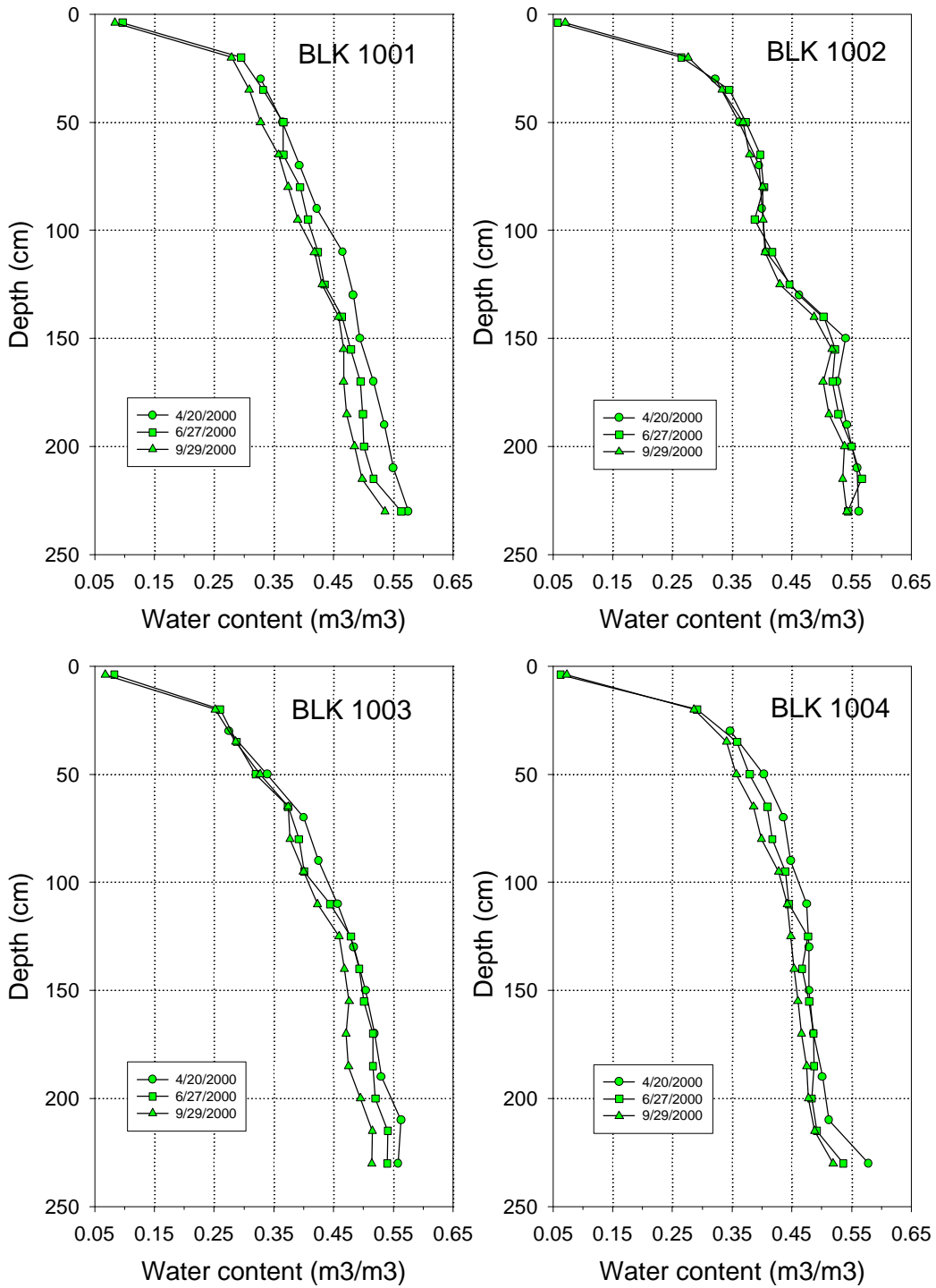


Figure 24. Soil water content θ profiles for spring, summer, and fall conditions in four access tubes at BLK100 in 2000.

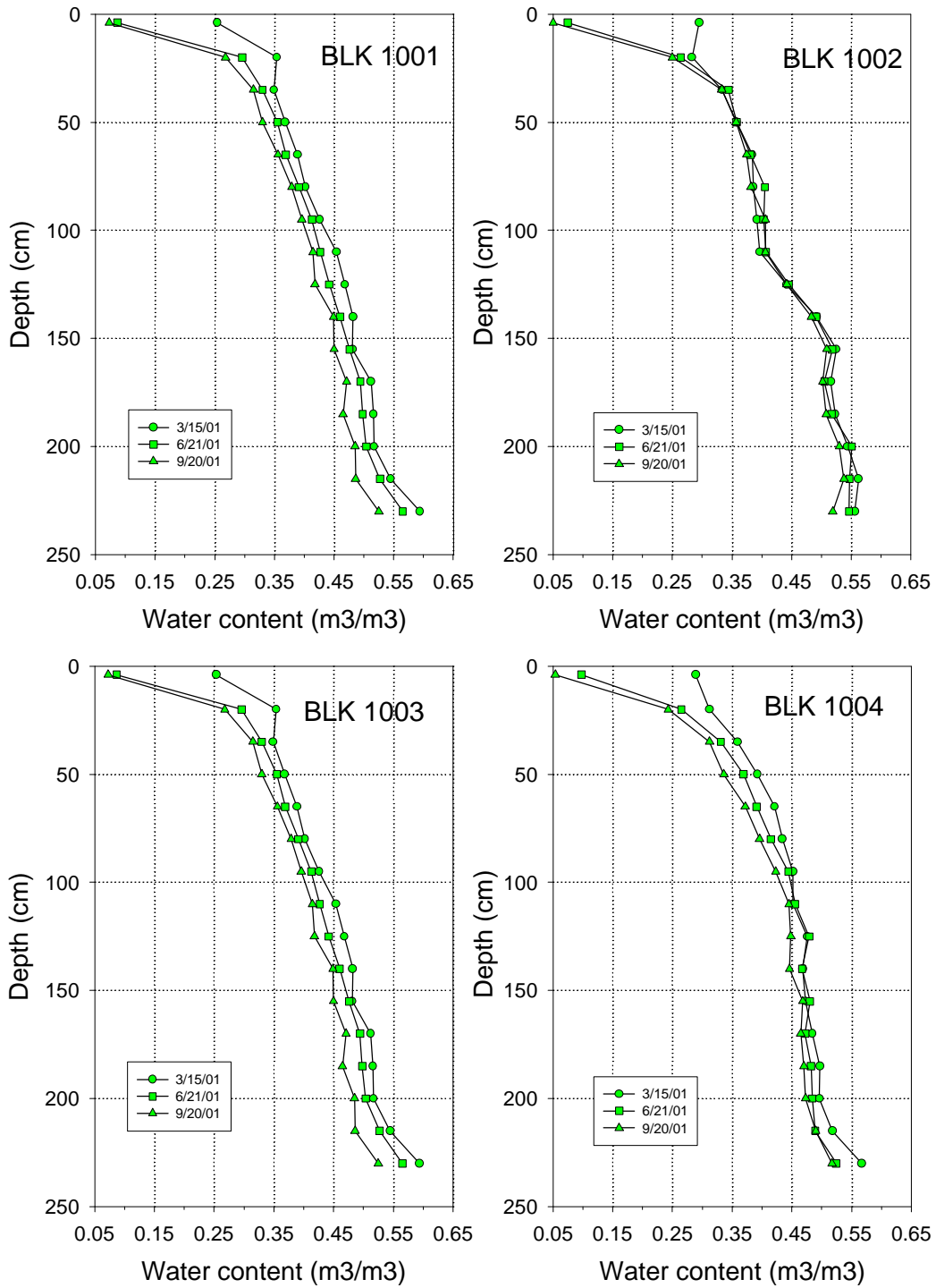


Figure 25. Soil water content 2 profiles for spring, summer, and fall conditions in four access tubes at BLK100 in 2001.

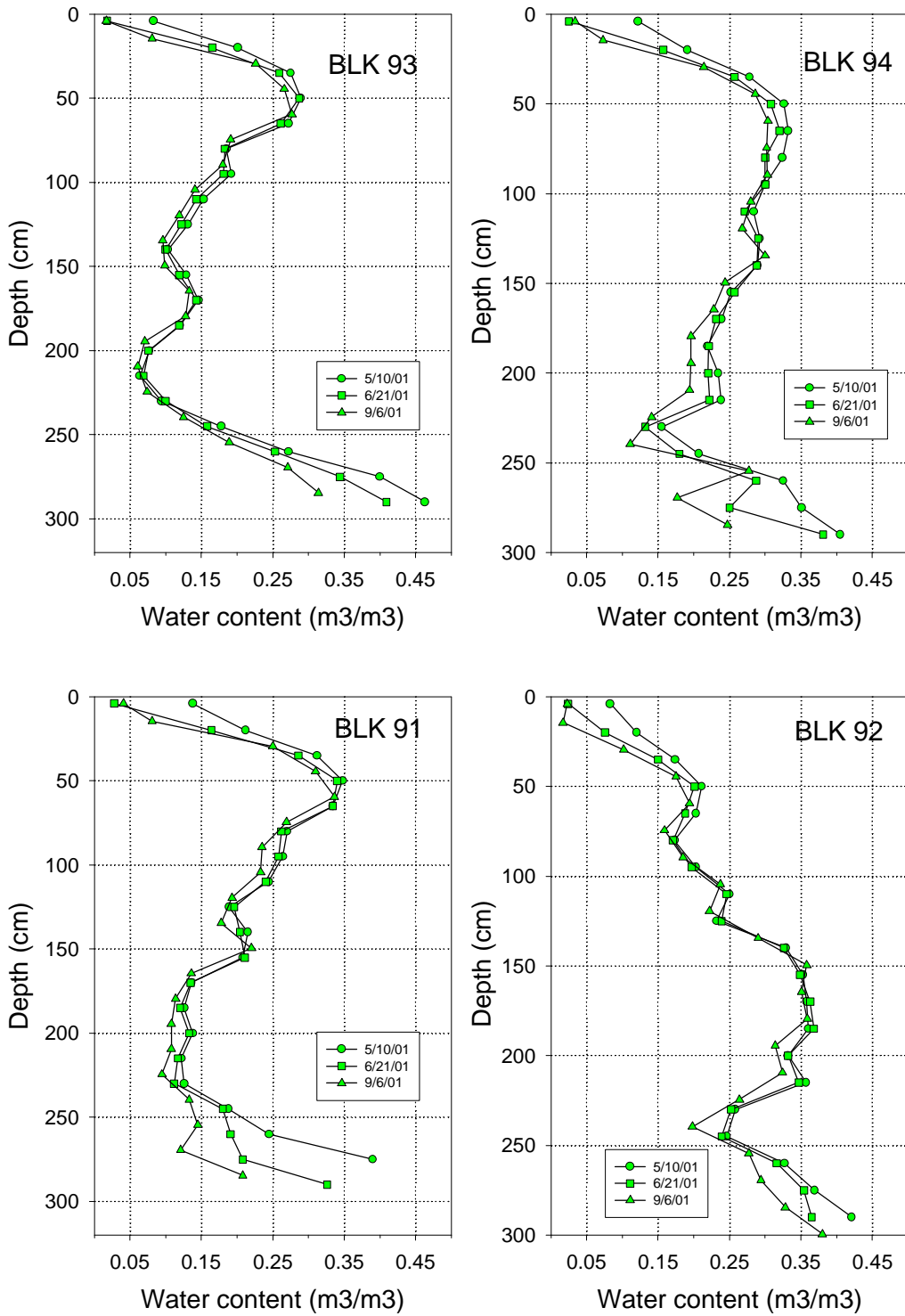


Figure 26. Soil water content 2 profiles for spring, summer, and fall conditions in four access tubes at BLK009 in 2001.

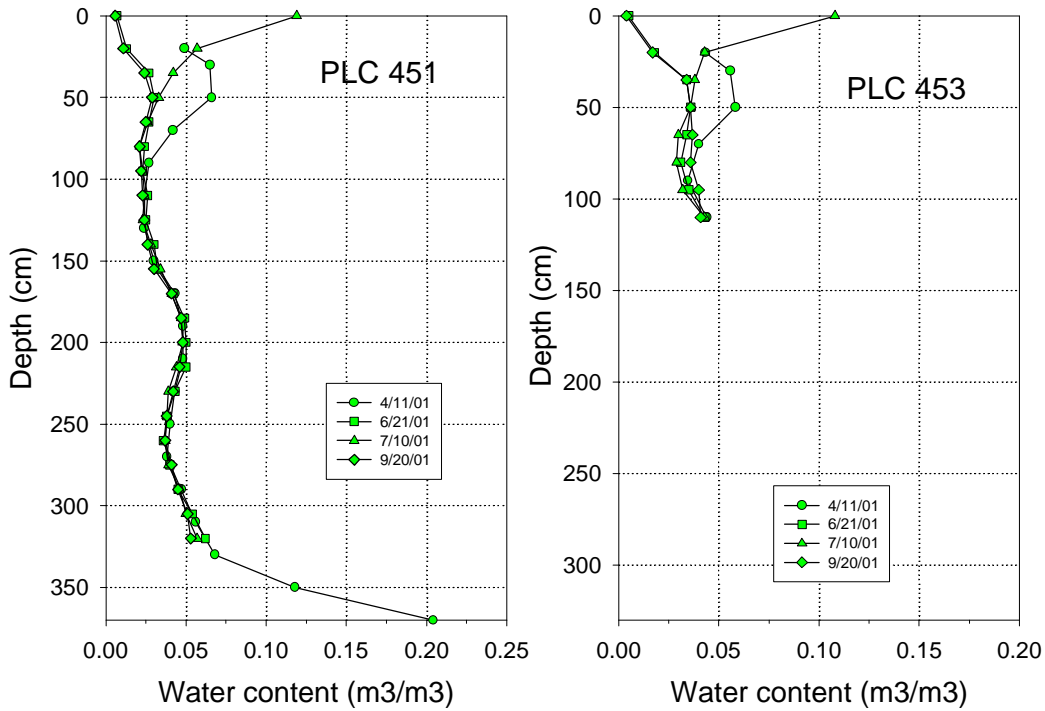


Figure 27. Soil water content 2 profiles for spring, summer, and fall conditions in two access tubes at PLC045 in 2001.

shallow (<3 m) and probably accessible to the vegetation. At two locations, the upper 1 m was relatively dry and decoupled from water table changes (Figure 31). At two other locations (tubes 742 and 744), soil water contents in the upper and lower profile were above limiting water contents and was difficult to distinguish whether the upper 1 m was coupled with the water table or whether it reflected uptake of precipitation-derived soil water. All locations were coupled to water table fluctuations at depths below 1 to 1.5 m. Like BLK009, the soil at PLC185 can be divided into three zones based on observed soil water fluctuations. Soil at PLC185 was dry in the upper 1 m except for precipitation inputs. Intermediate depths from 1 m to approximately 2.7

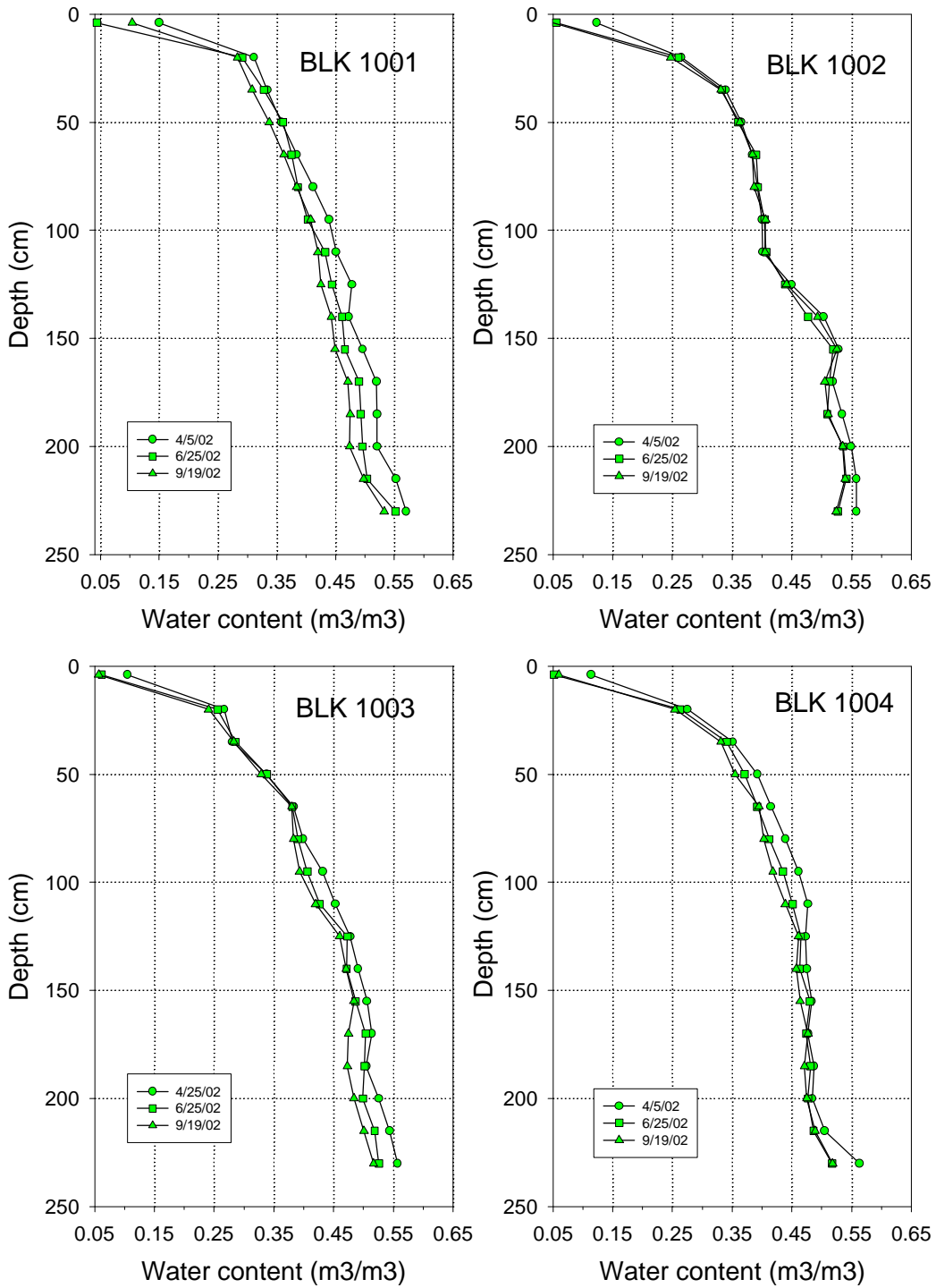


Figure 28. Soil water content θ profiles for spring, summer, and fall conditions in four access tubes at BLK100 in 2002.

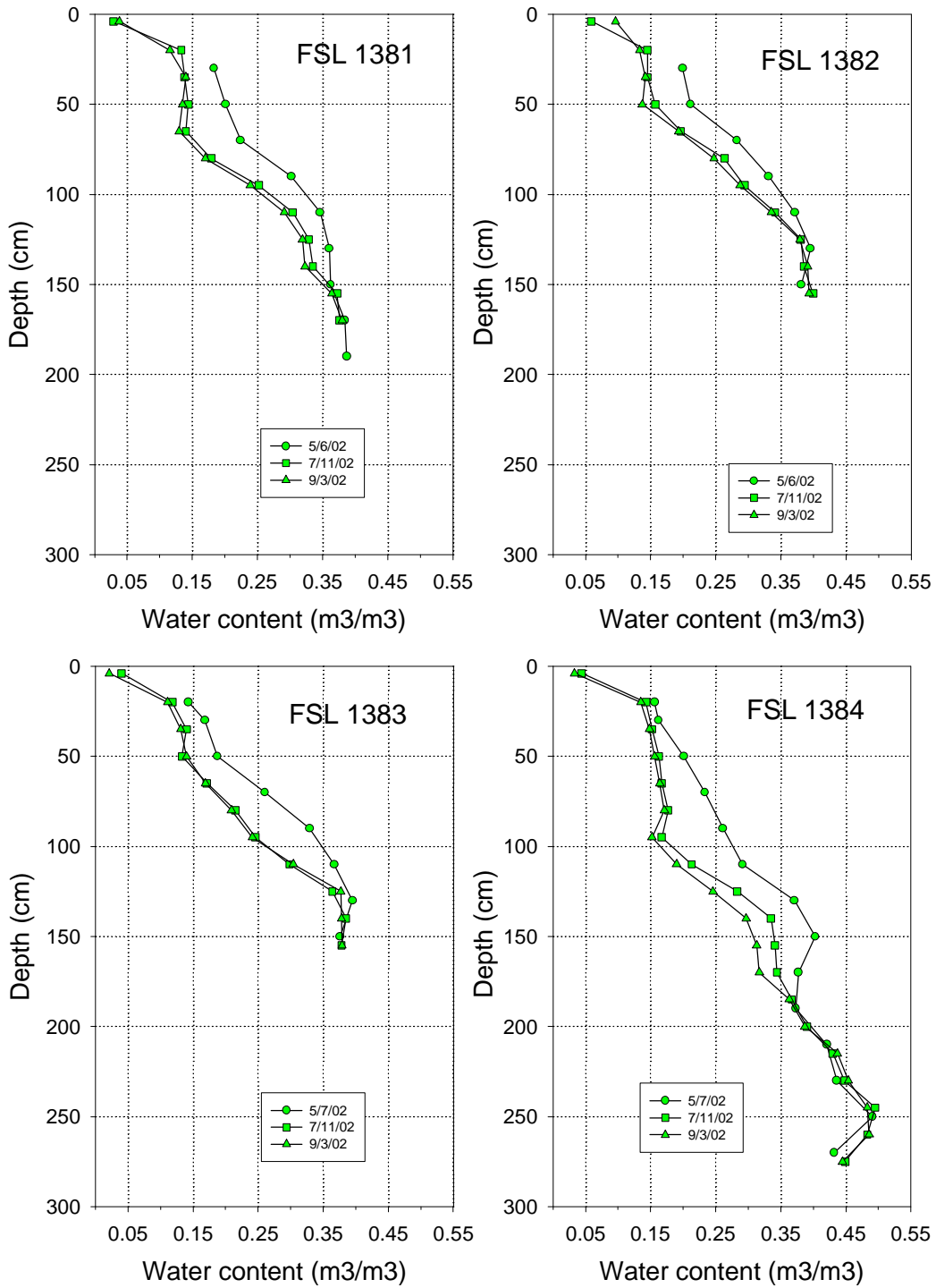


Figure 29. Soil water content 2 profiles for spring, summer, and fall conditions in four access tubes at FSL138 in 2002.

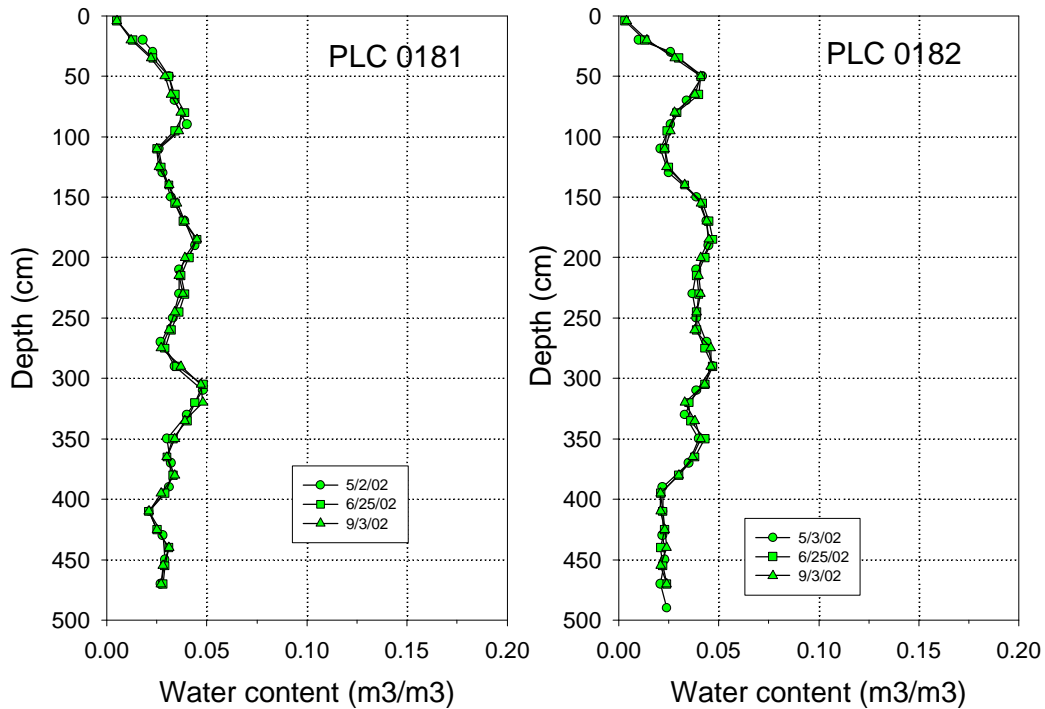


Figure 30. Soil water content 2 profiles for spring, summer, and fall conditions in two access tubes at PLC018 in 2002.

to 3.0 m, depending on location had nearly constant water content that varied according to soil texture (higher in finer textured soil). Under the drought conditions of 2002, water in this zone evidently was not available for uptake or uptake at this low cover site was negligible. At lower depths, soil water fluctuations were coupled to water table fluctuations, although the coupling was weak for two of the three locations.

Leaf area index (all species) differed between sites with wet and dry soils (Figure 33). At sites with deeper water tables and/or dry sandy soils (PLC045, PLC018, PLC074, and PLC185), LAI was small and peaked in the first two weeks of June. LAI at shallow water table sites with

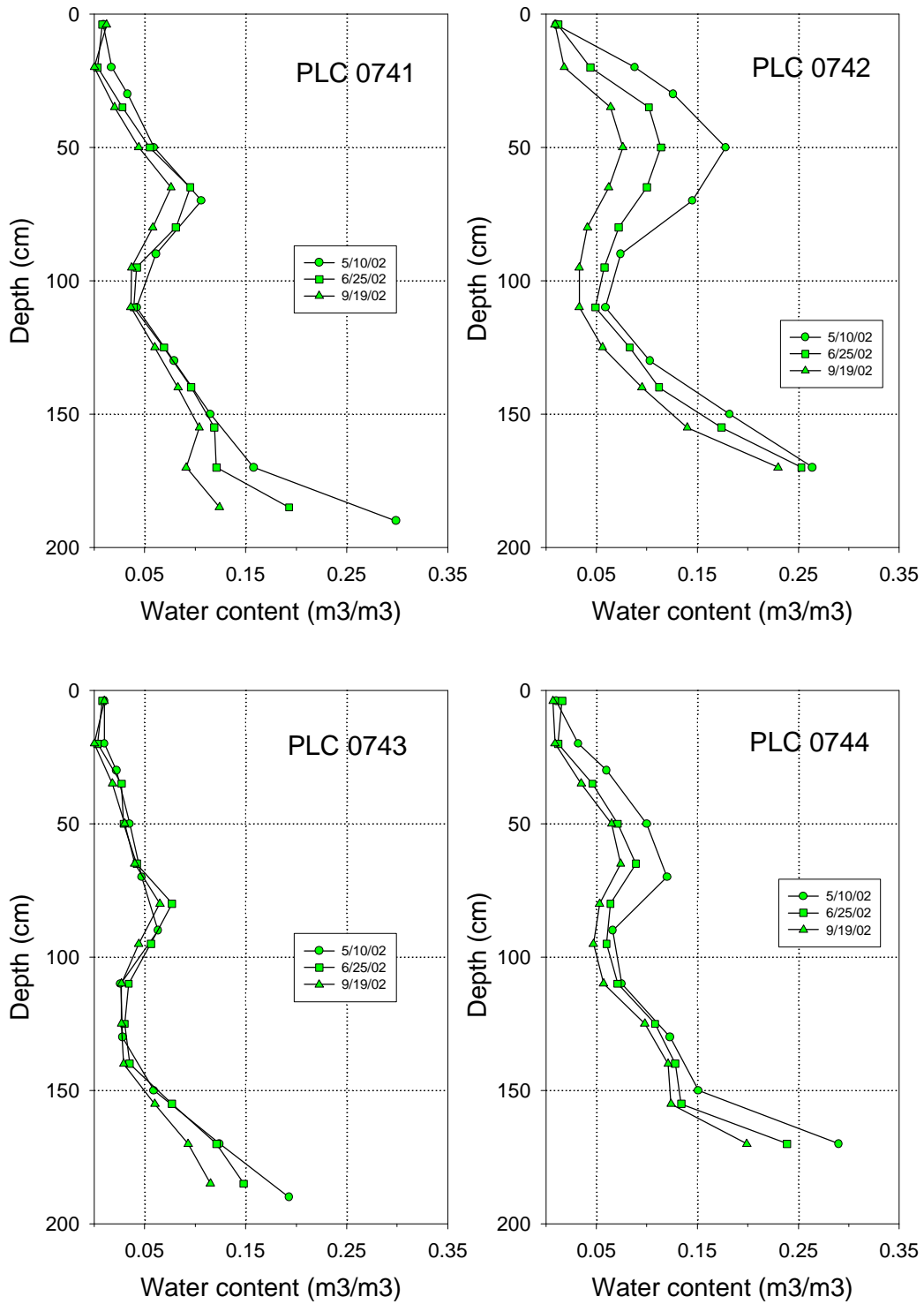


Figure 31. Soil water content 2 profiles for spring, summer, and fall conditions in four access tubes at BLK074 in 2002.

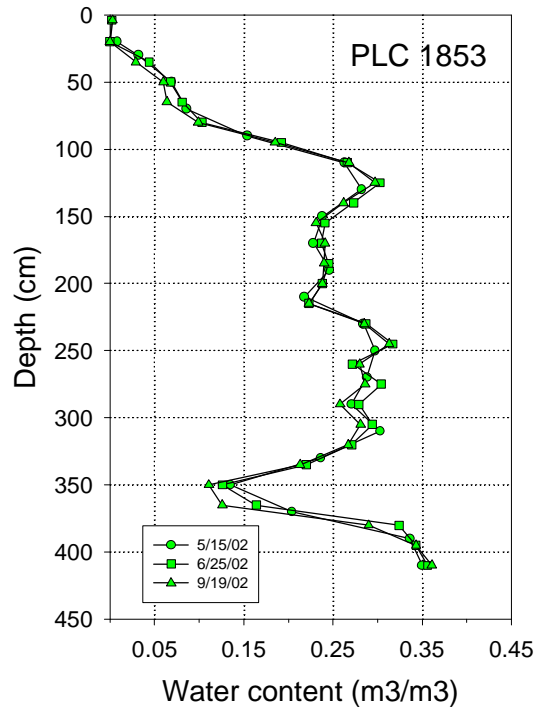
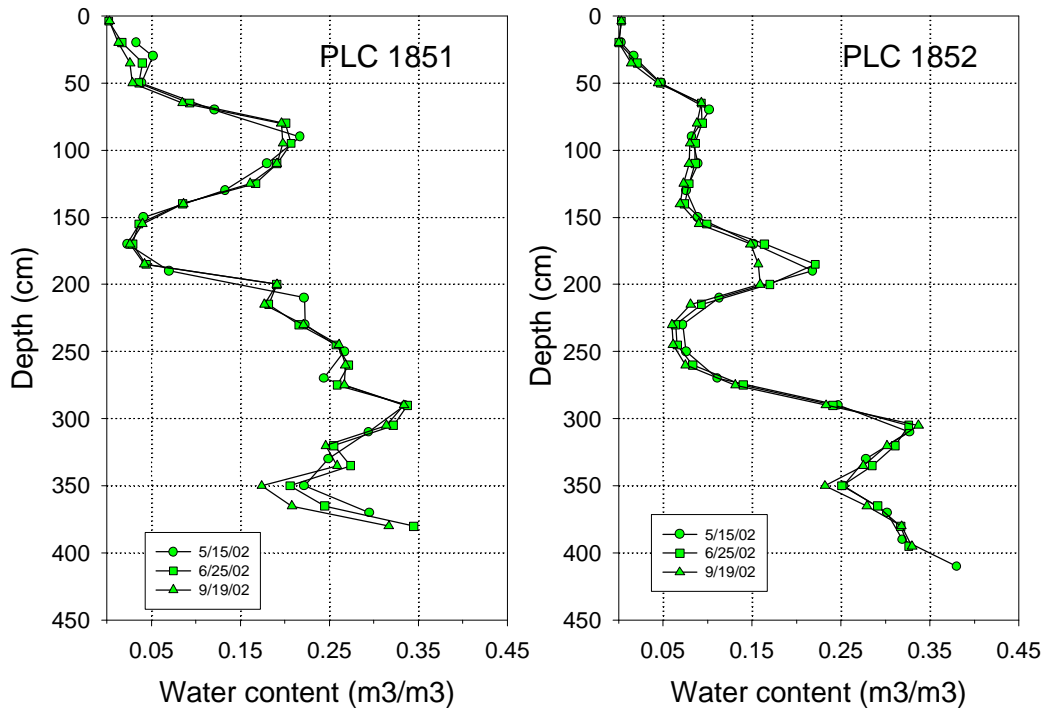


Figure 32. Soil water content **2** profiles for spring, summer, and fall conditions in three access tubes at PLC182 in 2002.

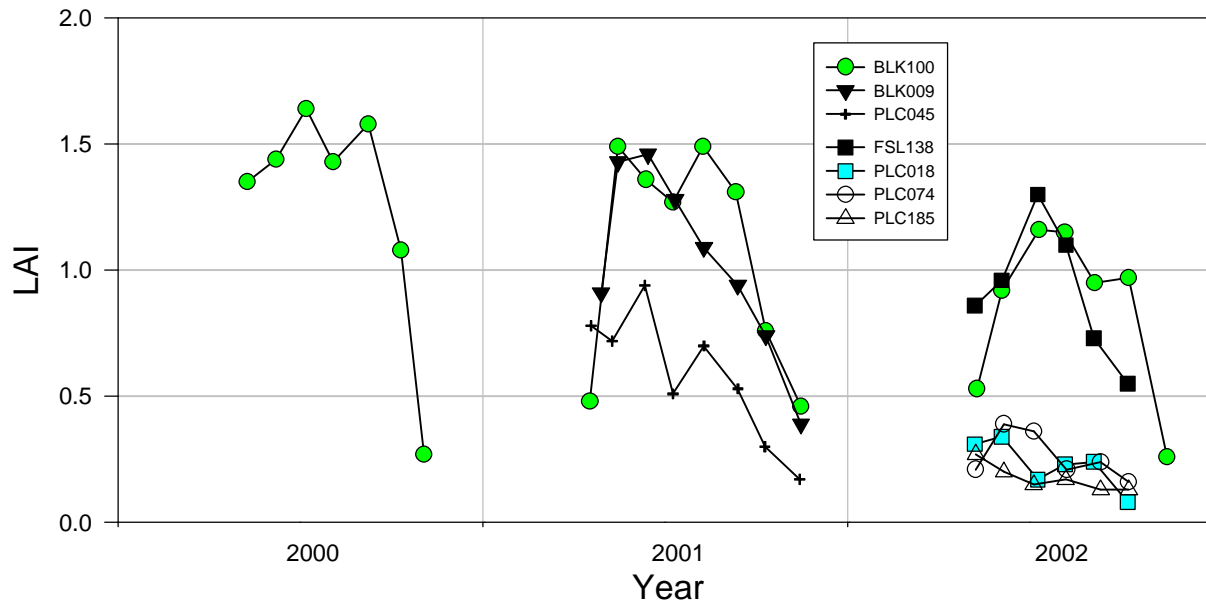


Figure 33. LAI for all sites. Values are the average of four transects.

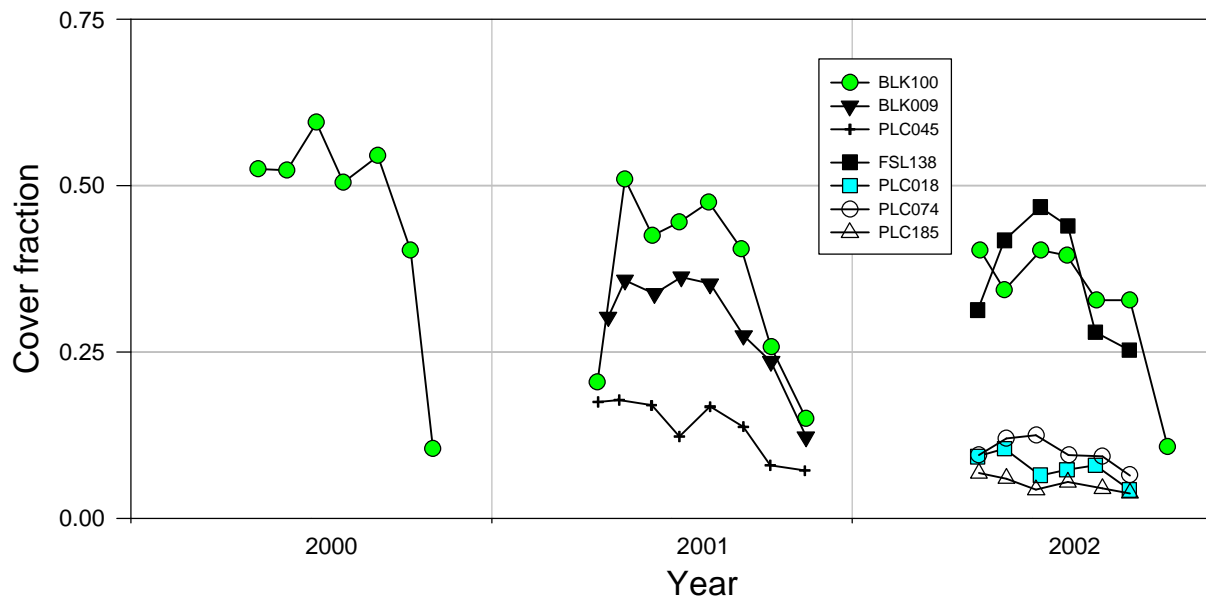


Figure 34. Plant cover of all species (fraction) for all sites. Values are the average of four transects.

relatively wet soils was greater and peaked later in the summer, usually the first week in July. Typically, BLK100 maintained a high leaf area through June, July, and August before declining in September (2000 and 2001) or October (2002). In contrast, FSL138 and BLK009 declined steadily after the peak LAI was attained in June (BLK009) or July (FSL138). Trends in plant cover closely tracked LAI (Figure 34) which was expected given the linear relationship between the quantities (Steinwand, 1999a and b).

EC energy balance components and closure

An example of half-hourly *EB* for the EC system at BLK 100 for several days in 2002 is given in Figure 35. *EB* ranged from (rarely) near zero to over 100 W m^{-2} with a mean *EB* closure error over the period of 43.9 W m^{-2} . Mean available energy during this period was 124.0 W m^{-2} , thus the turbulent fluxes did not account for over one-third of the available energy. During DOY 238, the energy balance closure error was greater than 150 W m^{-2} . The closure error tends to be highest during the afternoon, but persisted throughout the day. Comparison of Figures 35 and 36 shows that the *EB* error tends to be largest during periods of relatively higher wind speeds in the afternoon. The linear correlation coefficient between the horizontal wind speed and the *EB* error was $r = 0.46$. Except for DOY 238, winds were from the southeast during the afternoon, which should be the most favorable wind direction for the EC instruments, therefore the *EB* error maxima do not appear to be attributable to disruption of the flow by the sensors and mounting structure. The peak *EB* closure error occurred on DOY 238, and flow distortion may have contributed to the error that day.

For all sites, the mean *EB* calculated on a daily basis ranged from 56 to 75% (Figures 37 to 40). Highly erratic values of *EB* occurred before and after the growing season

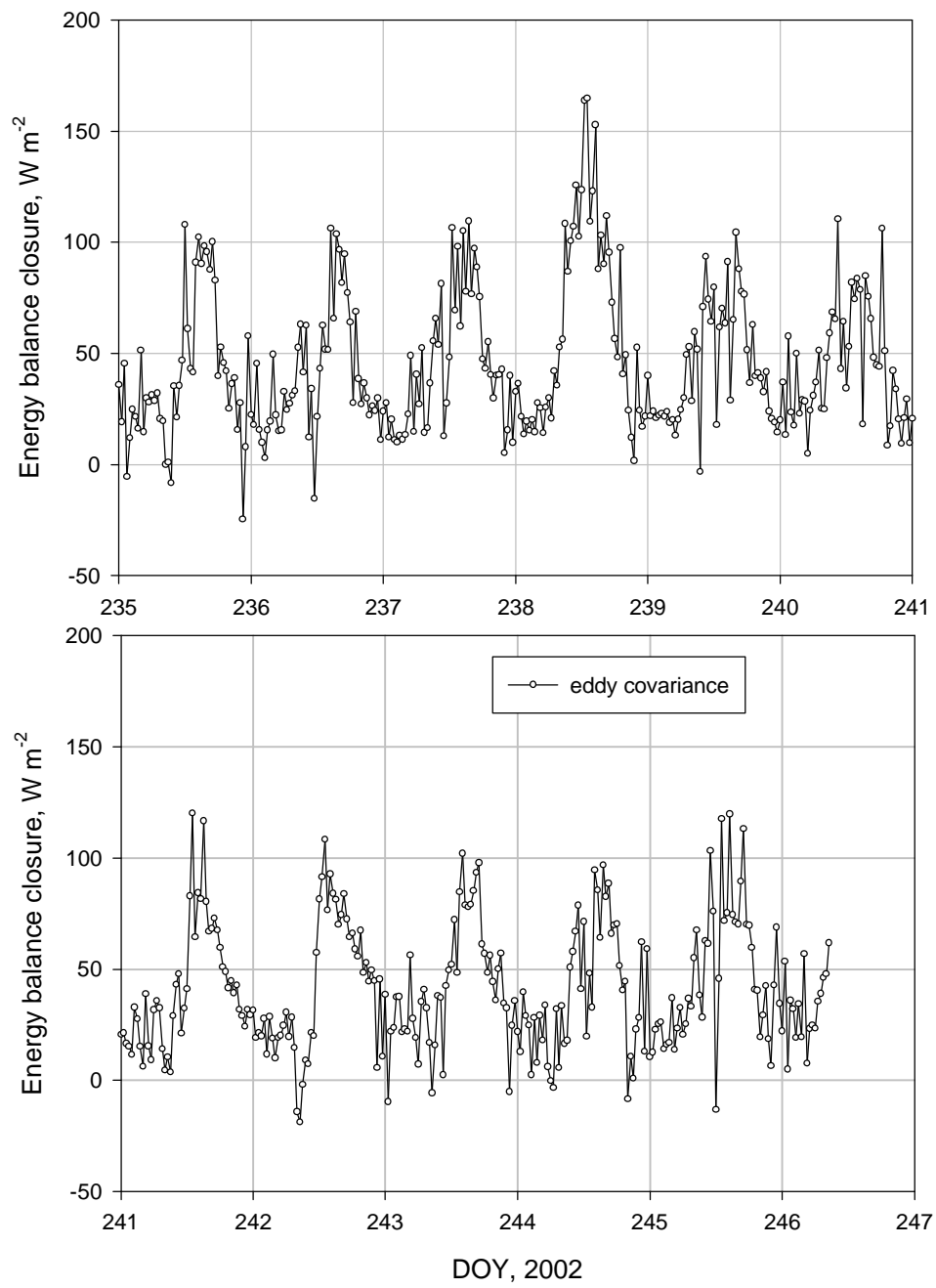


Figure 35. Example of the energy balance closure error for EC system on half hourly basis at BLK 100 during the period of BR system operation.

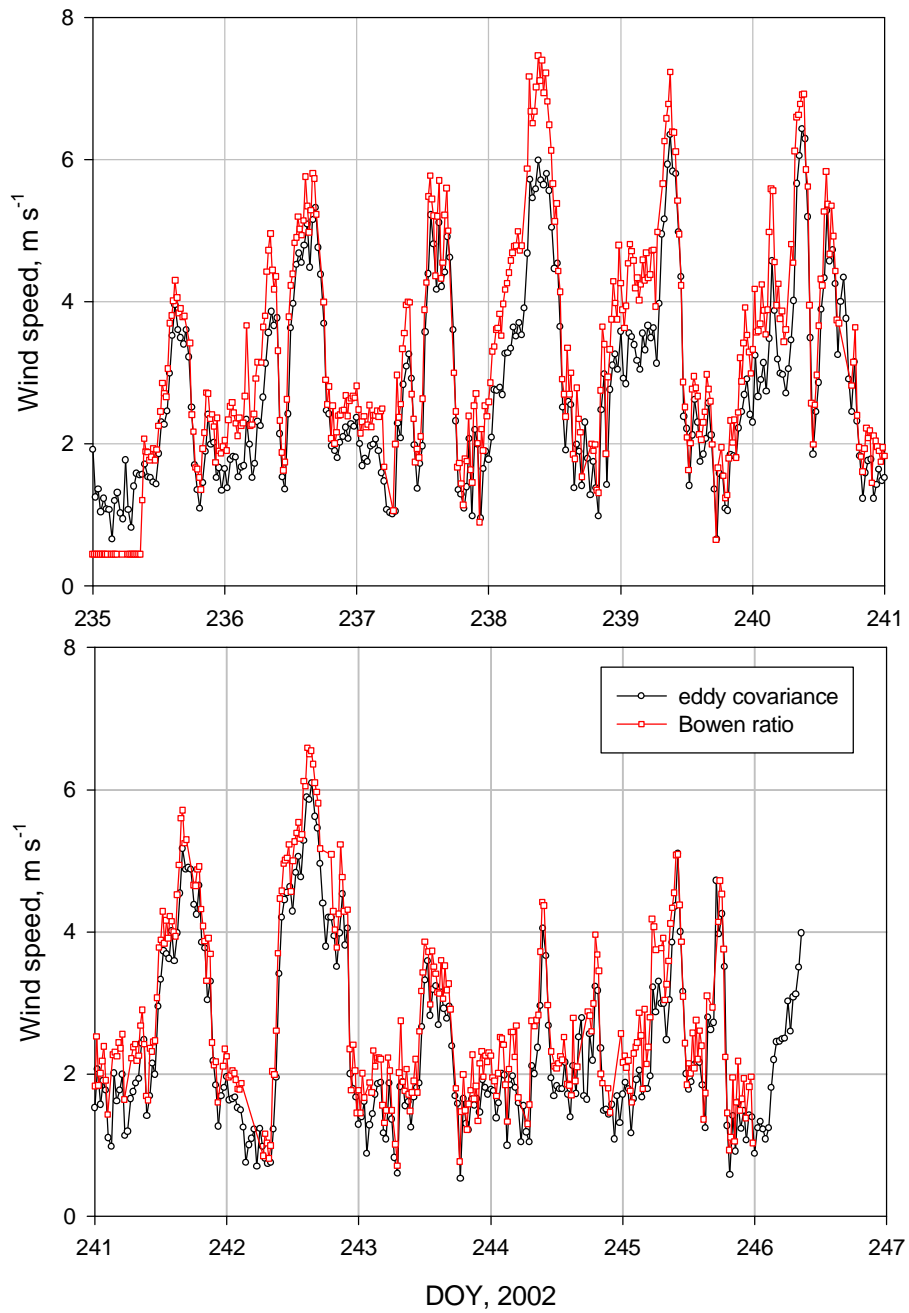


Figure 36. Wind speed at BLK 100 measured with eddy covariance and Bowen Ratio instruments in 2002.

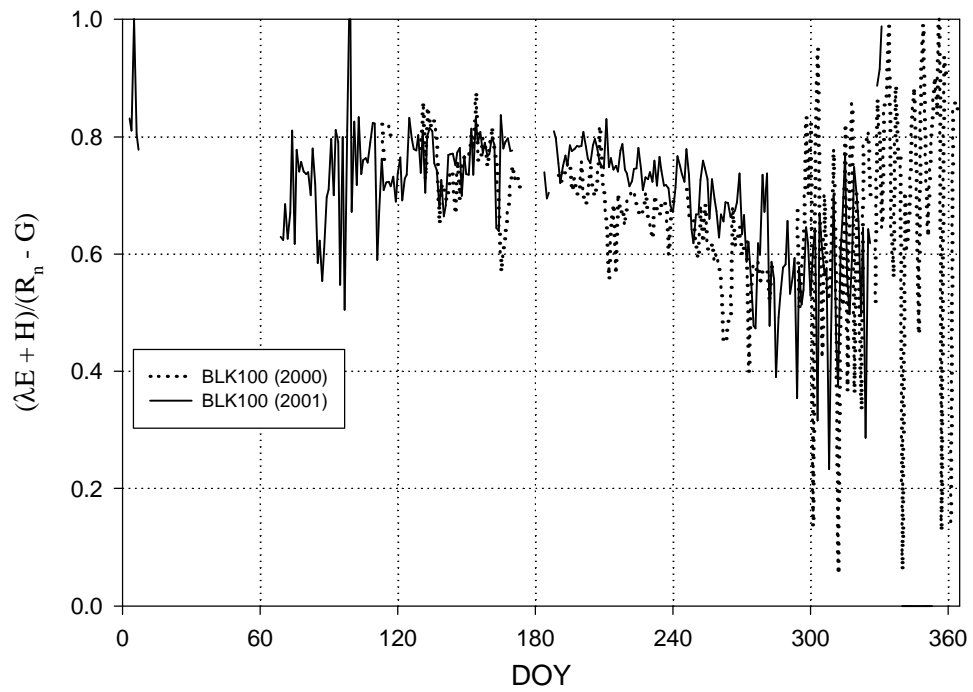


Figure 37. *EB* for BLK100 in 2000 and 2001.

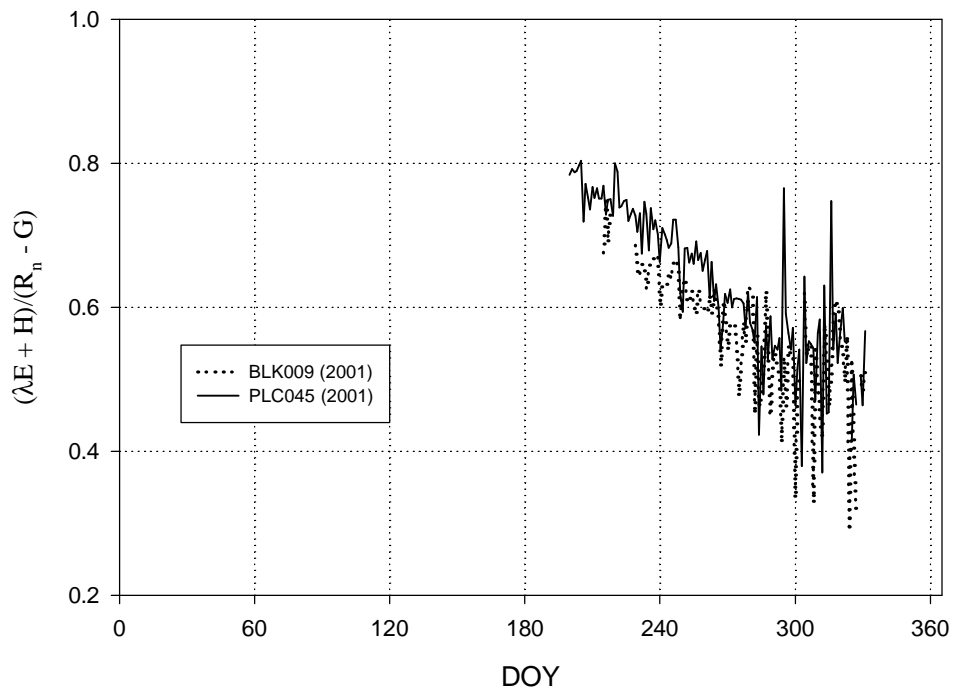


Figure 38. *EB* for BLK009 and BLK045 in 2001.

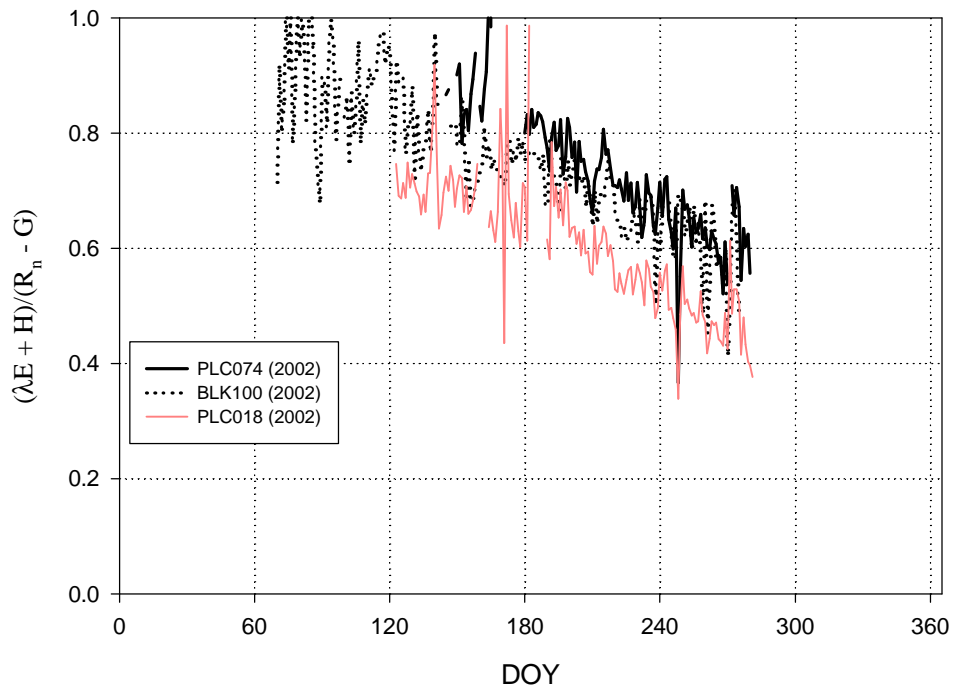


Figure 39. *EB* for PLC018, PLC074 and BLK100 in 2002.

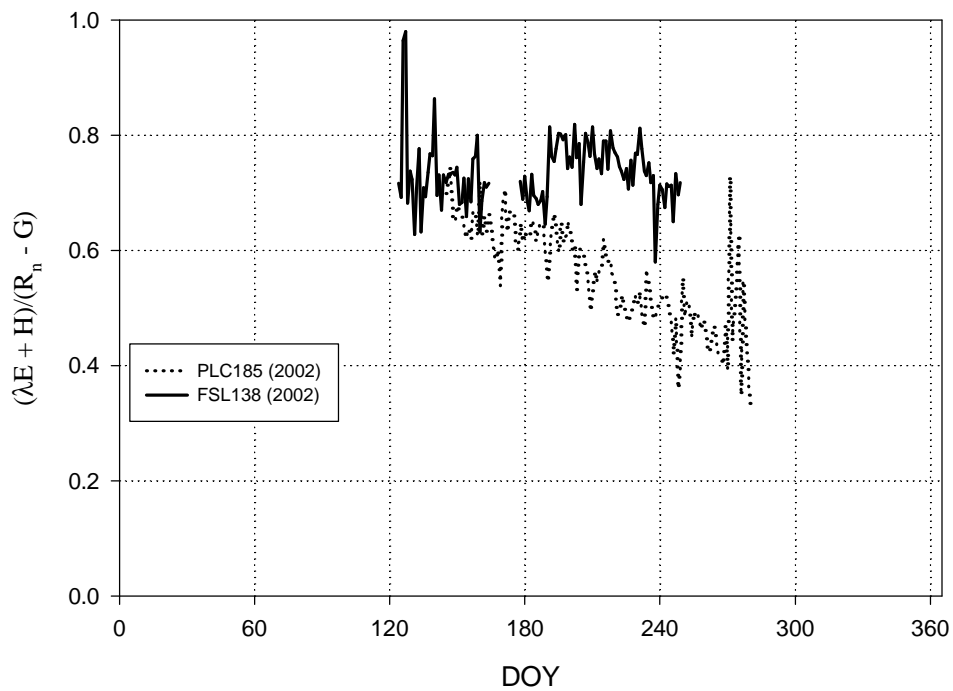


Figure 40. *EB* for PLC185 and FSL138 in 2002.

(84>DOY>288) when all the fluxes were relatively small. Generally, the closure error was least early in the growing season and increased approximately 20% by the end of the season. The increase in closure error usually began about midsummer (DOY 186) and was not evident before or after the growing season. Changes in EB seem related to H or IE individually or in combination rather than calibration drift, but the relationship is not understood. Interestingly, the EB trend at FSL138 was not similar to trends evident at other sites. The closure error at FSL138 was relatively stable except for a sharp decrease about DOY 191 that corresponded with a sudden decrease in IE suggesting the closure error was related to IE . At other sites, however, the late summer increase in the closure error was more gradual and increased as IE decreased.

Failure of EC systems to achieve EB closure has been observed in other studies, and various instrumental or theoretical explanations have been put forth. Zeller et al. (1989) and Massman et al. (1990) examined sources of error in EC turbulent flux measurements due to mismatches in sensor response times, sensor volume or line averaging effects, flow distortion around sensors and mounting structures, spatial separation of sensors, and sampling rate (aliasing) effects. Each source of error tends to reduce the covariance measured by the EC system, thereby causing the turbulent fluxes to be underestimated. After implementing corrections for each of these sources of error, their energy balance still failed to achieve closure, which they attributed to inaccuracy of the measurement of R_n and G .

In the event of non-closure of the energy balance, there are various strategies to correct the EC fluxes. Besides the formal frequency domain transfer function corrections used by Zeller et al. (1989) and Massman et al. (1990), several simple ad hoc corrections based on Equation 3

can be made, the choice of which depends on the suspected source of error. If the error is in the measurement of available energy, then no correction is necessary to the turbulent fluxes. If the error due to the hygrometer, energy balance can be achieved by assuming all the error is in the latent heat term. If the error is due to the sonic anemometer or due to a loss of covariance that affects H and IE in similar proportions, the turbulent fluxes can be corrected by assuming that b is measured correctly and adjusting the magnitude of the turbulent fluxes such that energy balance is achieved.

Examination of the EB from other EC systems operated as part of this project revealed that EB closure errors of similar magnitude as occur at sites with minimal ET (e.g. PLC018, Figure 39) suggesting that both turbulent fluxes are underestimated. Also, ET measured by the EC system at all sites was near 0 W m^{-2} during nighttime, as would be expected for the dry soil surface present at the site. Therefore, though the error may have been partly due to the hygrometer, ascribing the EB error solely to the IE term was unwarranted.

b measured with the BR and EC systems agrees during daylight hours, except at times when the BR system produced large erratic values (Figure 41). The b values are comparable between the two systems during the morning hours, climbing to a midday peak of ~ 1.7 , then during the afternoon hours BR b often grow very large while the EC b smoothly decline from their midday peak. The large afternoon b sometimes measured by the BR system are considered erroneous, because the clear dry conditions during the measurement period should produce smoothly varying b during daylight hours. The cause of these erroneous measurements is unknown. During periods of afternoon winds, the BR system often yielded unstable large

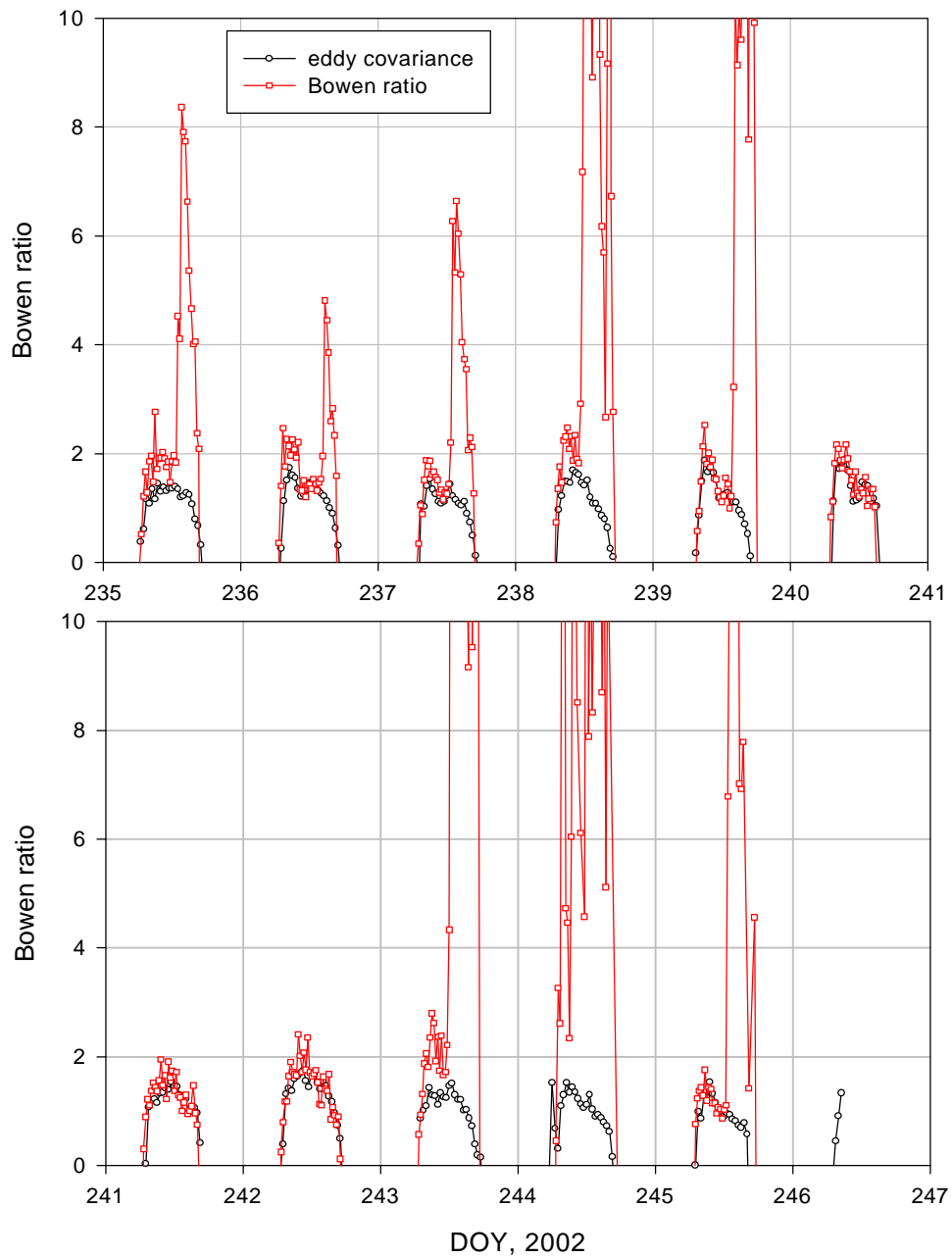


Figure 41. Daytime Bowen ratio (H/IE) at BLK100 measured with eddy covariance and Bowen Ratio instruments in 2002. Only daytime b are shown because for either system, nighttime b tended to be highly erratic due to the small magnitude and variable sign of IE .

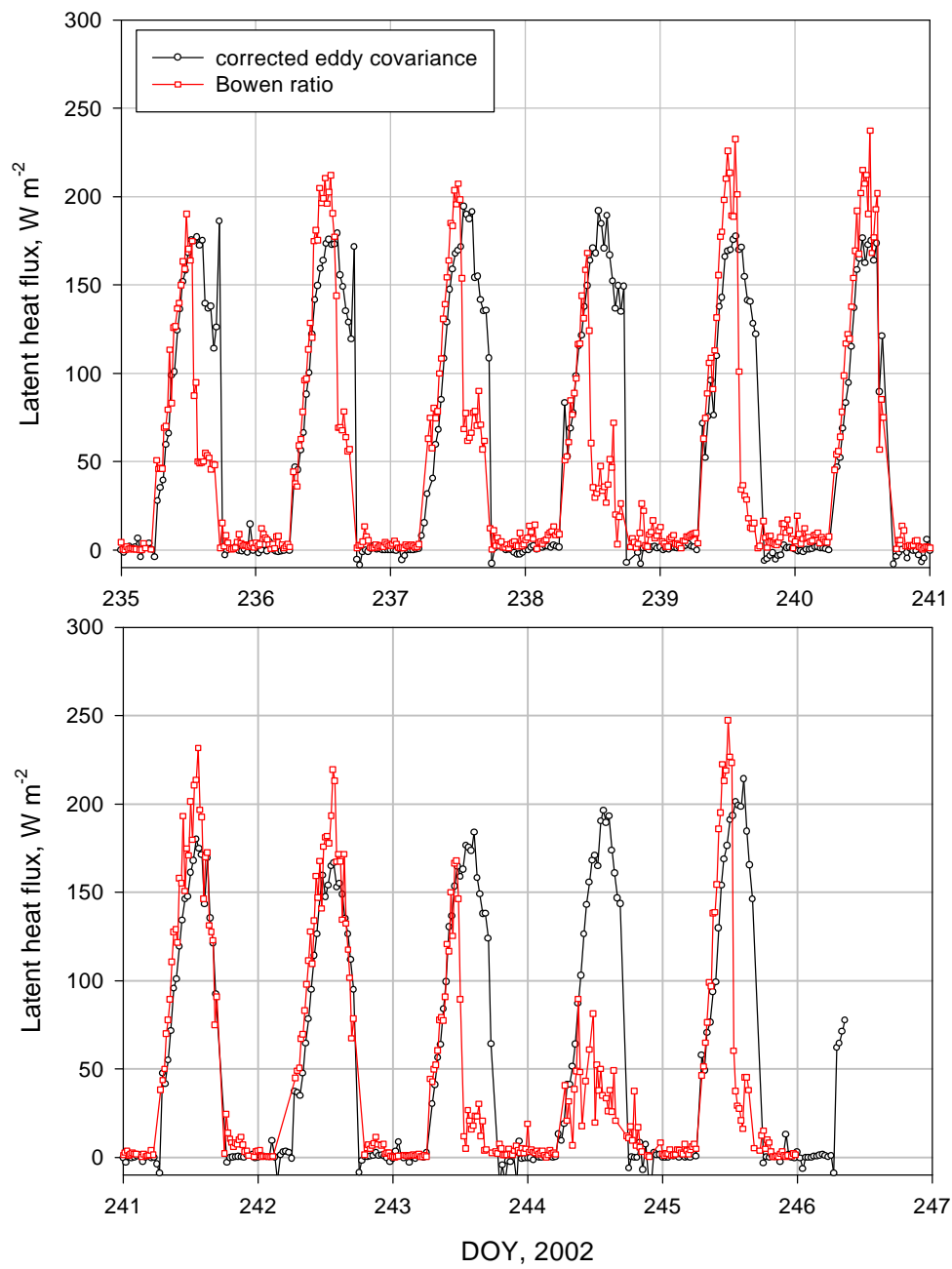


Figure 42. Latent heat flux at BLK 100 measured with eddy covariance and Bowen Ratio instruments in 2002. EC latent heat flux has been corrected using Equation 18.

Bowen ratios. Additionally, values of \mathbf{b} produced by the EC system followed a smoothly varying pattern repeated each day of increase from negative values in the early morning to a midday maxima followed by decrease to negative values in the evening. Thus, use of \mathbf{b} measured by the EC system is probably the most reliable way to correct the EC turbulent fluxes. The correction is applied as,

$$\mathbf{I}E_{corrected} = ET_{corr} = \frac{R_n - G}{\mathbf{b} + 1} \quad (18)$$

Of course, when Equation 18 is used to correct the EC measurements, the computed flux is no longer independent of the energy balance measurements. Additionally, measurements at dawn and dusk when \mathbf{b} is near -1 must either be discarded, similar to the processing of BR measurements, or not be corrected. Periods when \mathbf{b} is near -1 have little influence on daily or seasonal ET estimates, because ET is usually low during the time of day when this condition prevails. Prior to the application of Equation 18, the only corrections applied the EC measurement were the oxygen and air density corrections. Using \mathbf{b} as the correction factor thus assumes that other sources of error affect the turbulent fluxes in equal proportion (i.e., multiplicatively). When $\mathbf{I}E$ measured with the EC system is corrected using Equation 18, it produces similar results to $\mathbf{I}E$ measured with the BR system during periods when \mathbf{b} produced by each system was similar (Figure 42). During periods when \mathbf{b} measured with the BR system was erroneously large (e.g. at night), the corrected ET was greater than that measured with the BR system.

The corrected ET is usually, but not exclusively, greater than the uncorrected EC

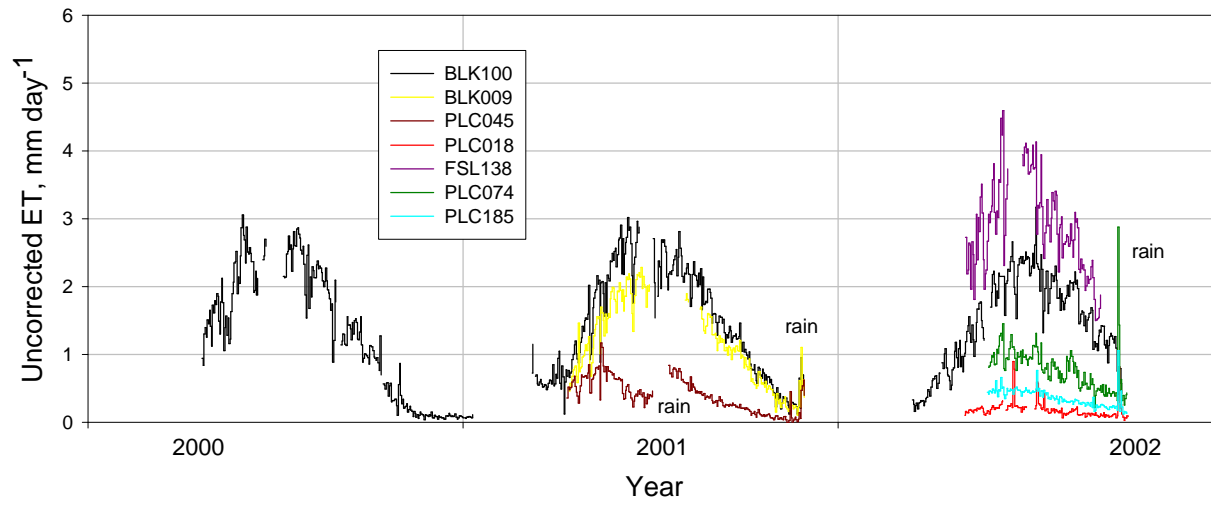


Figure 43. All uncorrected ET measured by EC systems.

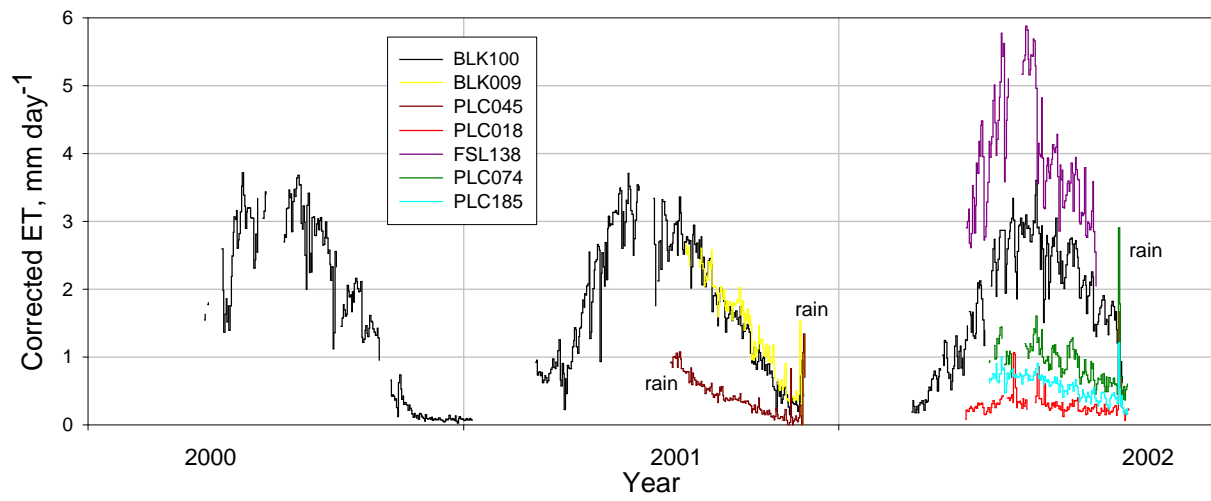


Figure 44. All corrected ET measured by EC systems.

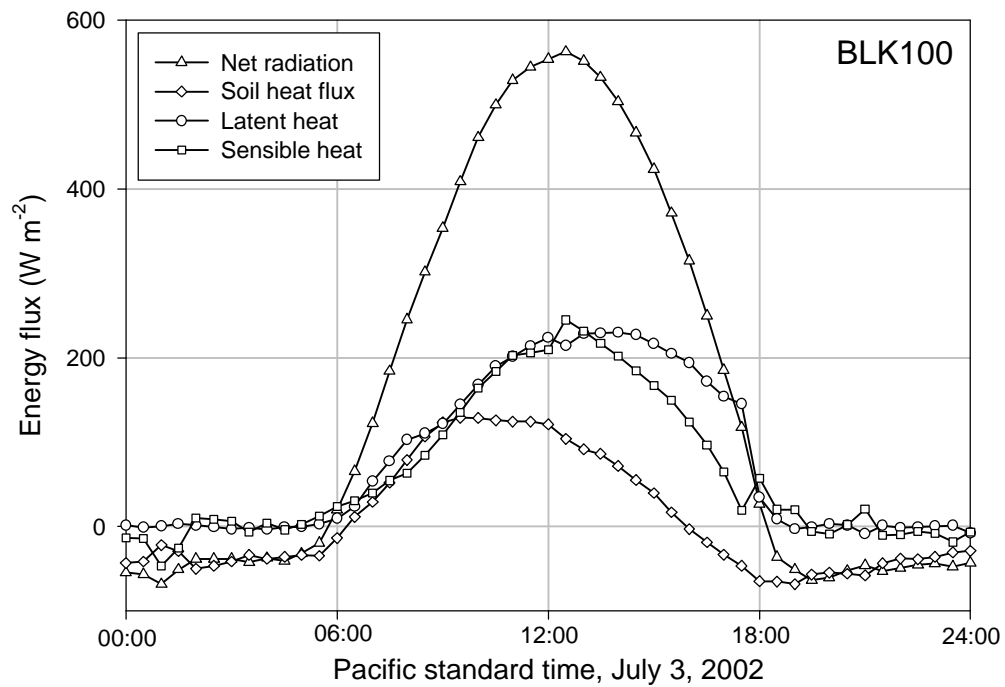
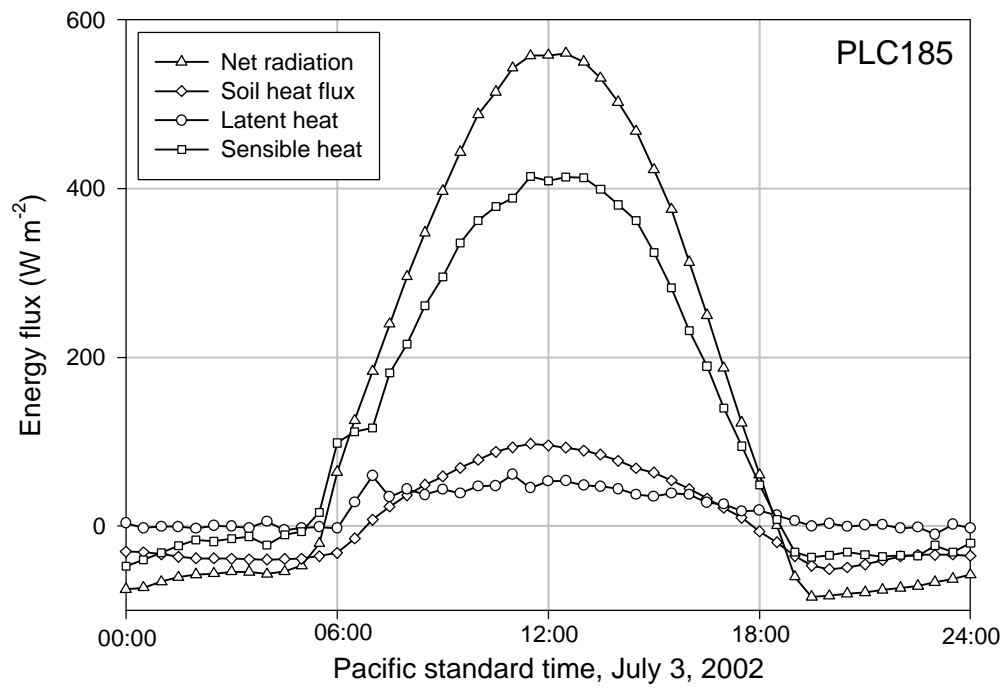


Figure 45. Half-hourly energy balance components measured at PLC185 (top graph) and BLK100 (bottom graph). Latent heat flux has been corrected for EB.

measurement. The correction (Equation 18) increased ET estimates a few tenths of mm day⁻¹ up to 1 mm day⁻¹ depending on the site (Figures 43 and 44). One disadvantage was the shorter record of corrected ET because there were fewer days when all instruments were functioning. The disadvantage was particularly acute at BLK009 and PLC045 where datalogger problems prevented collection of Rn and G for the first half of the growing season. As described above, this problem was partially alleviated by fitting the Fourier model to the available ET_{corr} data.

Eddy covariance results

Eddy covariance ET measurements were obtained for most of growing season at all sites (Table 7 and Appendix A). Two examples of the diurnal fluxes typical of summer conditions of the Owens Valley at sites with dry and wet soils are shown in Figure 45 where daytime surface heating due to solar radiation is partitioned into positive daytime sensible and latent heat fluxes. At night, net radiation was negative due to cooling of the land surface, latent heat flux was near zero due to the cessation of plant transpiration, and sensible heat flux was small and negative. Soil heat flux was a relatively small component of the energy balance and changed sign from negative to positive in mid-morning and from positive to negative in late evening. Note the different relative magnitudes of latent heat and sensible heat flux between sites with wet and dry soils. Latent heat flux accounted for a greater proportion of the available energy at wetter sites.

The Fourier model coefficients and fitting statistics are given in Table 10 and shown in Figures 46-54. The low r^2 for PLC018 and PLC185 (Table 9) was due in large part to the low and relatively flat seasonal ET trend (small variance). Visual inspection of Figures 52 and 54 suggests the agreement between the data and Fourier model was acceptable for the purpose of integration. ET_{corr} during the growing season ranged between 50 and 700mm (ET_r was greater

Table 10. ET_{corr} Fourier model coefficients and r^2 for each site-year.

Year	Site	mean mm day ⁻¹	A(1)	A(2)	B(1)	B(2)	r^2
2000	BLK 100	1.37	-1.62	0.26	-0.12	0.06	0.93
2001	BLK 100	1.33	-1.56	0.27	-0.13	-0.12	0.90
	BLK 9	1.43	-1.65	0.31	-0.14	-0.17	0.95
	PLC 45	0.50	-0.50	0.12	0.15	-0.08	0.85
2002	BLK 100	1.12	-1.33	0.30	-0.27	0.03	0.98
	FSL 138	1.94	-2.28	0.50	0.10	-0.20	0.70
	PLC 18	0.18	-0.14	0.01	-0.03	-0.02	0.54
	PLC 74	0.60	-0.49	0.02	0.06	-0.004	0.63
	PLC 185	0.35	-0.33	0.05	0.05	-0.05	0.57

than 1500mm) depending on water table depth and plant attributes (Table 11).

ET seasonal trends corresponded with the expected trends in evaporative demand throughout the summer and usually were greatest in late June or early July. The sharp decline in ET at FSL138 on July 11 (Figure 51) corresponded with termination of soil water decline at depths above 1 m and with the deepest water table depth (2.05 m). This site had the shallowest water table of all sites, and the ET decline may reflect a decrease in surface E derived from the soil and/or decrease in T as the water table approached the bottom of the saltgrass root zone of approximately 2m. Direct evaporation from the water table was negligible as discussed below in Section III. LAI began to decline steadily after the measurement on July 9 suggesting that curtailed transpiration constituted some fraction of the observed reduction in ET. Most of the decline in LAI was due to decline in DISP2, but vegetation at this site had a significant component of beardless wildrye, *Leymus triticoides*, and minor amounts of *Juncus sp.* It is not known if differing physiology of these species contributed to the observed ET step change.

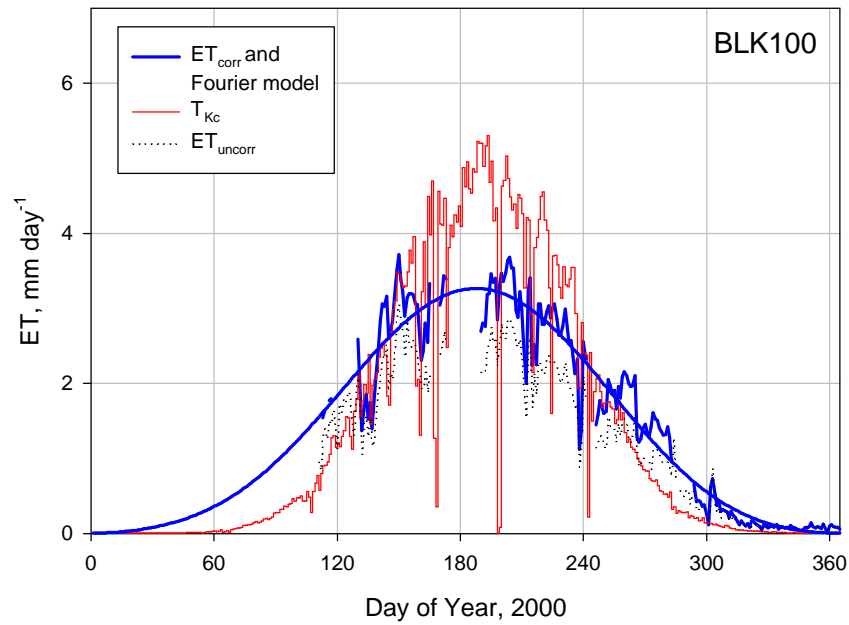


Figure 46. ET at BLK100 in 2000 measured with the EC system and estimated using field measurements and transpiration coefficients (Equation 17). EC measurements corrected and uncorrected for energy balance closure error are presented.

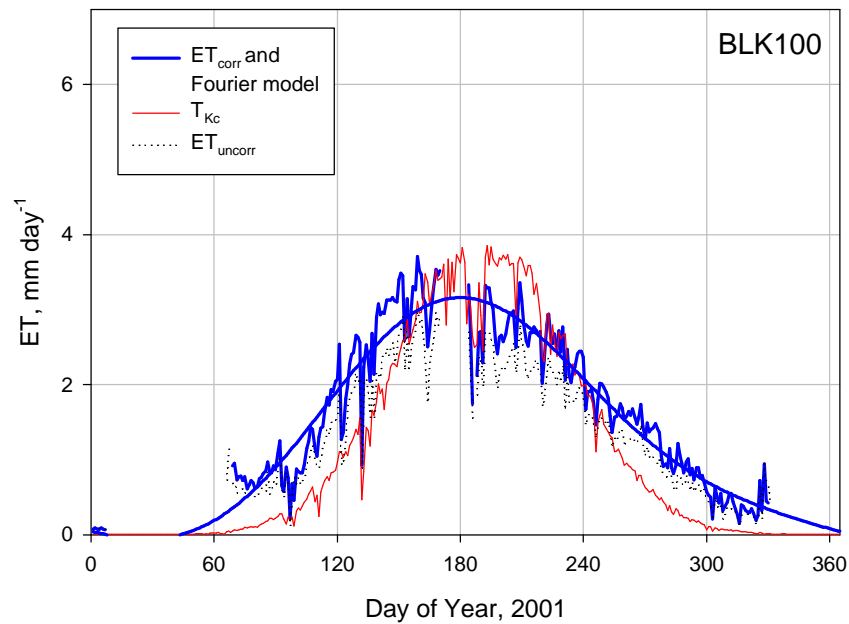


Figure 47. ET at BLK100 in 2001 measured with the EC system and estimated using field measurements and transpiration coefficients (Equation 17). EC measurements corrected and uncorrected for energy balance closure error are presented.

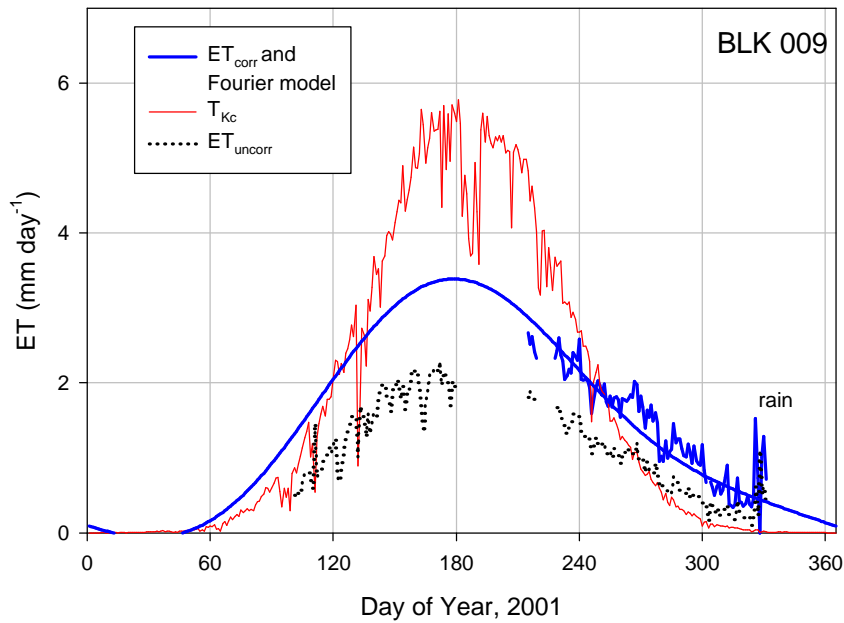


Figure 48. ET at BLK009 in 2001 measured with the EC system and estimated using field measurements and transpiration coefficients (Equation 17). EC measurements corrected and uncorrected for energy balance closure error are presented.

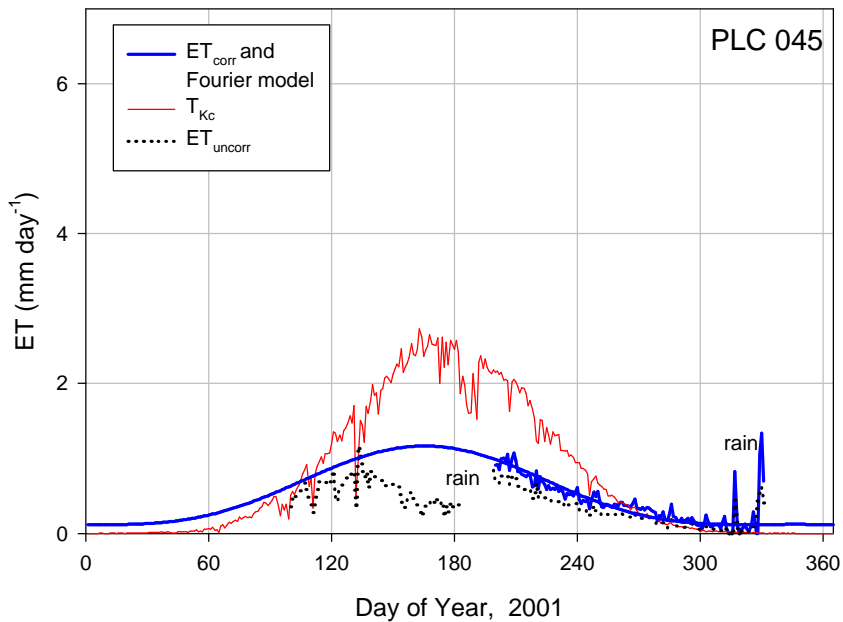


Figure 49. ET at PLC045 in 2001 measured with the EC system and estimated using field measurements and transpiration coefficients (Equation 17). EC measurements corrected and uncorrected for energy balance closure error are presented.

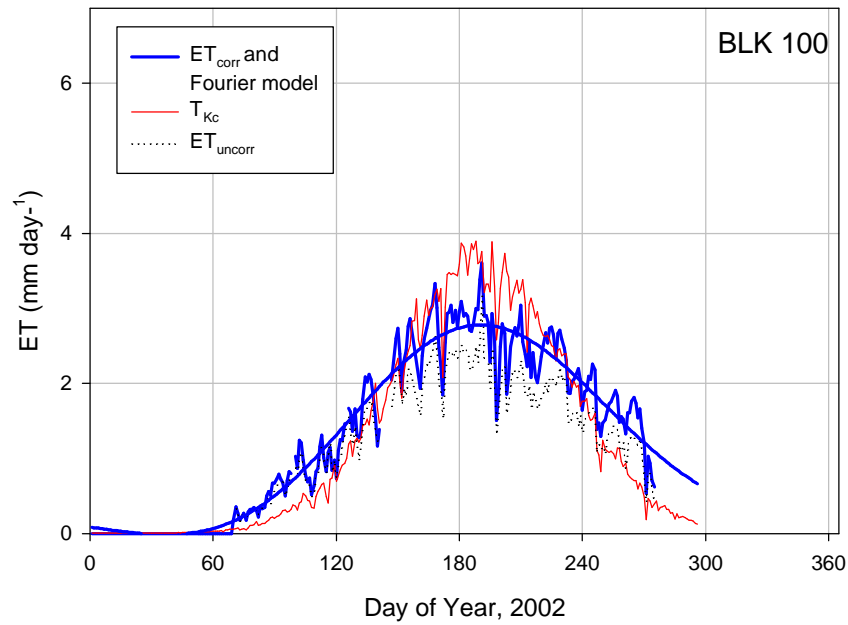


Figure 50. ET at BLK100 in 2002 measured with the EC system and estimated using field measurements and transpiration coefficients (Equation 17). EC measurements corrected and uncorrected for energy balance closure error are presented.

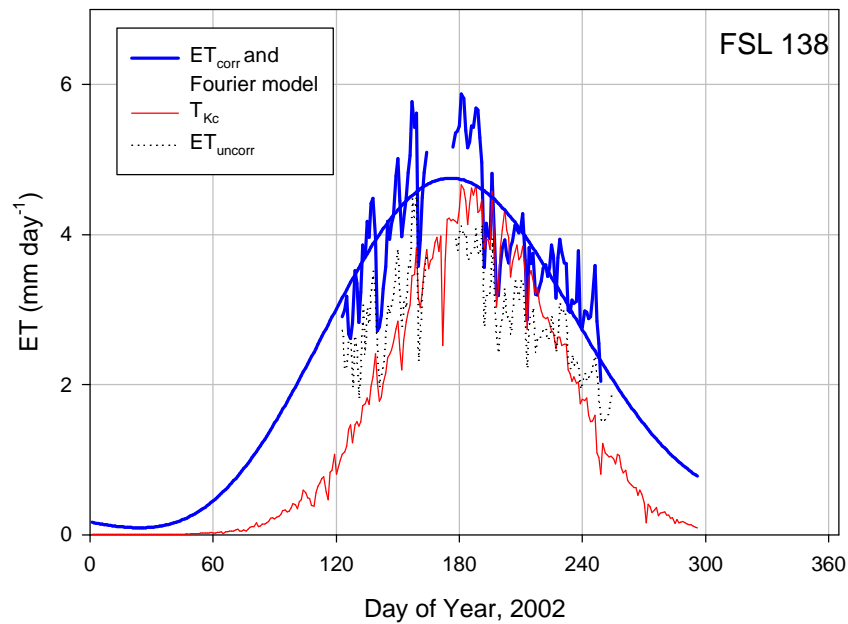


Figure 51. ET at FSL138 in 2003 measured with the EC system and estimated using field measurements and transpiration coefficients (Equation 17). EC measurements corrected and uncorrected for energy balance closure error are presented.

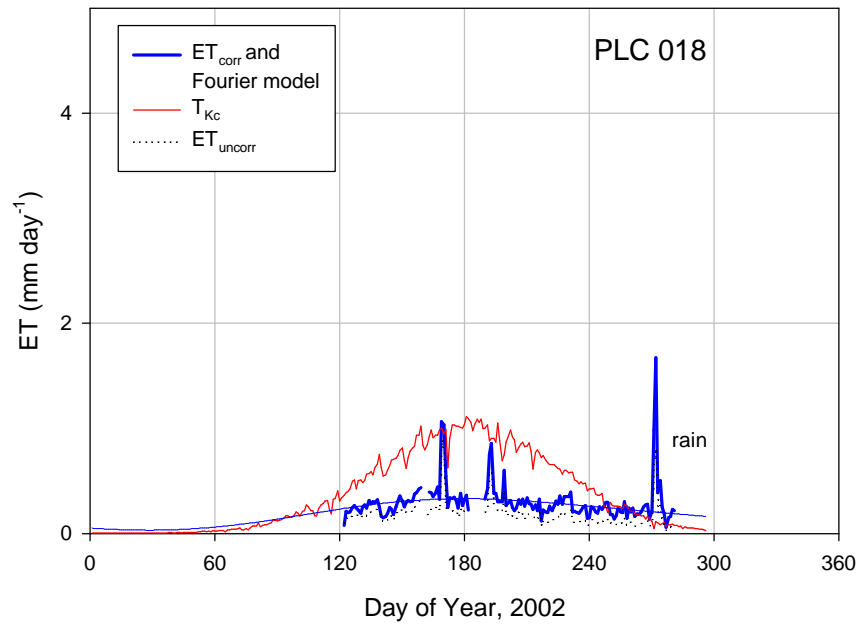


Figure 52. ET at PLC018 in 2002 measured with the EC system and estimated using field measurements and transpiration coefficients (Equation 17). EC measurements corrected and uncorrected for energy balance closure error are presented.

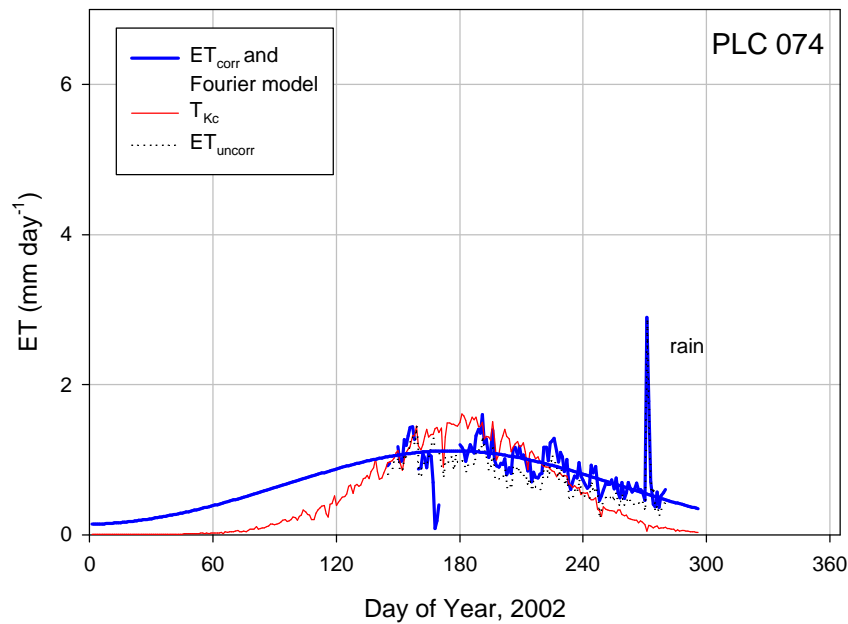


Figure 53. ET at PLC074 in 2002 measured with the EC system and estimated using field measurements and transpiration coefficients (Equation 17). EC measurements corrected and uncorrected for energy balance closure error are presented.

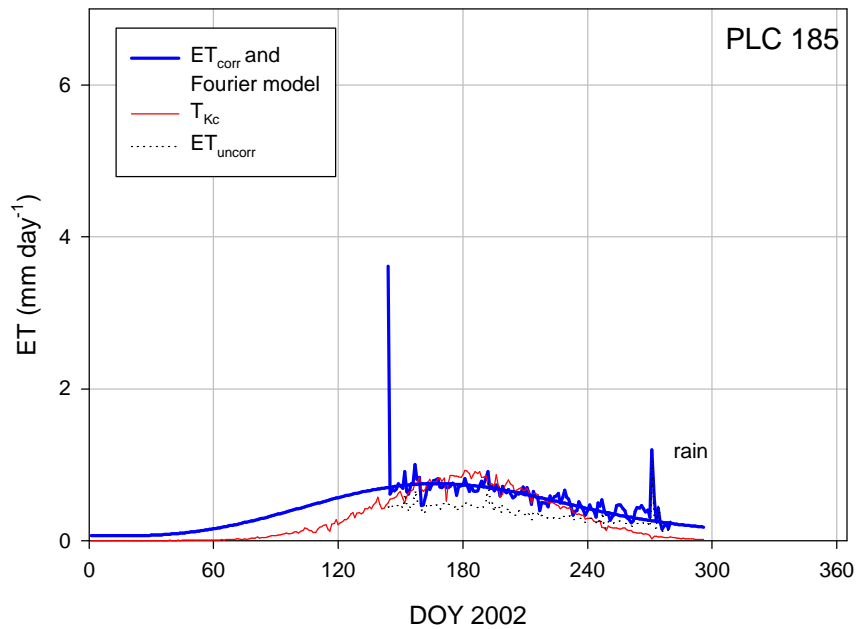


Figure 54. ET at PLC185 in 2002 measured with the EC system and estimated using field measurements and transpiration coefficients (Equation 17). EC measurements corrected and uncorrected for energy balance closure error are presented.

Comparison of EC and T_{Kc} results

Performance of the K_c models and vegetation measurements was evaluated to address three questions: 1) Did T_{Kc} approximate seasonal trends in ET measured by the EC stations? 2) Did the seasonal estimates of T_{Kc} compare favorably with measured seasonal totals? and 3) Did the LAI models for dominant species used to construct the K_c models agree with field measurements?

Daily values of ET measured by EC methods and corrected for the energy imbalance are presented in Figures 46 to 54 along with the daily T_{Kc} estimated using transpiration coefficients and LAI measurements (Steinwand, 1999b; Steinwand et al., 2001). Seasonal trends in T_{Kc} were

Table 11: Eddy covariance ET corrected for energy balance closure and T estimated from Kc models and measured LAI and ET_{r_i} . Vegetation measurements taken nearest the date of maximum LAI for the dominant species in Kc models were used (Table 9). Measured and predicted fluxes are the sum of daily totals for the period with available corrected eddy covariance measurements and integrated for the entire growing season using the fitted Fourier model (March 25-October 15).

Year	Site	ET_{corr}	T_{Kc}	T_{Kc} RMSE [^]	Growing season ET_{corr}	Growing season T_{Kc}	Growing season T_{Kc} RMSE
		mm	mm	mm day ⁻¹	mm	mm	mm day ⁻¹
2000	BLK 100	337	355	0.80	460	472	0.71
2001	BLK 100	434	341	0.66	446	384	0.72
	BLK 9	152	127	0.78	471	593	0.74
	PLC 45	55	85	0.53	165	266	0.49
2002	BLK 100	347	337	0.54	377	362	0.51
	FSL 138	450	328	1.27	646	414	1.48
	PLC 18	45	89	0.31	53	107	0.25
	PLC 74	112	101	0.42	177	147	0.40
	PLC 185	77	68	0.20	108	82	0.19

[^]: $RMSE = [3(ET_{corr-model})^2/n]^{0.5}$

similar to trends in ET_{corr} at BLK100 (all years), PLC074, and PLC185. At these sites (and FSL138), T_{Kc} tended to underestimate early and late season ET_{corr} but overestimated midsummer ET. Seasonal trends in T_{Kc} compared less favorably at BLK009, FSL138, PLC045, and PLC018. At FSL138, PLC045, and PLC018, the failure may be due to failure of site conditions to meet model assumptions. At PLC 045 and PLC 018, the water table was at or below the maximum rooting depth for saltbush and rabbitbrush and the upper 4 to 5 meters of soil was near limiting water content. The Kc models were developed from data collected at sites with sufficient soil water, and therefore, it was not surprising that T_{Kc} overestimated ET_{corr} . The decline in LAI and

ET (inferred from decline in uncorrected ET) during June at PLC045 corresponded with the exhaustion of available soil water within the monitored soil depth (3.2m) by June 21. Subsequently, leaf area and ET_{corr} at this site responded to approximately 2 cm rain in early July (Figure 49). The T_{Kc} and Fourier models cannot accommodate the bimodal response exhibited at this site. As described above, the fraction of E from the soil may have been sizeable at FSL138 due to the shallow water table and moist soils near the surface. T_{Kc} doesn't include soil E which could account for part of the underestimation. Failure of the models at BLK009 was not easily attributable to nonnegligible soil surface evaporation or plant water stress, and the failure may reflect an inherent inability of the models to estimate ET of the dominant species, CHNA2. This discrepancy, should be investigated further.

The model agreement with daily ET_{corr} was evaluated by calculating the root mean squared error (RMSE) between T_{Kc} or T_{GB} and measured daily ET_{corr} . The root mean squared error (RMSE) of T_{Kc} model and measured daily ET ranged from 0.23 to 1.45 mm d⁻¹ (Table 11). The low RMSE for BLK009 and PLC045 was deceptive, however, because the period with available ET_{corr} was limited to after late July. At both sites, values for ET_{corr} were not available for first half of the season and the differences were not included in the RMSE calculation (Figures 48 and 49).

The comparison of the daily ET measurements and T_{Kc} estimates are presented in Table 11. As shown above, the seasonal trends in T_{Kc} and ET_{corr} did not agree at some sites making the comparison of total ET based only the days for which data are available dependant on which portion of the growing season was measured. That problem also prevents site to site comparisons or for BLK100, year to year comparisons without relying on a model to integrate

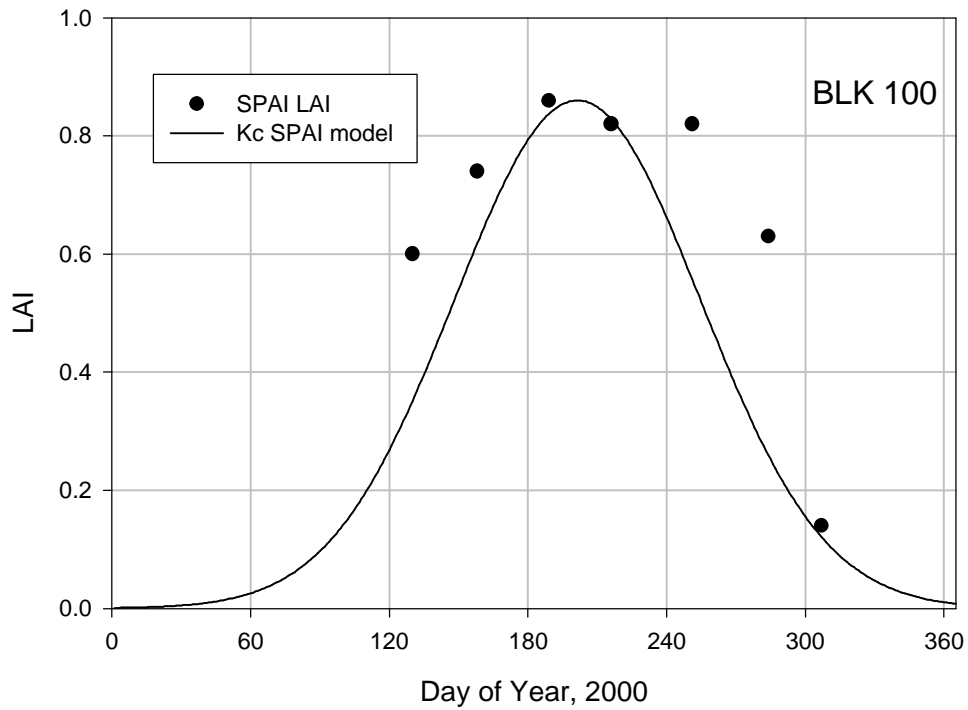
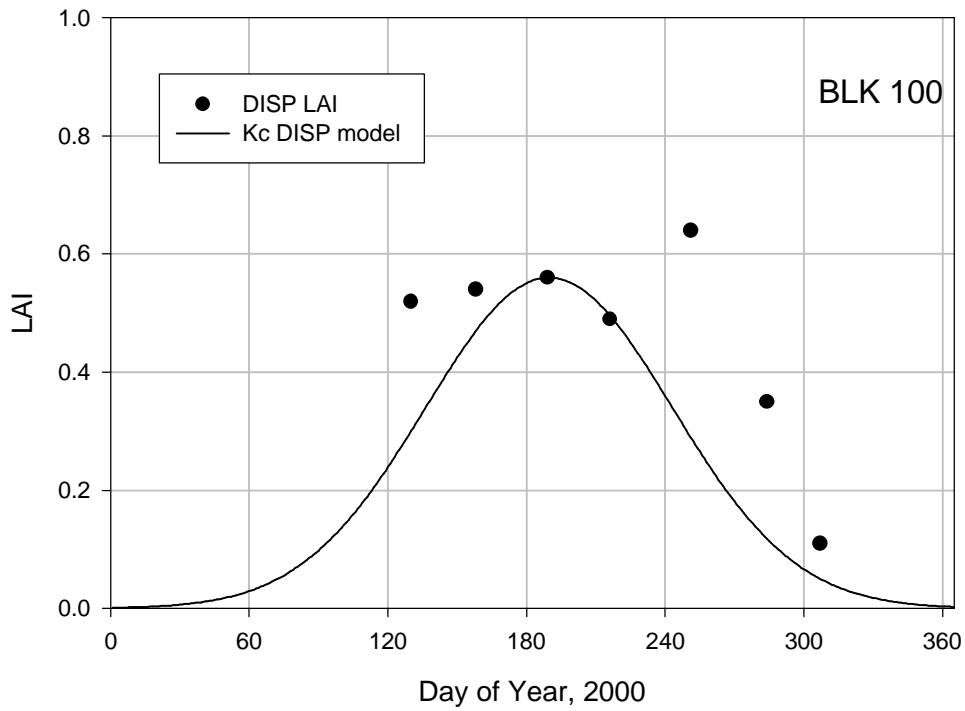


Figure 55. Measured LAI for dominant species at BLK100 in 2000 and LAI model in the Kc model scaled to the LAI used to calculate T_{Kc} . LAI is the mean of the four transects.

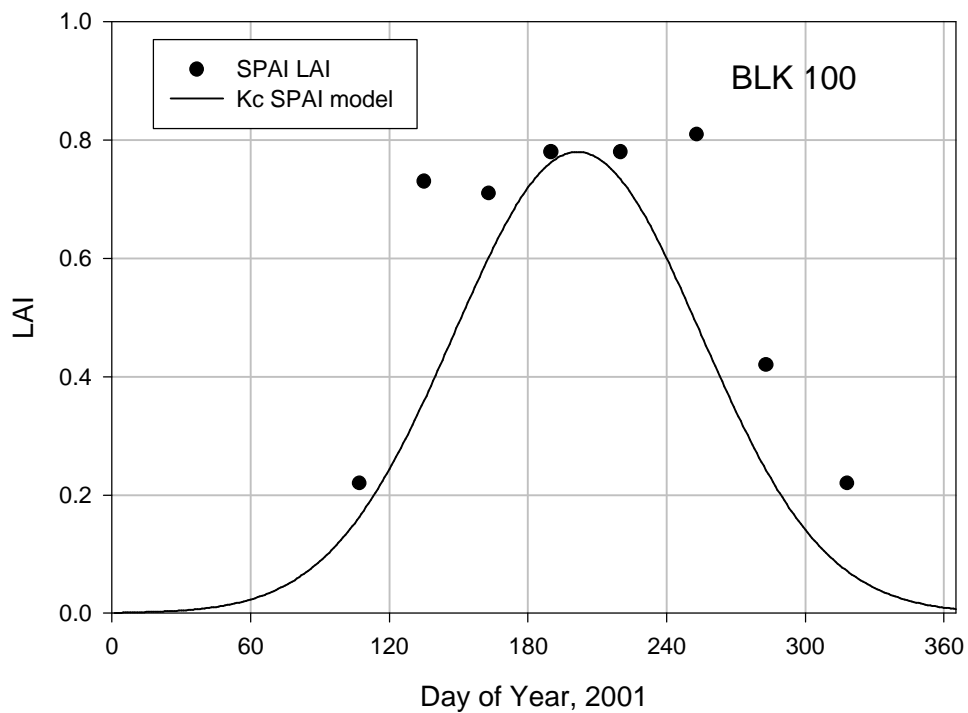
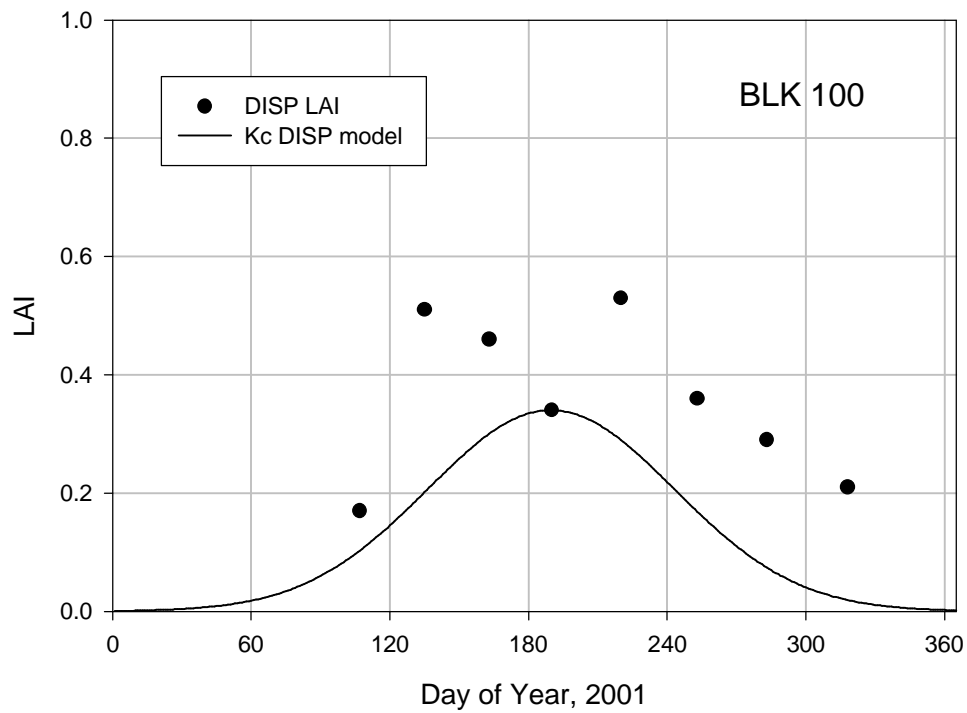


Figure 56. Measured LAI for dominant species at BLK100 in 2001 and LAI model in the Kc model scaled to the LAI used to calculate T_{Kc} . LAI is the mean of the four transects.

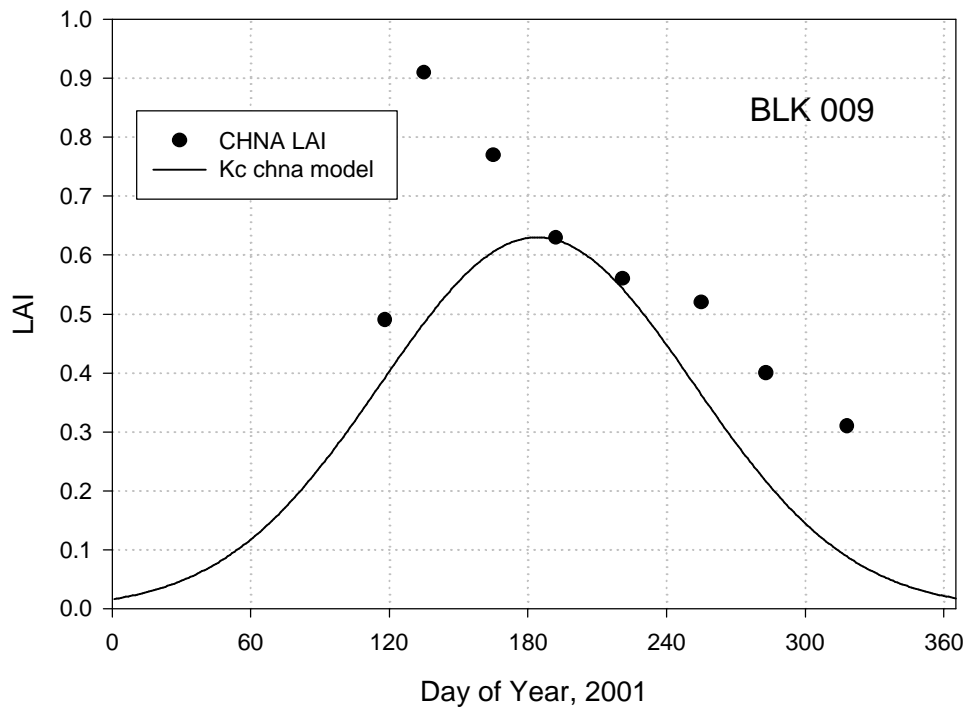
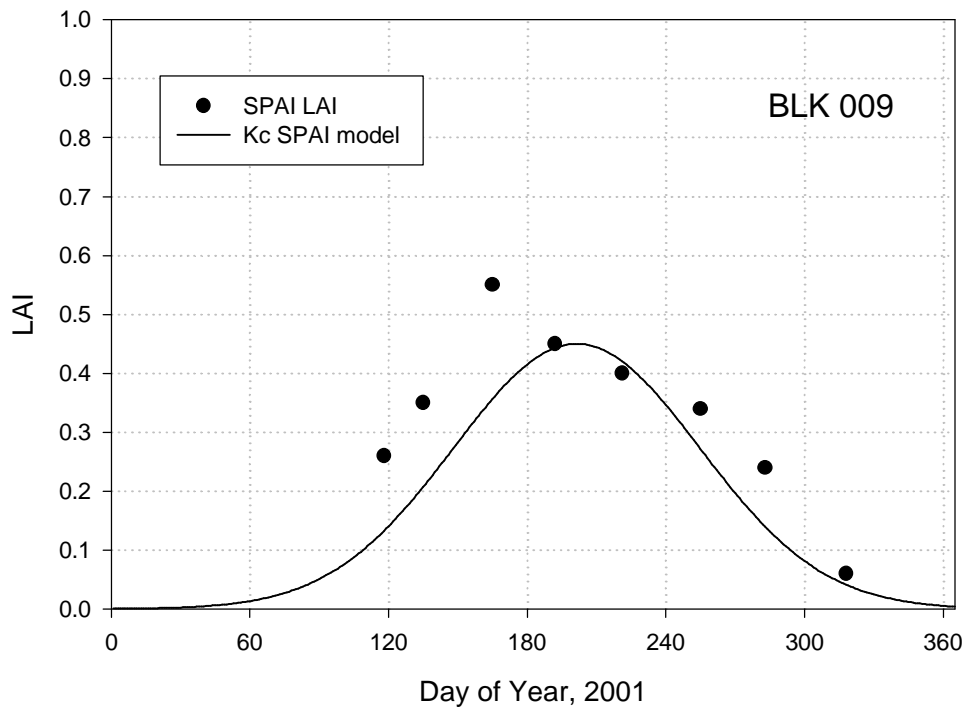


Figure 57. Measured LAI for dominant species at BLK009 in 2001 and LAI model in the Kc model scaled to the LAI used to calculate T_{Kc} . LAI is the mean of the four transects.

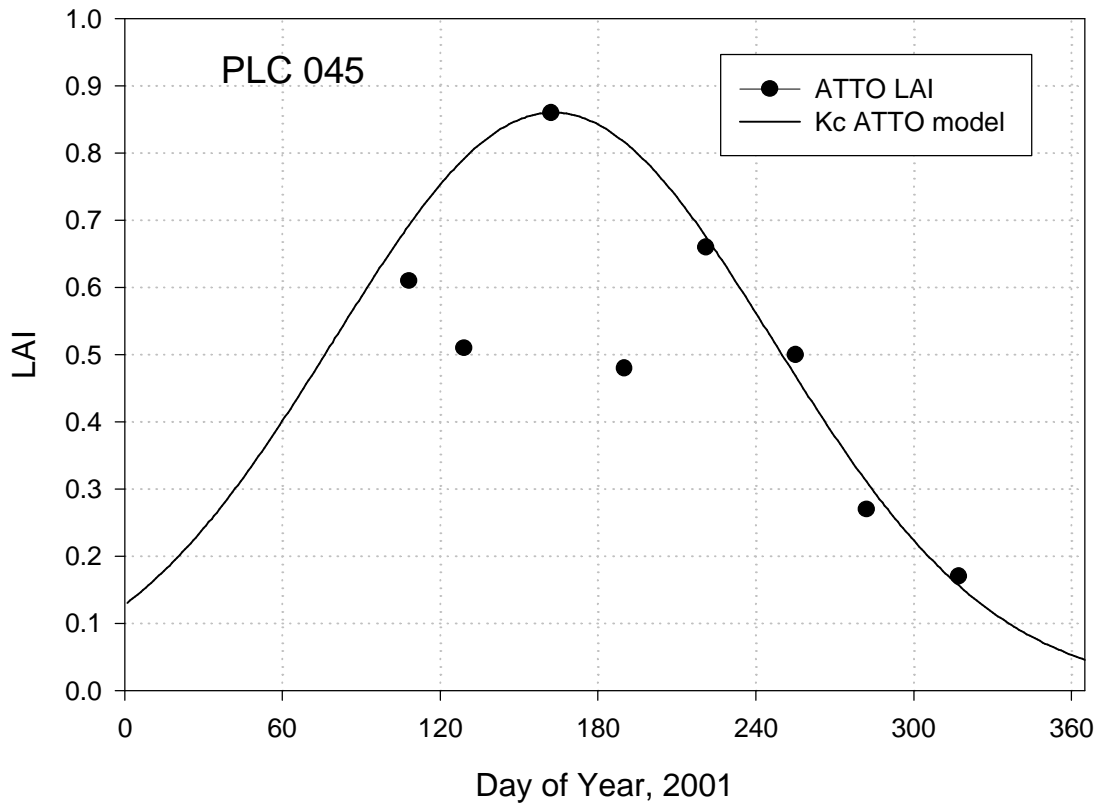


Figure 58. Measured LAI for dominant species at PLC045 in 2001 and LAI model in the Kc model scaled to the LAI used to calculate T_{Kc} . LAI is the mean of the four transects.

the seasonal total between uniform integration limits. The growing season values agreed best at well at BLK100 (all years) PLC074, and PLC185. The values were not expected to compare well for PLC046 and PLC018 for reason described above. Finally, T_{Kc} varies several centimeters if the LAI measurements bracketing the selected date for peak LAI are applied in Equation 16 indicating that reliance on a single midsummer measurement to represent the maximum LAI is a potentially large source of error if the peak LAI doesn't correspond with the sampling date because of site-specific or variable weather conditions.

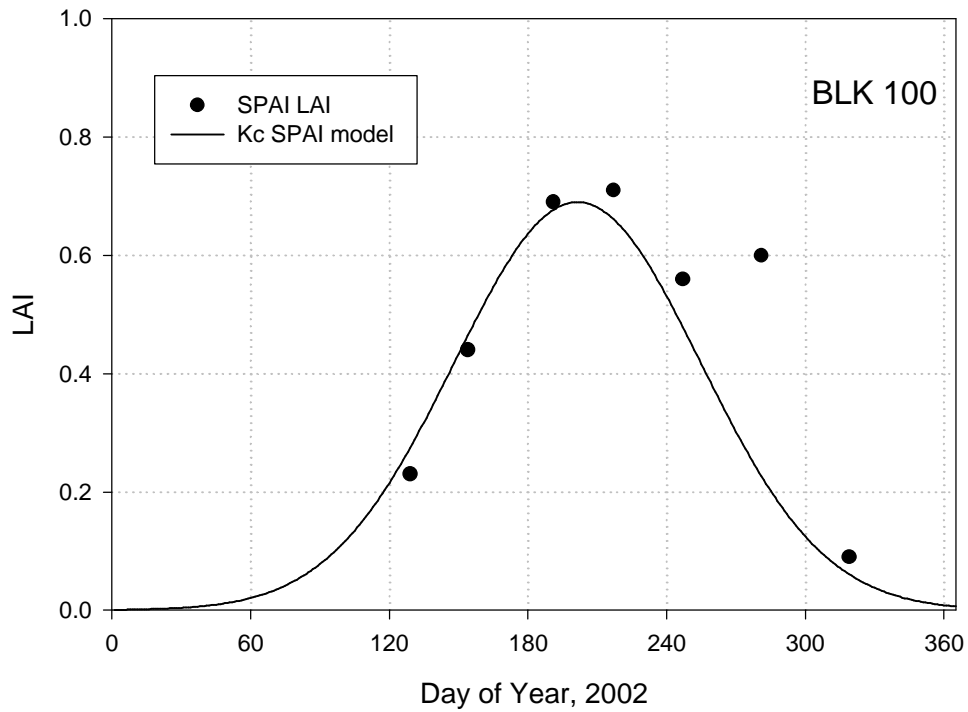
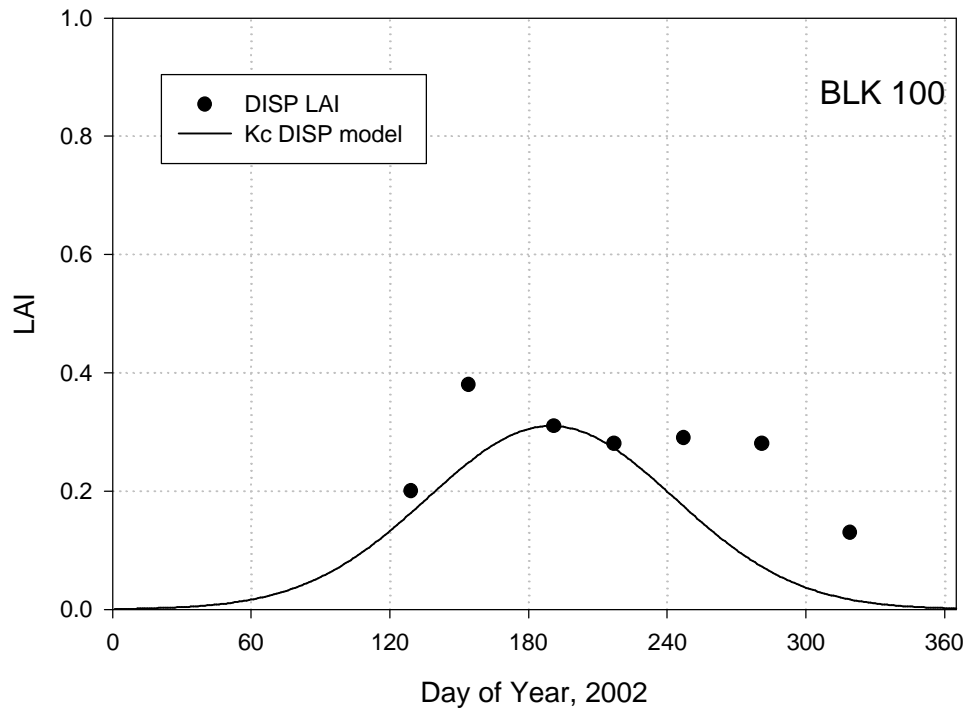


Figure 59. Measured LAI for dominant species at BLK100 in 2002 and LAI model in the Kc model scaled to the LAI used to calculate T_{Kc} . LAI is the mean of the four transects.

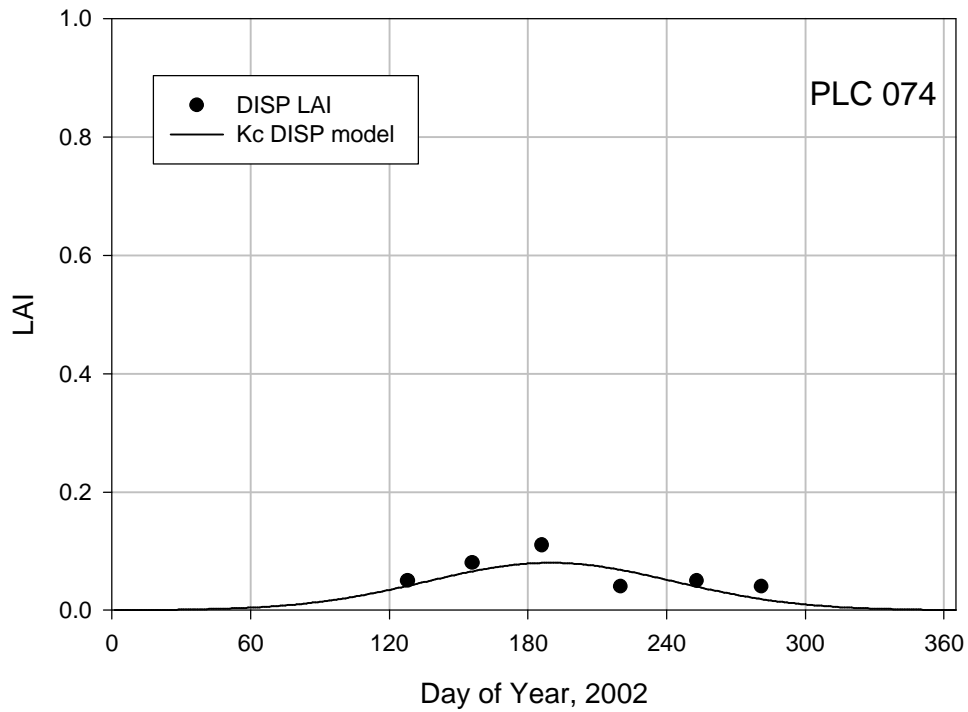
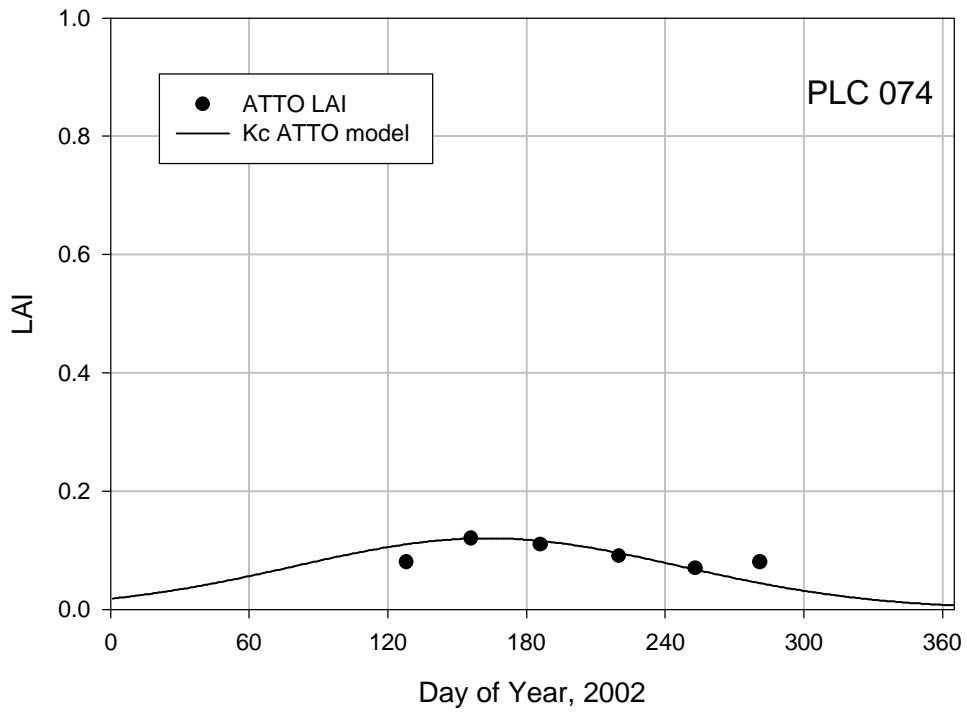


Figure 60. Measured LAI for dominant species at PLC074 in 2002 and LAI model in the Kc model scaled to the LAI used to calculate T_{Kc} . LAI is the mean of the four transects.

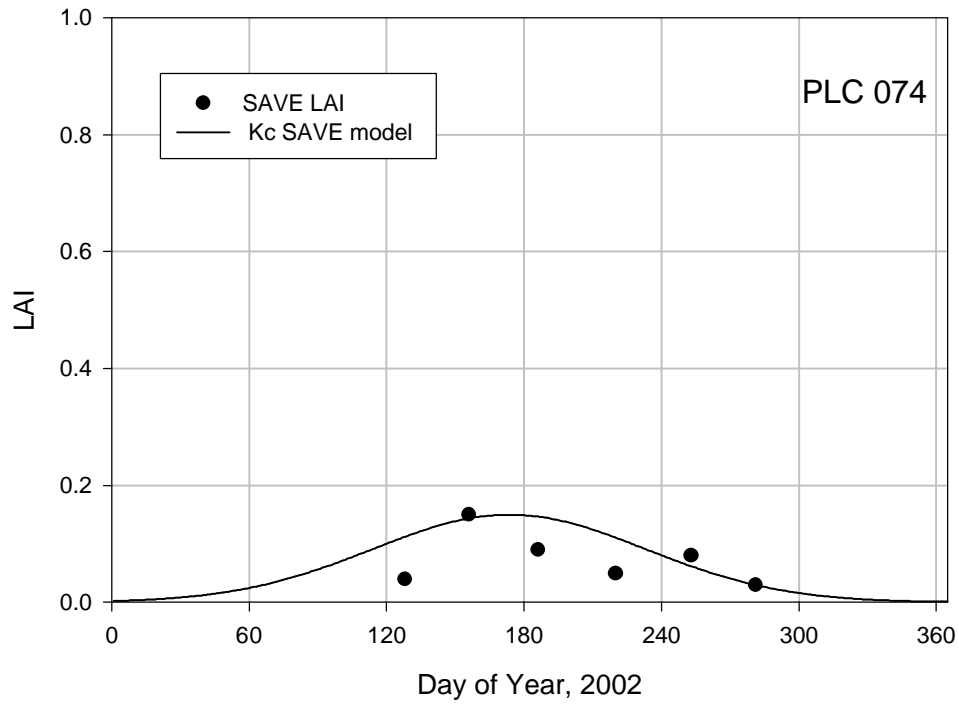


Figure 61. Measured LAI for dominant species at PLC074 in 2002 and LAI model in the Kc model scaled to the LAI used to calculate T_{Kc} . LAI is the mean of the four transects.

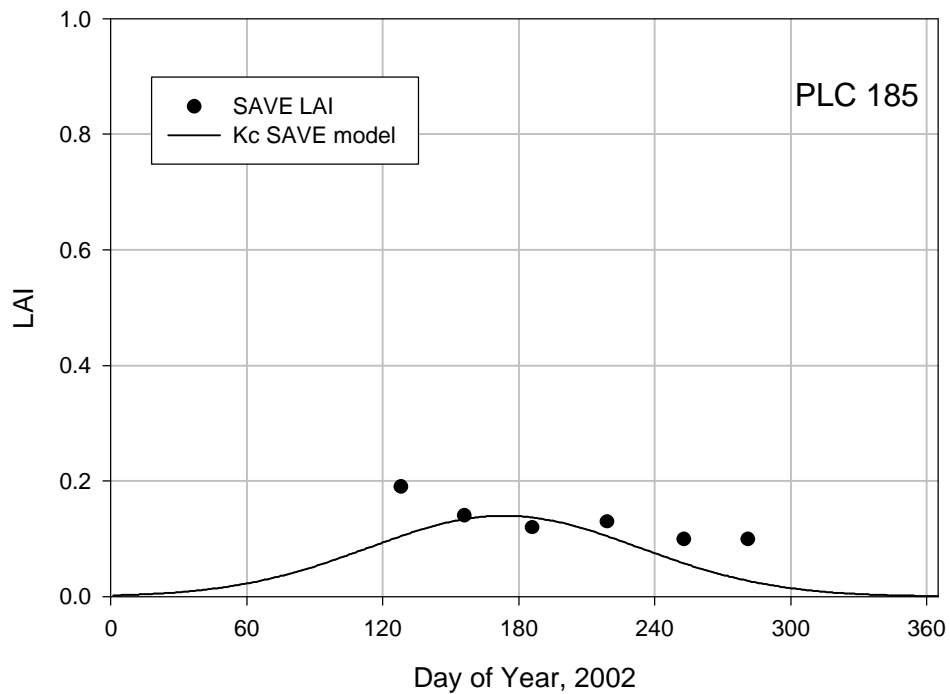


Figure 62. Measured LAI for dominant species at PLC185 in 2002 and LAI model in the Kc model scaled to the LAI used to calculate T_{Kc} . LAI is the mean of the four transects.

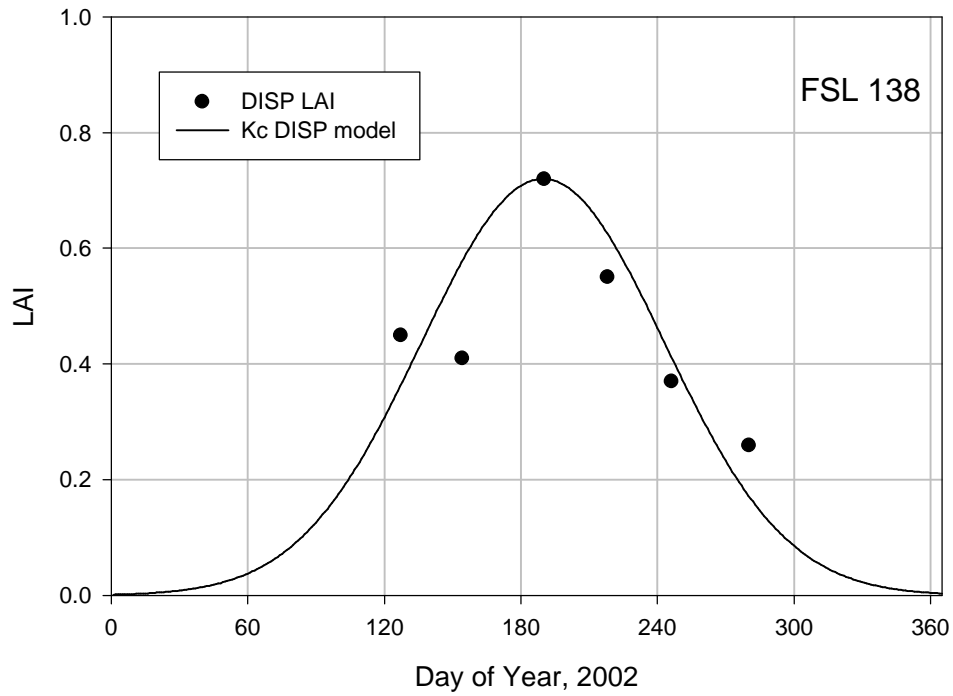


Figure 63. Measured LAI for dominant species at FSL138 in 2002 and LAI model in the Kc model scaled to the LAI used to calculate T_{Kc} . LAI is the mean of the four transects.

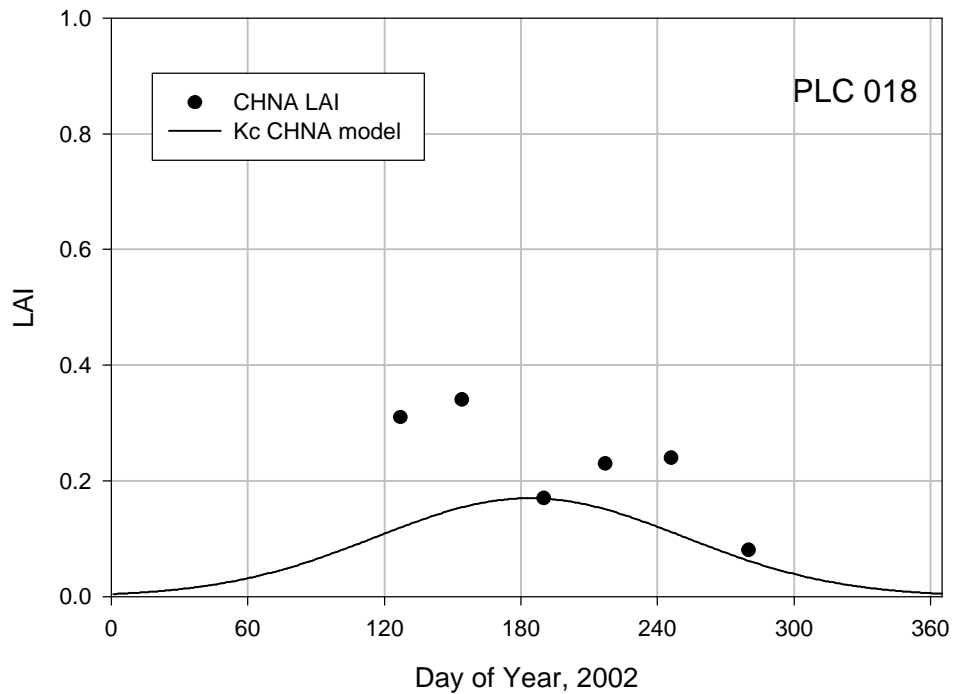


Figure 64. Measured LAI for dominant species at PLC018 in 2002 and LAI model in the Kc model scaled to the LAI used to calculate T_{Kc} . LAI is the mean of the four transects.

LAI of the dominant species at the EC sites was variable during the June-July period (midsummer). LAI for individual species generally showed fair correspondence between the observed maximum LAI and the timing of peak LAI in the Kc LAI models (Figures 55 to 64). Again, measured LAI used was the date nearest the average maximum LAI in the original Kc development. Examples of poor agreement were DISP2 at BLK100 in 2001, CHNA2 at BLK009 and PLC018, ATTO at PLC045. At these sites, the correspondence of the model and data could be improved considerably by better relying on vegetation measurements data collected on another date to fix the maximum LAI. Generally the shape of the model corresponded with field measurements; however, the models reflected trends in the data poorly and underestimated LAI for dominant species at BLK100, BLK009 and PLC018.

Conclusions

Turbulent fluxes measured by the EC system did not account for approximately one-third of the available energy. Similar discrepancies have been observed in other studies using EC methods. During periods when the BR system obtained stable measurements, the Bowen ratios measured by the two systems substantially agreed. It is recommended that EC measurements of IE be corrected by using the Bowen ratio measured by the EC system to account for all the available energy. Total ET corrected for the energy balance was measured by eddy covariance at seven sites with growing season totals ranged between 50 and 700mm (ETr greater than 1500mm) depending on water table depth and plant attributes. Seasonal total ET_{corr} generally agreed with estimates derived from Kc models and LAI measurements when the site conditions met assumptions of the Kc models. Variability in LAI among species during the peak months of the growing season (early June to early July) and the sensitivity of T_{Kc} estimates on correctly

sampling the peak LAI, however, is suggests that a single sampling date may be unacceptable.

III. Task 2: Vadose Zone model

This task was composed of two subtasks, field investigation of the soil water balance components and revision of a previously constructed vadose zone model that combined plant water use, soil water storage, and water table fluctuations to predict future water storage and plant water availability (Or and Groeneveld, 1994).

Field investigation

Introduction

Phreatophytes are known to utilize groundwater, but quantifying the portion of ET during the growing season drawn from groundwater is difficult. Plant uptake (T) largely drives changes in stored soil water and possibly depth to water table in the absence of hydrologic manipulations. Understanding the partitioning of T between soil water and groundwater sources, therefore, is essential to prepare an accurate model of the vadose zone water balance for phreatophytes. Field experiments were conducted to provide an accounting of the depths and magnitudes of water uptake by plant roots at sites instrumented with EC stations. The purpose of this task was collect field data to examine sources of plant uptake necessary to examine conceptualization of specific components of the vadose zone water balance model.

Materials and Methods

Site selection and instrumentation

Monitoring locations distributed vertically and laterally through the vadose zone near the

EC stations were visited periodically during this project. Detailed measurements of soil water content were conducted using a combination of time domain reflectometry (TDR), neutron probe access tubes, and gravimetric sampling. In the original proposal, matric potential monitoring was planned to support detailed numerical soil water modeling. The purpose of that effort was to assist parameterization of groundwater uptake in the vadose zone water balance model, but the intensity of that field and modeling effort was deemed infeasible and unnecessary. That methodology was replaced by the combination of soil hydraulic property measurements and simpler analytical models described below. The site selection and instrumentation are described in Section II

Soil characterization

Particle-size analyses by the hydrometer method (Gee and Bauder, 1986) were completed on sixty-five soil samples collected during access tube installation. Samples were selected to represent obvious textural differences observed during field sampling. Samples were analyzed for all sites except PLC074. Soil characterization data for PLC074 were available from previous research conducted at this site by LADWP, Inyo County, and Natural Resources Conservation Service (Appendix B).

Soil water retention measurements were collected on intact core samples collected at approximately 0.3m depth near each access tube. Retention measurements were collected using pressure cell methods (Dane and Hopmans, 2002). Parametric models of van Genuchten (1980) and Maulem (1976) and the retention curve data were used to derive parameters necessary to perform analytic modeling for the vadose zone model development. These results are given in Appendix B.

Saturated paste extracts were prepared to measure salinity of surface samples at BLK009, BLK100, and PLC045 (Rhoades, 1982). These data were used to assess the possibility for successful TDR measurements. TDR instruments often fail if soil salinity is greater than 5 dS/m.

TDR measurements were made of the surface soil layer in conjunction with the gravimetric samples to determine the potential of using TDR for routine measurements of θ . Surface TDR measurements are less destructive and quicker than the gravimetric samples. Surface (0-12 cm) measurements were collected using a Hydrosense TDR system (Campbell Scientific) after calibration using soils from Owens Valley several sites. The instrument was most reliable at sites with dry sandy soils (PLC074, PLC185) and least reliable at BLK100 when the soil was moist, probably due to soil salinity. Data from gravimetric sampling was used when the TDR failed.

Soil Water Balance (SWB) and Partitioning

This study determined the partitioning of ET between groundwater (ET_{gw}) and soil water (ET_{soil}) sources by measuring or estimating the water balance components and closure of the water balance,

$$(i) \quad ETa = ET_{soil} + ET_{gw}, \quad (ii) \quad ET_{soil} = P + \Delta S, \quad (iii) \quad ET_{gw} = E_{gw} + T_{gw} \quad (19)$$

$$(iv) \quad T_{gw} = ETa - E_{gw} - P - \Delta S$$

where ET_{corr} is as defined previously, ΔS is change in soil water storage, P is precipitation, and T_{gw} and E_{gw} are transpiration and evaporation derived from groundwater, respectively. Runoff, runoff, and deep percolation of precipitation were negligible. Partitioning calculations were made for the growing season (March 25 to October 15) because of vegetation phenology and

availability of field ET measurements. This period encompassed the majority of annual ET because vegetation is senesced during the winter. Determination of the each component of the water balance is described in the sections below.

ET_{corr}, Actual ET. *ET_{corr}* was the derived by summing the daily *ET_{corr}* values of the Fourier model. Please refer to Section II for a description of the EC methods and model fitting.

E_{gw}, Evaporation from Water Table. Under the arid conditions of Owens Valley, with relatively fine-textured soils in some of the sites, and in the presence of relatively shallow water table (<2 m) this component of the water balance may represent a significant contribution to the seasonal water balance. Availability of continuous eddy covariance measurements allowed us to estimate the magnitude of direct evaporation from the water table through the soil when plants were not actively transpiring, i.e. at night. *E_{gw}* was determined by summing nighttime *ET_{corr}*. This should be a generous estimate because it discounts soil E and leakage through plant stomata. To test whether this procedure gave realistic estimates, we compared nighttime *ET_{corr}* at BLK100 with theoretical predictions. BLK100 was chosen because it had the longest period of record and the finest textured soil (Appendix B), i.e. the greatest capillarity above the water table. Gardner (1958) derived an analytical expression for relating the maximum evaporation flux from a dry soil surface (*E_{gw}* [m/h]) as a function of soil properties (saturated hydraulic conductivity *K_s* [m/h], and an extinction parameter " [1/m])) and water table depth *L* [m],

$$E_{gw} = \frac{K_s}{\exp^{(aL)} - 1} \quad (20)$$

The expression shows that for a water table depth of zero (at the soil surface) the soil-controlled rate of evaporation would be the saturated hydraulic conductivity. For a deep water table (large

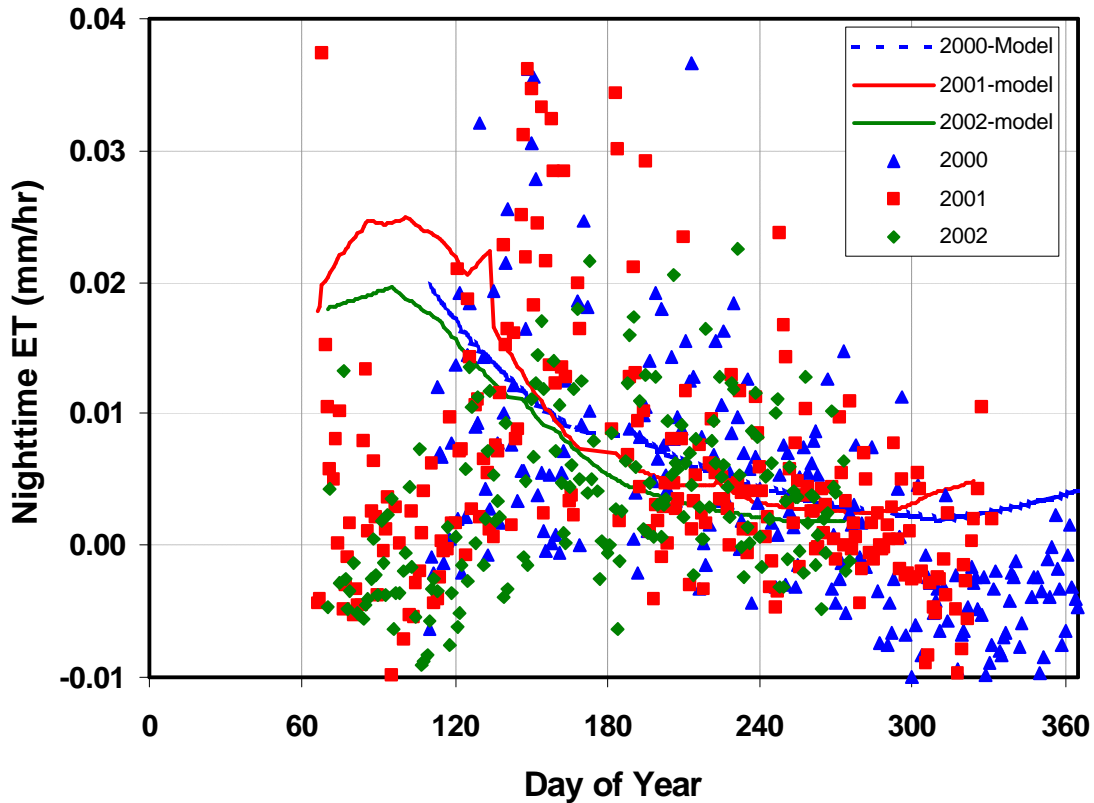


Figure 65. Nighttime soil evaporation measured by EC method at BLK100. Note the strong seasonal trend. Lines represent model predictions based on water table depth (Equation 20).

L) the direct evaporation would be zero. The analytical model results and nighttime ET_{corr} for BLK100 are presented in Figure 65. The results for show that for measured K_s of 8.5 mm/h (from soil water retention curve measurements), and water table range of depths from 2000 to 2500 mm, the best fit to the EC data was obtained with an estimated $\mu=0.0027$ [1/mm] which was consistent for the fine textured soil at this site. The magnitudes of theoretical E_{gw} and nighttime ET_{corr} were similar except for the early growing season (about DOY 90-130) when the water table was shallowest. The poor agreement for these months is not unusual because the

Gardner model only considers soil factors controlling evaporation rate and ignores that evaporation demand early in the growing season is small. The similarity of the two estimates for most of the growing season, however, and the small magnitudes of estimates derived using either method suggest that summing nighttime ET provided an acceptable and conservative (high) value for E_{gw} .

) *S, Change in Stored Soil Water.* Methods for neutron and gravimetric soil water measurements are described in Section II . Soil water stored in the soil (S) (cm/soil depth) was calculated according to,

$$S_{tube} = \sum q_i \Delta z_i \quad (21)$$

where q_i is volumetric water content depth i and Δz_i is the thickness of the soil interval represented by z_i . The storage calculation was calculated for the entire monitoring depth or for specific portions of the root zone to differentiate uptake groundwater from soil water uptake and then averaged to derive S . The change in soil water was taken as the maximum change observed between a measurement in the spring (usually the time S is greatest) and a measurement in the late summer or fall when S was smallest.

P, Precipitation. Precipitation was measured after each event by Inyo County or daily by the National Oceanic and Atmospheric Administration (NOAA). Rain gauges assigned to the sites were: Inyo County RG-6: BLK100, BLK009; Bishop Airport NOAA: PLC045, PLC074, PLC018; Inyo County RG-3: PLC185; Inyo County RG-1: FSL138. Equation 19 assumed that all P is utilized by vegetation. This assumption was probably inaccurate as some P evaporates directly back into the atmosphere and contributes to ET_{corr} . This will have no effect on

Table 12: Soil water balance components and calculation of T_{gw} for EC sites. The values represent growing season totals (March 25 to October 15).

Year	Site	T_{gw}	ET_{corr}	P	$)S_{max}$	E_{gw}	T_{gw}/ET_{corr}
		(mm)	(mm)	(mm)	(mm)	(mm)	
2000	BLK 100	338	460	11	99	12	0.73
2001	BLK 100	310	446	15	104	17	0.70
	BLK 9	310	471	15	131	15	0.66
	PLC 45	96	165 [^]	35	34	0	0.58
2002	BLK 100	294	377	1	68	14	0.78
	FSL 138	490	646	2	97	57	0.76
	PLC 18	13	53	3	37 ^{^^}	0	0.25
	PLC 74	102	177	3	72	0	0.57
	PLC 185	36	108	3	69 ^{^^}	0	0.33

[^]: As described in the test this value may be exaggerated slightly because of the poor correspondance with actual ET trends and shape of the Fourier model.

^{^^}:Initial soil water measurement was 1 month into growing season and soil was near limiting suggesting maximum was $)S_{max}$ underestimated. $)S_{max}$ determined by adding winter precipitation depleted before first S measurement: PLC18, 35mm+2mm, PLC185, 35mm+34mm.

calculation of T_{gw} because the fraction of P contributing directly to ET_{corr} would have to be subtracted from variables on the same side of the equation (Equation 19iv). Double counting of P that infiltrated into the soil was avoided by defining S as the difference between measurements early and late in the growing season and ignoring P -driven increases in S during the summer.

Results and Discussion

Soil Water Balance (SWB) and Partitioning

All components of the seasonal soil water balance are given in Table 12. The portion of T derived from the water table was estimated from the water balance as the difference between ET_{corr} , soil water depletion, precipitation, and evaporation. The component of E derived from the water table was a negligible fractions of the SWB for all sites. P was negligible for all sites

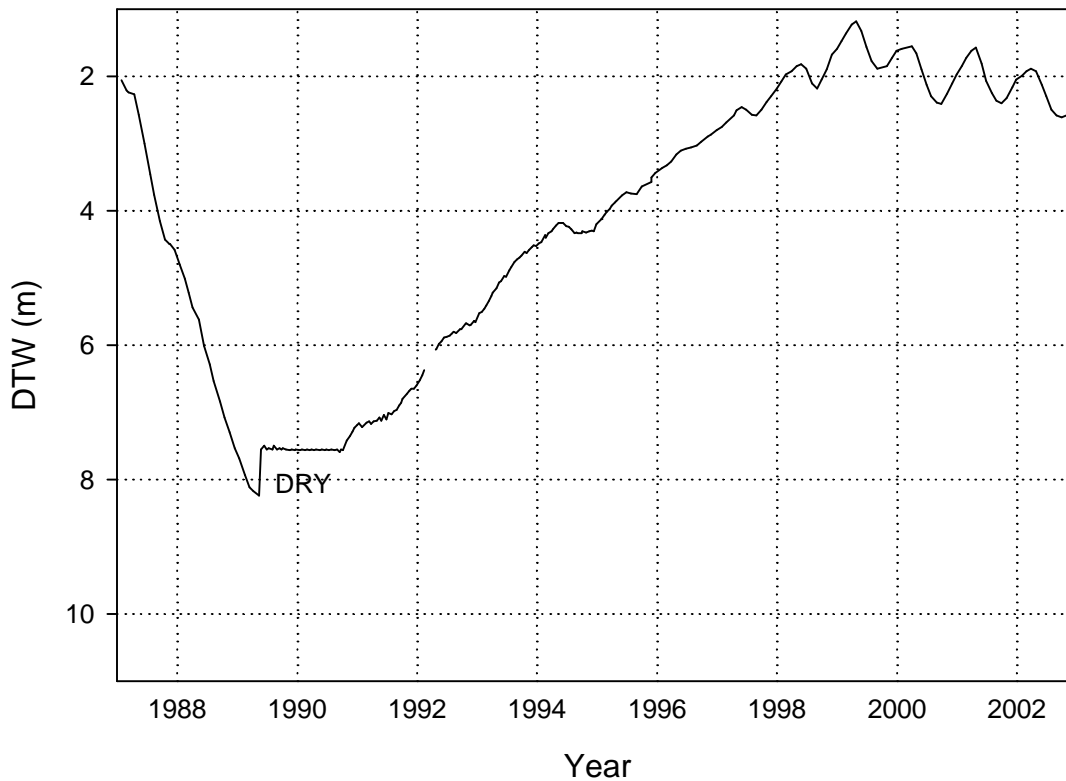


Figure 66. Hydrograph for monitoring well 419T. The magnitude of the intra-annual fluctuations do not correspond with pumping 1991 to 2003 and increase when the water is near the root zone (2m).water table to well below the root zone (approximately 2 m).

except PLC045. Direct uptake accounted for 66 to 80% of ET_{corr} for high cover sites with water table depths of 1 to 3 m. The site with the lowest contribution from the water table was PLC018. This site probably wasn't coupled to groundwater (DTW >5 m) suggesting this is the limit on the precision of our estimate of T_{gw} .

Determination of T_{gw} as the residual in the SWB lumps error for each component into the estimate. Because of this uncertainty, it was important to compare the results with an

independent estimate of T_{gw} . An important hydrologic signature that could assist quantification of plant uptake from groundwater is the rate and magnitude of water table drawdown (Freeze and Cherry, 1979). Evidence from recent water table recovery in a monitoring well, 419T, in an alkali meadow plant community (Figure 66) provides an example of the expected signature of vegetation uptake on seasonal water table fluctuations. The dramatic water level decline from 1987 to 1990 corresponded with a period of heavy pumping in this wellfield which lowered the Beginning in 1991, pumping was curtailed substantially with all occurring from one or two wells greater than 4.6 km from 419T. Notice that during the recovery from 1990 to 1997 when water levels were deeper than 3.0 m there was practically no seasonal variations in water table depths (other than those influenced by regional hydrological processes). In contrast, from 1997 to 2002 a clear seasonal fluctuation is evident that starts every year near the beginning of April coinciding with the onset of significant plant activity. Seasonal fluctuations in 419T did not correspond with pumping suggesting that ET may be controlling the intra-annual fluctuations.

We examined the relationship between plant water uptake and water table fluctuations to establish independent support for the values of T_{gw} derived from water balance closure. A key step to establishing that plants indeed drive the observed fluctuations in water table depth, was to measure water table depth at high temporal resolution and differentiate between behavior during the day time when plants transpire and during nighttime when T is substantially reduced. Results of high temporal water table depth measurement at BLK100 and PLC074 are depicted in Figures 67 and 68. In contrast to a relatively constant water table drawdown during the day (when plants are transpiring), during the night, there was practically no change in water table depth. Daily water table drawdown and concurrent related ET_{corr} results are summarized in

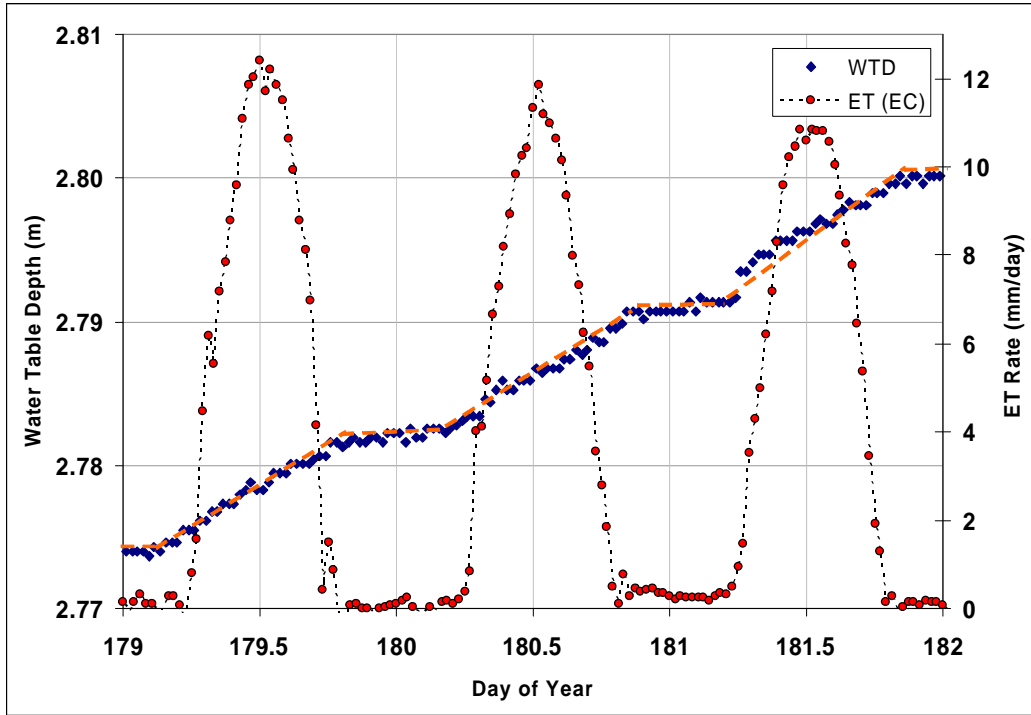


Figure 67. Diurnal fluctuations in water table depth (WTD) near EC station in BLK100 (well 850T). Notice a reduction in drawdown rate (smaller slope) during nighttime. $ET(EC)=ET_{corr}$.

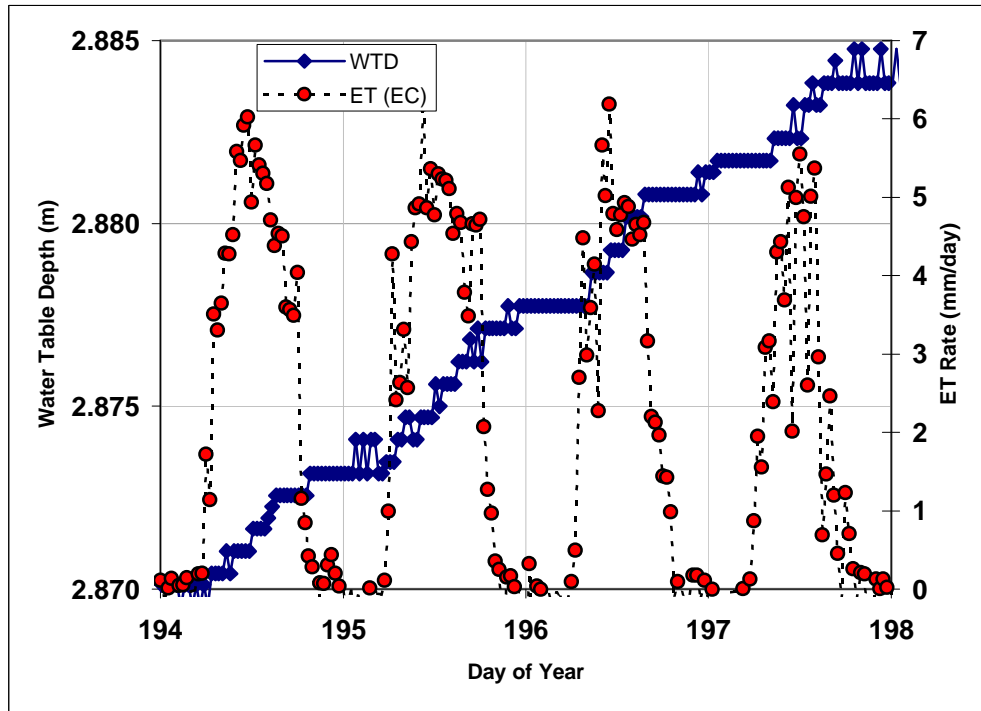


Figure 68. Diurnal fluctuations in water table depth (WTD) near EC station in PLC074 (well 012UT). Notice a reduction in drawdown rate (smaller slope) during nighttime. $ET(EC)=ET_{corr}$.

Table 13. Measured diurnal changes in water table depths, daily ET (eddy covariance method), and estimated specific yield for BLK 100 during summer of 2003 (Specific yield is estimated assuming ET was a result of uptake from water table only).

Site	Day of Year	Diurnal Change in WTD (mm)	Daily ET (mm)	Specific yield (-)
BLK100	178	8.84	4.07	0.46
	179	8.24	4.13	0.50
	180	8.53	4.00	0.47
	181	9.45	3.96	0.42
	182	10.0	3.96	0.40
	183	8.24	3.89	0.47
	184	8.84	3.88	0.44
	185	7.62	4.03	0.53
	186	7.62	4.27	0.56
	187	8.84	4.11	0.46
	188	8.23	4.09	0.49
	189	9.46	3.93	0.41
	<i>mean</i>	8.66	4.03	0.47
	PLC074	193	4.27	2.3
194		3.97	2.32	0.58
195		3.65	2.3	0.63
196		3.97	1.9	0.48
197		2.44	1.43	0.59
198		2.44	1.62	0.66
<i>mean</i>		3.46	1.98	0.58

Table 13. Assuming that the entire drawdown was driven by ET_{corr} (primarily plant transpiration) that was independently measured by the EC station, we estimated an effective yield for the site by taking the ratio of daily ET to daily water table drawdown distance (r),

$$S_y = \frac{ET_{gw}}{r} \quad (22)$$

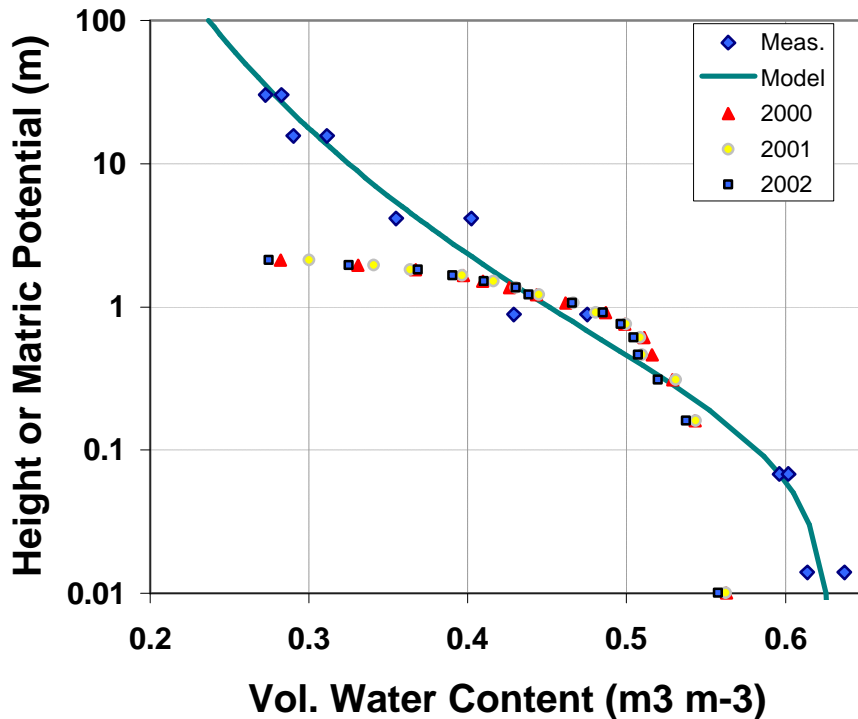


Figure 69. Soil water characteristic for BLK100 soil measured in the lab (and fitted model) and inferred from measured water content vs. height above the water table during April of 2000, 2001, and 2002.

The resulting value of specific yield for BLK100 was 0.47 and was 0.58 for PLC074. These values are considerably higher than expected for a profile under hydrostatic conditions. Freeze and Cherry (1979) suggested that the specific yield for unsaturated soil profiles with fluctuating shallow water table should be less than the drainable porosity for the soil, and could be estimated from a soil water characteristic curve. The primary flaw with this argument is that in the presence of plant uptake the soil profile is far from the quasi-equilibrium state expected for gravity drainage of a hydrostatic profile. The change in water table depth is brought about by

direct uptake through a soil profile that is much drier than a hydrostatic profile. The processes can be viewed as one of a propagating drying front induced by plant roots. At shallow depths, plants preferentially take up soil water due to presence of nutrients and typically higher root densities. An example from BLK100 is illustrated in Figure 69 showing water content measurements vs. height above the water table at its shallowest position in early April for three consecutive years. Notice the strong divergence of the water content profile from a hydrostatic one based on the measured soil water retention curve that occur at an elevation of about 1 m above water table.

Extrapolating for the period between high and low DTW measurements, seasonal plant water uptake was estimated using Equation 22 and the mean S_y for BLK100 and PLC074. At BLK100, the calculated seasonal ET from these fluctuations between DOY 90 and 260 resulted in ET_{gw} of 383 mm, and ET of 393 mm in 2001 and 2002, respectively. For PLC074, ET_{gw} estimated from water table change for the period DOY112 to 246 as 133mm. These values based on seasonal water table fluctuations include E and T_{soil} and should overestimate T_{gw} by ~0.71 and 0.80 at BLK100 and ~0.57 at PLC074 if the T_{gw} estimates from the SWB are accurate. Multiplying the values derived from groundwater fluctuations by the fractions in Table 12 gave: 272 mm at BLK100 (2001), 314 mm at BLK100 (2002), and 75 mm at PLC074. Comparable values of T_{gw} for the same period determined by water balance closure were 293 mm in 2001 and 277 mm in 2002 at BLK100 and 59 mm at PLC074. Given the similarity of the values and the imprecision of the unrelated methods, we concluded that SWB estimates of T_{gw} were reliable for these shallow water table sites. This method was not tested for sites like PLC185 or PLC018 with deep water tables because of the absence of DTW monitoring.

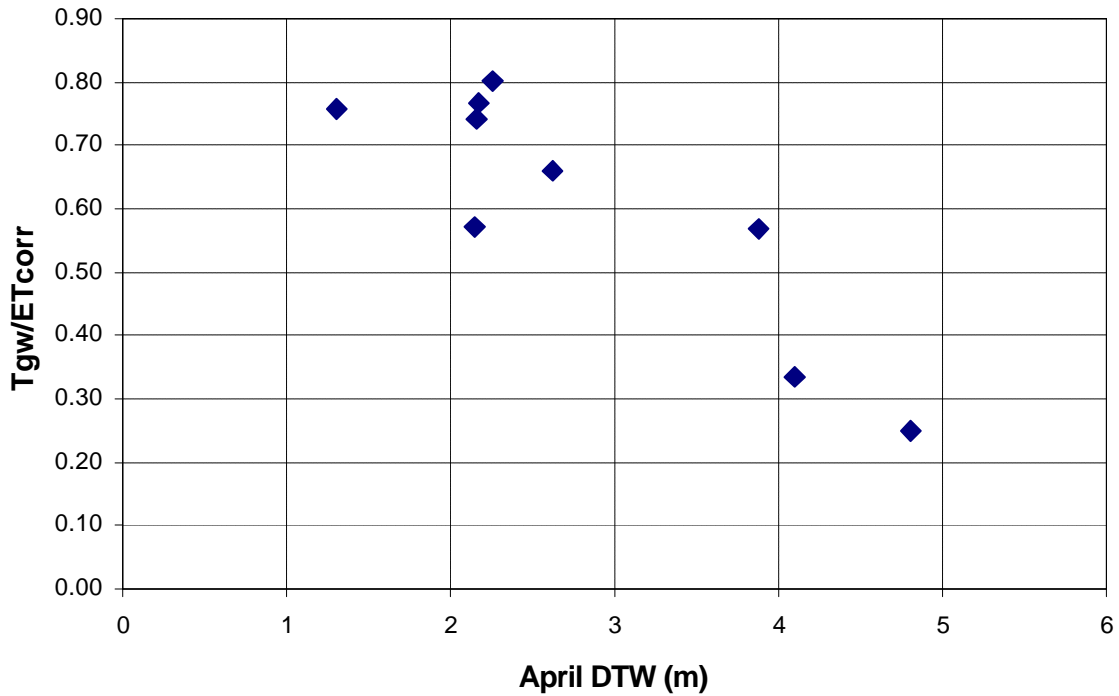


Figure 70. Fraction of ET supplied by direct uptake from the water table as a function of DTW at the beginning of the growing season. DTW values for PLC018 is an estimate and could be deeper (i.e. >4.8m). DTW for PLC185 was determined at the time of access tube installation.

Analysis of the water balance closure quantified the contribution to ET_{corr} from the water table when the root zone and the water table were “coupled”. Groundwater pumping may lower the water table and “decouple” the water table from the root zone. Under such conditions, it would be expected that the contribution from the water table would decrease and reliance on stored soil water would increase (and/or T would decrease). Thus, modeling the soil water balance also requires an expression to reduce T_{gw} as the water table declines. Also, an expression is needed to describe the expected reduction in T as water table decline induces plant stress.

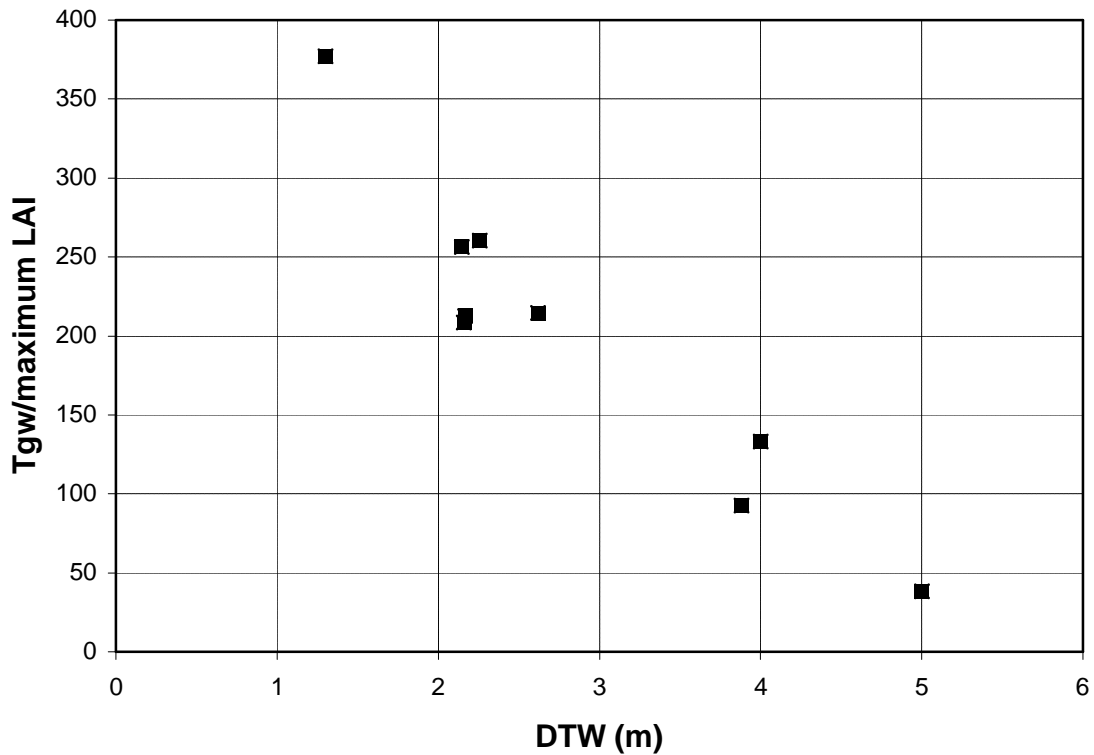


Figure 71. T_{gw} scaled by maximum LAI as a function of DTW. DTW values for PLC018 is an estimate and could be deeper (i.e. >5.0m). DTW for PLC185 was determined at the time of access tube installation.

The vadose model currently contains a parameter to account for water table uptake as a function of DTW, (KW, see below), but the parameter is related to maximum rooting depth and not well quantified. This study did not artificially lower the water table during the growing season preventing direct observation of this function. The study sites, however, included a range of water table and vegetation conditions including coupled and decoupled sites. The fraction of ET supplied by water table uptake (T_{gw}/ET_{corr}) was related to DTW as shown in Figure 70.

Alternatively, simple inspection suggested that T_{gw} was related to LAI and/or DTW (the latter are weakly correlated for this set of locations). The relationship between T_{gw} , LAI, and DTW is presented in Figure 71. Normalizing T_{gw} by peak LAI accounted for inherent site differences in plant community due to other soil factors or stress induced reduction in leaf area. Depending on the method to derive ET estimates (if based on LAI for example) this function may be able to accommodate the groundwater uptake for coupled sites and for sites affected by pumping. Further experimentation with the vadose zone model is necessary to determine which function is most applicable to reformulate the KW model parameter.

Conclusions

At sites with high leaf area and shallow water tables, 70-80 % of the ET_{corr} was derived from the water table directly and is not reflected in changes in soil water content. Quantifying this value has direct bearing on the parameterization of the vadose zone water balance model. Additionally, multiple functions relating T_{gw} , LAI and DTW were prepared to guide future conceptualization of the vadose zone model.

Vadose Zone KF model development/improvements

Introduction

Previous studies cooperatively conducted by the County and LADWP developed a mass balance model to determine changes in water storage in the vadose zone (Or and Groeneveld, 1994). The model uses transpiration coefficients, precipitation, and changes in water table depth to account for changes in vadose water storage and Kalman filtering to optimally update predictions as data become available. The Kalman filter utilizes uncertainty in both measurements and model predictions to determine the overall uncertainty in predicted soil water

storage. An important characteristic of the existing model is that the ET, water table fluctuation, and water table contribution to plant uptake can be modified, updated, or replaced without reference to the other model components. Key to the success of the model is proper accounting of sources for water uptake, groundwater or soil water by phreatophytes based on the depth to the water table.

The simplified soil water balance between two time periods, i and $i+1$ is,

$$SW_{i+1} = SW_i + P + \Delta SW_{DTW} - ETa \quad (23)$$

where, SW is soil water stored in the soil layer of interest, P is precipitation, ΔSW_{DTW} is change in soil water caused by change in DTW, and ETa is actual ET (ET_{corr} in this study). ΔSW_{DTW} is only calculated when the water table is within the root zone. The water balance model of Or and Groeneveld (1994) estimates the ETa by the following expression:

$$ETa = Kc \cdot KW \cdot ETr \quad (24)$$

where ETr is potential evapotranspiration as determined by atmospheric-climatic conditions (e.g., Penman's equation); Kc is a transpiration coefficient which provides the ratio of ETa to potential evapotranspiration ETr (Equation 15). KW is a coefficient based on water table depth which partitions some of the ETa to direct uptake from the water table without depletion of stored soil water. When KW is 1 or greater, all ETa is drawn from the soil. The dominance of T_{gw} in the soil water balance when the water table was shallow pointed the need to focus on how to construct KW before making extensive revisions or tests of the model.

The objective of this task was to revise the vadose water balance model to update its components based on results obtained in this study.

Materials and Methods

Modeling was conducted using data collected at BLK100 because that site had the longest record. Because of the predominance of T_{gw} , model runs were primarily to evaluate the KW component by relying on measured ET, DTW and soil water information. All data used for this portion of the project were collected during the field investigation of the water balance closure described above.

Results and Discussion

Specific changes or improvements to the model are described in the sections below.

CIMIS ETr model

The vadose zone model requires predictions of plant water demand (Kc) that are adjusted for weather conditions using ETr. A stochastic model for generating synthetic ETr sequences for Owens Valley, CA was estimated from a 19 years (1983-2001) sequence of ETr based on observations collected at Bishop, California (CIMIS, 2002). A modified Penman equation was used to compute daily ETr, from which mean daily ETr and a corresponding standard deviation (STD) were obtained using the available data set (Figure 72). A clear seasonal trend existed in the ETr time series which was removed prior to fitting a stochastic model. A Fourier series was fitted to the daily ETr using procedures described by Salas et al., (1980). The first two harmonics series is given by,

$$\overline{ETr}(i) = \langle ETr \rangle + \sum_{j=1}^2 \left[A(j) \cos\left(\frac{2\pi ij}{365}\right) + B(j) \sin\left(\frac{2\pi ij}{365}\right) \right] \quad (25)$$

where i is the day of year, $\langle ETr \rangle$ is mean daily ETr for the entire year (4.12 mm/day), $A(1)=-2.73$; $A(2)=-0.112$; $B(1)=0.187$; and $B(2)=0.097$. We used the first harmonic only as it was

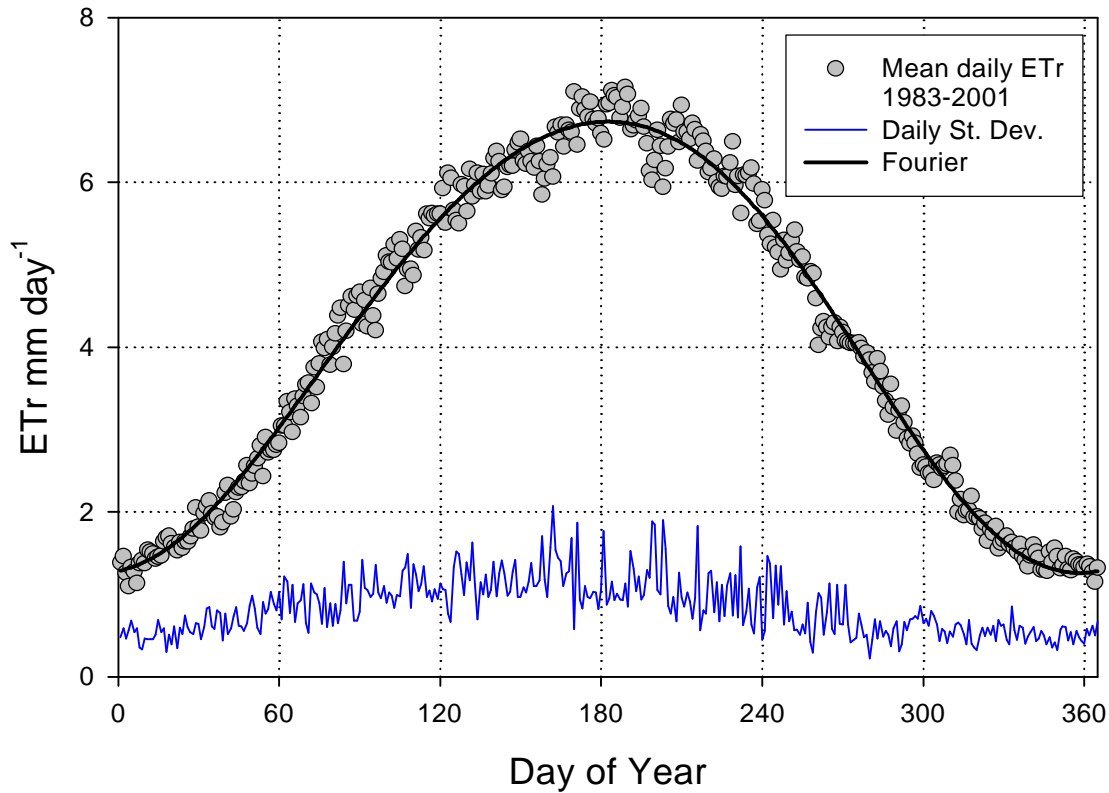


Figure 72: Mean daily ET_r and its standard deviation (STD) estimated by the modified Penman equation from climatic data collected at Bishop, California (CIMIS, 2002, station #35).

capable of explaining more than 98% of the variance in average daily ET_r indicating a strong seasonal (periodic) trend as evident from the data.

An approach based on classic time-series analysis was adopted for fitting a stochastic model to the residuals of mean daily ET_r series, i.e., after removing the deterministic trend. Several possible ARMA(p,q) stochastic models were tested based on criteria of best fit and parsimony. Estimated parameters by the maximum likelihood method, statistics, and tests of the

Table 14. Estimated model parameters for standardized mean daily ETr series for 1983-2001 in Bishop, California. Data are from CIMIS Station #35).

ARMA(p,q) Model Order				
Parameters		AR(1)	AR(2)	ARMA(1,1)
ϕ_1		0.438	0.421	0.506
ϕ_2			0.031	
θ_1				0.085
Goodness-of-Fit and Parsimony Tests				
Residuals variance s_e^2		0.050	0.055	0.050
Porte Manteau Test - $Q_{L=90}$		98.8	97.0	97.2
AIC		-1088	-1086	-1087

residuals are given in Table 14. An ARMA(1,1) model was selected as the best model for the daily ETr data based on goodness-of-fit test results (Table 14), and capability to be reduced into a predictive model for ETr as shown next. The ARMA(1,1) model is given by,

$$ET_i = \phi_1 ET_{i-1} - \theta_1 e_{i-1} + e_i \quad (26)$$

where ϕ_1 is an autoregression parameter, θ_1 is a moving average parameter, and e_i is a normally distributed zero mean term with variance equal to s_e^2 . The adequacy of the ARMA(1,1) was also confirmed by its best-fit to the autocorrelation of ETr residuals.

We adopted a method proposed by Graupe and Krause (1973) for improving the ETr model by transforming the ARMA(1,1) of ET_i estimates which are based on inaccurate measurements that include error into a first order autoregressive model, AR(1) of the

unobservable "true" state,

$$\tilde{ET}_{i+1} = \mathbf{j}_1 \tilde{ET}_i + u_i \quad (27)$$

where $ET_i = ET_i + v_i$, and $s_u^2 = s_e^2 [1 + \sigma_1^2 / \sigma_1^2 + \sigma_1^2 / \sigma_1^2]$ ($s_u^2 = 0.06$). An estimate of the measurement variance is given by: $s_v^2 = s_e^2 [\sigma_1^2 / \sigma_1^2]$ (with $s_v^2 = 0.0084$).

Site-Scale Transpiration Coefficients

Initially we planned to use detailed information on vegetation cover and composition for each study site, coupled with vegetation based Kc to derive estimates for diurnal and seasonal transpiration fluxes. The Kc models were a subject of this study. Therefore, the vadose zone model was revised to rely on site-specific Kc derived from eddy covariance and *ETr* measurements rather than the approach described in the original proposal. This was necessary to insulate the investigation of *KW* from variability introduced by less direct estimates of ET. Site-scale Kc were derived from the eddy covariance *ET_{corr}*, CIMIS *ETr* measurements, and Equation 15. Although the data set is fragmentary, daily Kc from three measurement seasons at BLK100 (2000-2002), revealed a clear and repeatable trend (Figure 73). Subsequently, we fitted a Fourier series to mean daily Kc with some patching of missing periods in January and February when the instruments were being calibrated with linear trends depicted by the continuous line on Figure 73.

KW evaluation and model simulation

The water balance model estimates the actual evapotranspiration by Equation (24) given above. The relative portion of ETa satisfied by uptake directly from the water table (*KW*) was computed by three methods assuming that: (i) the uptake is proportional to the depth occupied by

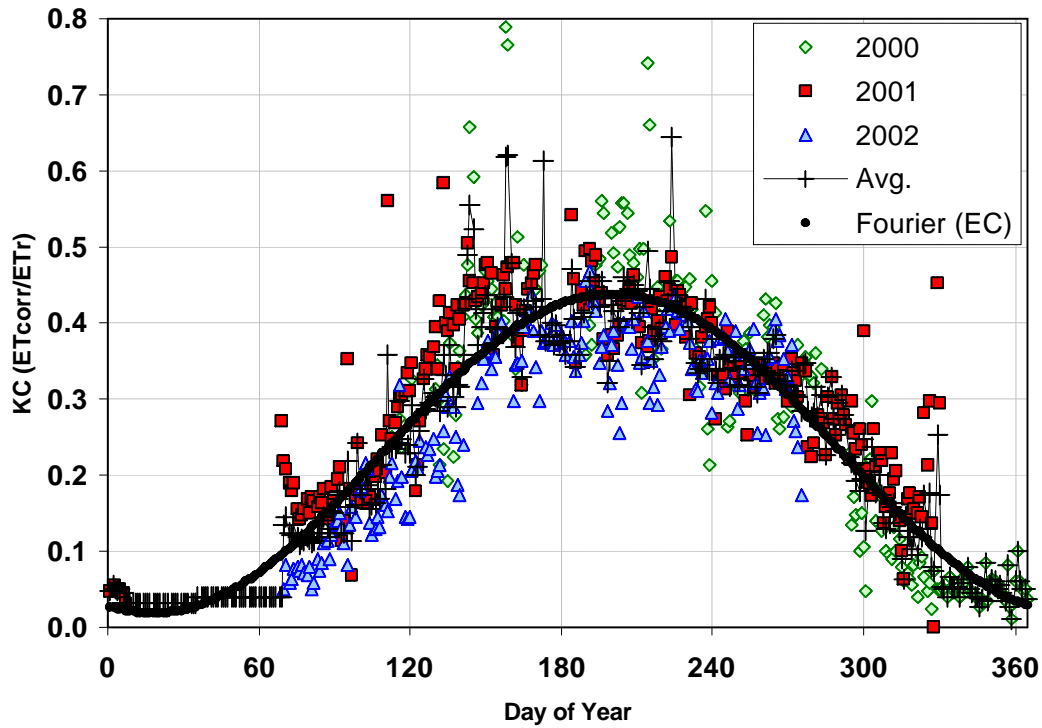


Figure 73. Site-scale Kc data, average, and fitted Fourier model for BLK100. Fourier model coefficients: A(1) -0.20, B(1)-0.064, A(2) and B(2) 0.0; $r^2 = 0.91$.

the water table within the rooting zone (Or and Groeneveld, 1994); (ii) a newly-developed expression proposing that uptake is proportional to the depth occupied by the water table raised to a power ($4 > b > 2$); and (iii) the uptake follows a pattern of exponential-decay with depth given below by,

$$(i) \quad KW_i = \frac{DTW_i}{RTD_{max}}; \quad (ii) \quad KW_i = \left(\frac{DTW_i}{RTD_{max}} \right)^b; \quad (iii) \quad KW_i = 1 - \exp\left(-\frac{a \cdot DTW_i}{RTD_{max}} \right) \quad (28)$$

where RTD_{max} is the maximum rooting depth and all other variables as defined previously. All variables are expressed in units of equivalent water depth. Unfortunately, the short time frame of

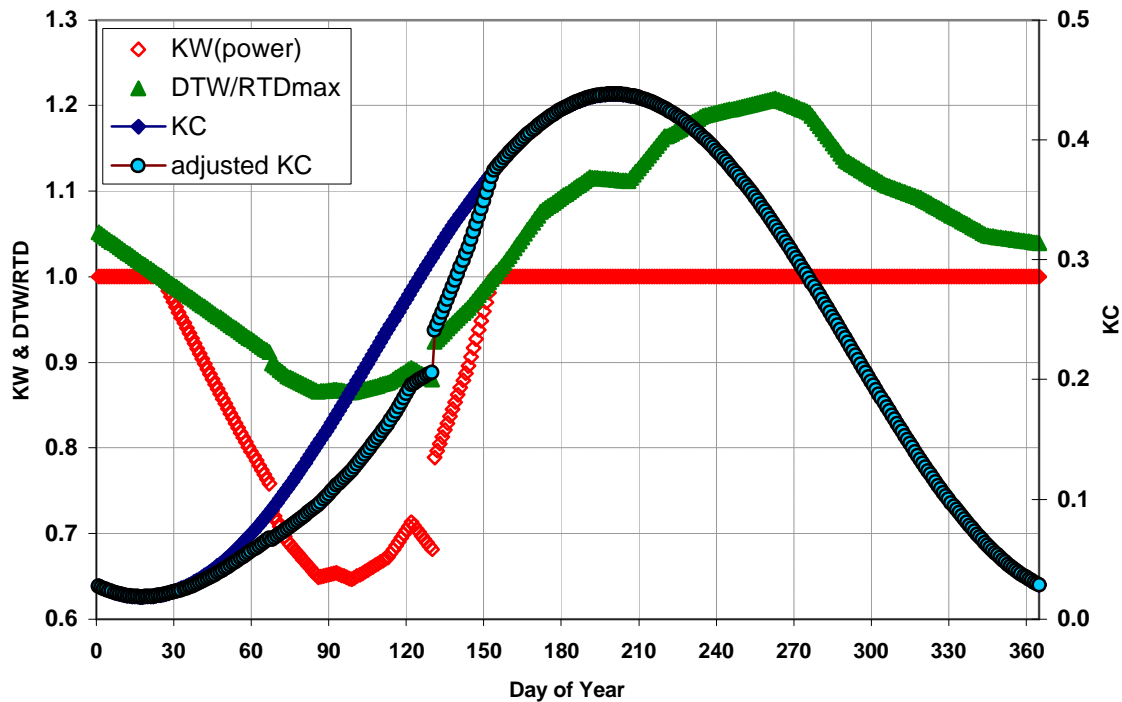


Figure 74. Changes in relative water table depth (DTW/RTD , where $RTD_{max}=2500$ mm) in BLK100 during 2001. KW was based on the power function with $b=3$, and the site Kc adjusted by the water table contribution as reflected by KW [calculated as: adjusted $Kc = (1 - KW) * Kc(EC)$]. The area between the Kc curves reflects the contribution of direct uptake from water table to site ET_{corr} .

the study did not allow for relying on function derived from the SWB. In previous studies we have used (iii) with $a=2$ (Or and Groeneveld, 1994). In this study we use (ii) with $b=3$ based weight for greater uptake of water from the water table when it was located within the rooting zone based on the field investigation results (Figure 74). This version gave the highest fraction of groundwater uptake, but still was lower than suggested by the SWB.

For all versions, $KW \geq 1$ for $DTW_i > RTD_{max}$. RTD_{max} was set at the multi-year water

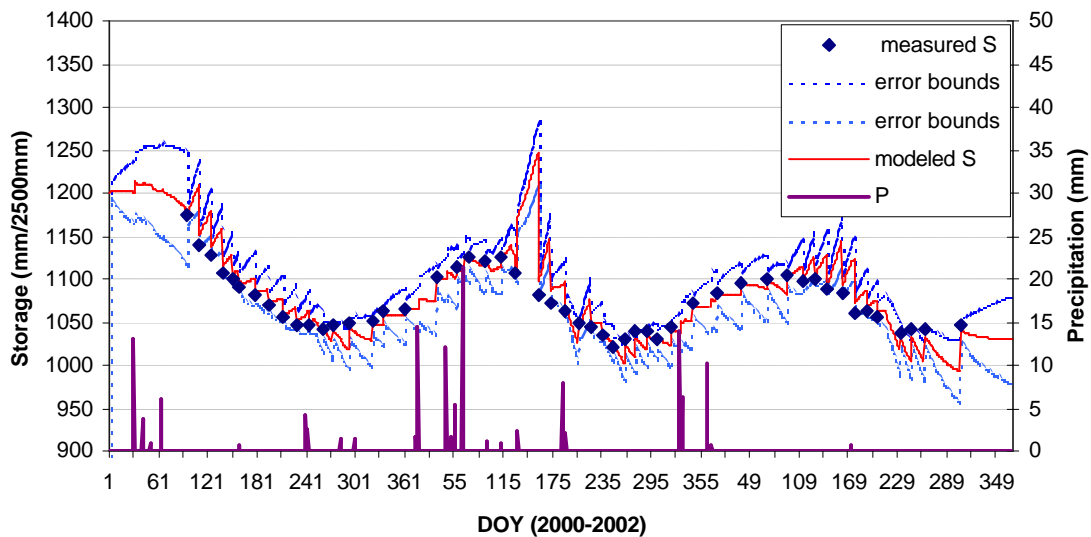


Figure 75. Measured and modeled changes in S at BLK100 for 2000-2002 using the revised water table uptake expression.

table average depth of about 2.5m. Conveniently this was the measurement depth for calculation of S . This site had fine-textured soils (Appendix B), and the saturated zone extended above the water table and into the active root zone ($<2.5\text{m}$).

An example of simulation results of the vadose zone model with the power version of KW is given in Figure 75. The model overestimated soil water content the during the growing season (especially in April and May) and underestimated the soil water content as the water table rose each winter. The SWB showed that groundwater uptake occurred after DOY 160 after the water table dropped below the RTDmax used for the simulations (2.5m). The model assumed that groundwater uptake ceased after DOY 160 (i.e. $KW = 1$). The model needs further refinement to determine the best formulation of the KW based on the SWB results. The

relationship between KW and RTD_{max} will be particularly important to refine.

Conclusions

Starting from the model reported by Or and Groeneveld (1994) we performed the following updates and key modifications: (1) the ETr stochastic model was updated by incorporating additional 10 years of ETr data obtained from the CIMIS station in Bishop, CA; (2) our estimates were improved on the amount of water taken up directly from the water table in sites with different water table depths to refine the partitioning function between uptake from vadose water and groundwater (3) the water balance model was revised to make use of these new functions.

IV. Public Outreach and Technical Presentations

Inyo County Water Department published an annual report called the *Monitor* to present summaries of significant policy developments, monitoring results of the environmental conditions in the Valley and to provide updates on current research by science staff including work performed for this project. The Monitor was produced in June 2003, and a copy is attached. The Water Department maintains a web site (www.inyowater.org) where reports and publications arising from this project will be posted. Drs. Harrington and Steinwand presented results from this project at national meetings in 2002 of the American Geophysical Union and Soil Science Society of America (SSSA). References for these presentations are given below. Drs. Steinwand and Or are scheduled to present a results of this study in a poster entitled: *Water Balance Closure for Owens Valley Phreatophytes Combining Water Table, Eddy Covariance,*

and Soil Water Measurements at the SSSA meetings in November 2003. Two internal Inyo County reports related to this project have been completed. Copies of those are attached to this report.

Presentations

Harrington, R.F., and A.L. Steinwand. 2002. Regional groundwater discharge estimated using micrometeorological measurements, plot-scale measurements of vegetation cover, and remotely-sensed vegetation cover. American Geophysical Union

Steinwand, A.L., R.F. Harrington, P.J. Hubbard, and D. Martin. 2002. Transpiration coefficients and eddy covariance estimates of evapotranspiration of Great Basin phreatophytes. In Agronomy Abstracts, ASA, Madison, WI.

V. References

- Allen, R.G., L.S. Pereira, D. Raes, and M. Smith. 1998. Crop Evapotranspiration: Guidelines for Computing Crop Water Requirements. United Nations FAO, Irrigation and Drainage Paper 56. Rome, Italy. 300 p.
- Arya, S.P. 2001. Introduction to Micrometeorology, Second Edition, Academic Press.
- Ball, J.T., J.B. Picone, and P.D. Ross. 1994. Evapotranspiration by riparian vegetation along the lower Colorado River. Final report to U.S. Bureau of Reclamation. 188pp.
- Bastiaanssen, W.G.M., M. Menenti, R.A. Feddes, and A.A. M. Holtslag. 1998a. A remote sensing surface energy balance algorithm for land (SEBAL). Part 1: Formulation. J. of Hydrology 198-212.
- Bastiaanssen, W.G.M., H. Pelgrum, J. Wang, Y. Ma, J.F. Moreno, G.J. Roerink, R.A. Roebeling, and T. van der Wal. 1998b. A remote sensing surface energy balance algorithm for land (SEBAL). Part 2: Validation. J. of Hydrology 212-213:213-229.
- Bastiaanssen, W.G.M. 2000. SEBAL-based sensible and latent heat fluxes in the irrigated Gediz Basin, Turkey. J. of Hydrology 229:87-100.
- Bastiaanssen, W.G.M., M.D. Ahmad and Y. Chemin. 2002. Satellite surveillance of evaporative depletion across the Indus Basin. Water Resources Research 38, no. 12, 1273. 9 p.
- Berger, D.L., M.J. Johnson, and M.L. Tumbusch. 2001. Estimates of Evapotranspiration from the Ruby Lake National Wildlife Refuge Area, Ruby Valley, Northeastern Nevada, May 1999-October 2000. USGS Water Resources Investigations Report 01-4234.
- Bidlake, W.R. 2001. Evapotranspiration from a Bulrush-Dominated Wetland in the Klamath Basin, Oregon. J. of Amer. Water Res. Assoc. 36(6), 1309-1320.
- Bidlake, W.R. 2002. Evapotranspiration from Selected Fallowed Fields on the Tule Lake National Wildlife Refuge, California, During May to October 2000, USGS Water Resources Investigations Report 02-4055.
- Blaney, H.F. 1954. Consumptive use of groundwater by phreatophytes and hydrophytes. Pub. no. 37. de l'Association Internationale d'Hydrologie. Presented at the Tenth General Assembly of the Int'l. Union of Geology and Geophysics, Rome, Italy. September 1954.
- Branson, F. A., R. F. Miller, and I. S. McQueen. 1976. Moisture relationships in twelve northern desert shrub communities near Grand Junction, Colorado. Ecology. 57:1104-1124.

- Brutsaert, W. 1982. Evaporation into the atmosphere. D. Reidel.
- Campbell Scientific Inc. 1998a. CSAT Three Dimensional Sonic Anemometer Instruction Manual, Revision 3/98.
- Campbell Scientific Inc. 1998b. Eddy Covariance System Operator's Manual CA27 and KH20, Revision 7/98.
- Campbell Scientific Inc. 1989. KH20 Krypton Hygrometer, Revision 11/89.
- Campbell Scientific Inc. 1996. Q-7.1 Net Radiometer, Revision 5/96.
- Campbell Scientific Inc. 1996. CS615 Water Content Reflectometer Instruction Manual, Version 8221-07, Revision 10/96.
- Campbell Scientific Inc. 1999. HFT3 Soil Heat Flux Plate, Revision 2/99.
- Campbell, G.S., and J.M. Norman. 1998. An Introduction to Environmental Biophysics, Second Edition, Springer.
- Cheatham, N. H. and J. R. Haller. 1975. An annotated list of California habitat types. Unpublished mimeograph.
- CIMIS, California Irrigation Management Information System. 2002. Agric. Water Conservation Section, Dept. of Water Resources, Sacramento, CA.
- Danskin, W.R. 1998. Evaluation of the Hydrologic System and Selected Water-Management Alternatives in the Owens Valley, California, U.S. Geological Survey Water-Supply Paper 2370-H.
- Dane, J.H. and J.W. Hopmans. 2002. Water Retention and Storage. pp. 671-796 *In*. J.H. Dane and G.C. Topp (eds.) Methods of soil analysis, Part 4. Soil Sci. Soc. Am. Book 5. SSSA. Madison, WI.
- Duell, L.F.W. 1990. Estimates of Evapotranspiration in Alkaline Scrub and Meadow Communities of Owens Valley, California, Using the Bowen-Ratio, Eddy-Correlation, and Penman-Combination Methods. USGS Water Supply Paper 2370-E.
- Duell, L. F. W. 1992. Eddy-correlation measurements at site L, Chapter D, USGS WRI 91459.
- Elmore, A.J., J.F. Mustard, S.J. Manning, and D.B. Lobell. 2000. Quantifying vegetation change in semiarid environments: Precision and accuracy of spectral mixture analysis and the normalized difference vegetation index. *Remote Sens. Environ.* 73:87-102.

- Farah, H.O. 2001. Estimation of regional evaporation under different weather conditions from satellite and meteorological data. A case study in the Naivasha Basin, Kenya. Doctoral Thesis Wageningen University and ITC.
- Franks, S.W. and K.J. Beven. 1997. Estimation of evapotranspiration at the landscape scale: a fuzzy disaggregation approach. *Water Resour. Res.* 33:2929-2938.
- Freeze, R.A., and J.A. Cherry. 1979. *Groundwater*. Prentice-Hall, Englewood Cliffs, New Jersey.
- Gardner, W.R. 1958. Some steady state solutions of the unsaturated moisture flow equation with applications to evaporation from a water table *Soil Sci.* 85:228-232.
- Gash, J.H.C. 1986. A note on estimating the effect of a limited fetch on micrometeorological evaporation measurements. *Bound.-Layer Met.* 35:409-413.
- Gay, L. W. 1992. Bowen ratio measurements at sites C and L, Chapter A, USGS WRI 91-4159.
- Gay, L.W. and L.J. Fritschen. 1979. An energy budget analysis of water use by saltcedar. *Wat. Res. Res.* 15:1589-1592.
- Gee, G.W., and J.W. Bauder. 1986. Particle-size analysis. pp. 383-411 *In*. A.Klute (ed.) *Methods of soil analysis, Part 1*. 2nd ed. Agron. Monogr. 9. ASA and SSSA. Madison, WI.
- Goodall, D. W. 1952. Some considerations in the use of point quadrats for the analysis of vegetation. *Australian Journal of Scientific Research.* 5:1-41.
- Graupe, D. and D.I. Krause. 1973. On the identification of input-output noise models. *Int. J. Syst. Sci.* 4:617-621.
- Groeneveld, D.P. 1997. Vertical point quadrat sampling and an extinction factor to calculate leaf area index. *J. Arid Env.* 36:475-485.
- Hendrickx, J.M.H., S.-H. Hong, T. Miller, E. Small, P. Neville, J. Cleverly, and W.G.M. Bastiaanssen. 2002. Abstract. Actual ET rates derived by SEBAL in the Middle Rio Grande Valley Annual Meeting of American Geophysical Union, San Francisco, December 6-10.
- Holland, R. F. 1986. Preliminary descriptions of the terrestrial natural communities of California. Unpublished mimeograph.
- Hollett, K.J., W.R. Danskin, W.F. McCaffrey, and C.L. Walti. 1991. *Geology and Water Resources of Owens Valley, California*. USGS WSP 2370-B.
- Iqbal, M. 1983. *An introduction to solar radiation*. Academic Press, Toronto.

- Kuchler, A. W. 1967. *Vegetation Mapping*. New York, Ronald Press Co. 472 pp.
- Kustas, W.P. and J.M. Norman. 1996. Use of remote sensing for evapotranspiration monitoring over land surfaces. *Hydrol. Science J.* 41:495-515.
- Laczniak, R.J., G.A. DeMeo, S.R. Reiner, J.LaRue Smith, and W.E. Nylund. 1999. Estimates of ground-water discharge as determined from measurements of evapotranspiration, Ash Meadows area, Nye County, Nevada. U.S.G.S Water-Res. Invest. Rep. 99-4079.
- Lee, C.H. 1912. An intensive study of the water resources of a part of the Owens Valley, California. USGS Water Supply Pap. 294.
- Manning, S.J, J.F. Mustard and A.J. Elmore. 1999. Patterns of vegetation response to groundwater pumping detected with field monitoring and LandSat TM data. *Ecological Society of America*. August 1999. Spokane, WA. *Ecological Society of America abstracts* vol. 84.
- Massman, W.J., D.G. Fox, K.F. Zeller, and D. Lukens, Verifying Eddy Correlation Measurements of Dry Deposition: A Study of the Energy Balance Components of the Pawnee Grasslands. USDA Rocky Mountain Forest and Range Experiment Station Research Paper RM-288, 1990.
- Maulem, Y. 1976. A new model for predicting the hydraulic conductivity of unsaturated porous media. *Water Resour. Res.* 12:513-522.
- Miller, R.F. 1988. Comparison of water use by *Artemisia tridentata* spp. *wyomingensis* and *Chrysothamnus viscidiflorus* spp. *viscidiflorus*. *J. Range Manage.* 41:58-62.
- Miller, R.F., F.A. Branson, I.S. McQueen, and C.T. Snyder. 1982. Water relations in soils as related to plant communities in Ruby Valley, Nevada. *J. Range Manage.* 35:462-468.
- Nichols, W.D. 2000. Regional ground-water evapotranspiration and ground-water budgets, Great Basin, Nevada. U.S.G.S. Prof. Pap. 1628.
- Or, D., and D.P. Groeneveld. 1994. Stochastic estimation of plant-available soil water under fluctuating water table depths. *J. Hydrol.* 163:43-64.
- Pelgrum, H. and W.B.M. Bastiaanssen. 1996. An intercomparison of techniques to determine the area-averaged latent heat flux from individual in-situ observations: a remote sensing approach using the European Field Experiment in a Desertification-Threatened Area data. *Water Res. Res.* 32:2775-2786.
- Robinson, T.W. 1970. Evapotranspiration by woody phreatophytes in the Humboldt River

- Valley near Winnemucca, Nevada. U.S.G.S. Prof. Paper 491-D.
- Roerink, G.J. et al. 1997. Relating crop water consumption to irrigation water supply by remote sensing. *Water Resources Management* 11:445-465.
- Salas, J.D., W. Delleur, V. Yevjevich, and W.L. Lane. 1980. Applied modeling of hydrologic time series. Water Resource Publications, Fort Collins, Co.
- Schillinger, W.F. and F.L. Young. 2000. Soil water use and growth of Russian thistle after wheat harvest. *Agron. J.* 92:167-172.
- Shuttleworth, W. J., 1993. Evaporation, *In* D. R. Maidment (ed.) *Handbook of Hydrology*, McGraw-Hill.
- Snedecor, G. W. and W. G. Cochran. 1980. *Statistical Methods*, Iowa State University Press, Ames, Ia..
- Stannard, D. I. 1992. Bowen ratio measurements at sites C and F, Chapter B, USGS WRI 91-4159.
- Steinwand, A.L. 1998. Evaluation of methods to calculate vegetation water requirements for the Owens Valley, Ca. Report to the Inyo/Los Angeles Technical Group, February 28, 1998. 55pp.
- Steinwand, A.L. 1999a. Transpiration coefficients for three Great Basin shrubs. Report to the Inyo/Los Angeles Technical Group, May 12, 1999. 41pp.
- Steinwand, A.L. 1999b. Transpiration coefficients for two Great Basin phreatophytic grasses. Report to the Inyo/Los Angeles Technical Group, November 24, 1999. 91pp.
- Steinwand, A.L., R.F. Harrington, and D.P. Groeneveld. 2001. Transpiration coefficients for three Great Basin shrubs. *J. Arid Env.* 49:555-567.
- Sumner, D.M., Evapotranspiration from Successional Vegetation in a Deforested Area of the Lake Wales Ridge, Florida. USGS Water Resources Investigations Report 96-4244, 1996.
- Van den Hurk, B.J.J.M., W.G.M. Bastiaanssen, H. Pelgrum, and E. van Meijgaard. 1997. A new methodology for assimilation of initial soil moisture fields in weather prediction models using Meteosat and NOAA data. *J. of Applied Meteorology* 36:1271-1283.
- van Genuchten, M.Th. 1980. A closed-form equation for predicting the hydraulic conductivity of unsaturated soils. *Soil Sci. Soc. Am. J.* 44:892-898.

Wang, J., W.G.M Bastiaanssen, Y. Ma, and H. Pelgrum. 1998. Aggregation of land surface parameters in the oasis-desert systems of Northwest China. *Hydr. Processes* 12:2133-2147.

Webb, E. K., G. I. Pearman, and R. Leuning. 1980. Correction of flux measurements for density effects due to heat and water vapor transfer. *Quart. J. R. Meteorol. Soc.*, 106, 85-100.

Zeller, K.F., W. Massman, D. Stocker, D.G. Fox, D. Stedman, and D. Hazlett. 1989. Initial Results from the Pawnee Eddy Correlation System for Dry Acid Deposition Research. USDA Rocky Mountain Forest and Range Experiment Station Research Paper RM-282.

VI. Summary of Costs and Disbursements

Inyo County Salaries and Benefits	\$75,686
Consultants	\$78,605
Equipment	\$60,721
General Operating	\$13,507
Total Expense	\$228, 519
Total Disbursement from DWR	\$242,975

Appendix A: Daily eddy covariance, energy balance component, and transpiration model results.

Appendix B: Soil characterization data for EC sites.